TECHNISCHE UNIVERSITÄT MÜNCHEN

Lehrstuhl für Nanoelektronik

Modeling and Simulation of Carbon Nanotubes Networks: Toward a Multiscale Approach

Simone Colasanti

Vollständiger Abdruck der von der Fakultät für Elektrotechnik und Informationstechnik der Technischen Universität München zur Erlangung des akademischen Grades eines

Doktor-Ingenieurs (Dr.-Ing.)

genehmigten Dissertation.

Vorsitzender: Prof. Gordon Cheng, Ph.D.

Prüfer der Dissertation:

1. Prof. Paolo Lugli, Ph.D.
2. Prof. Stephen Goodnick, Ph.D.

Die Dissertation wurde am 10.10.2016 bei der Technischen Universität München eingereicht und durch die Fakultät für Elektrotechnik und Informationstechnik am 21.10.2016 angenommen.

To my family,

"Essentially, all models are wrong, but some are useful."

George E. P. Box

Abstract

In the last decade, the interest in novel electronic materials has dramatically increased, opening new possibilities and offering new scenarios that few years ago were considered only research curiosities. Terminologies such as flexible electronic and organic electronic are day by day acquiring more appeal and driving not only the research in academia but also a conspicuous amount of resources in global leading companies. Among the many emerging technologies, carbon nanotubes (CNTs) thin-films represent certainly one of the most interesting from an application-oriented point of view. Such interest increases the demand for a clear understanding of the physical phenomena that dominate the transport through these devices. For this reason, theoretical studies based on numerical approaches are fundamental for the design and development of high-performance devices.

In this regard, this work is focused on the development of a multi-scale simulation software that has the ultimate goal of helping in the design of CNT film devices for various applications. The model is based on a stochastic algorithm that can generate non-rigid solid objects in a three-dimensional space, emulating with high accuracy the typical fabrication processes involved. The transport mechanisms are modeled according to the theory of one-dimensional ballistic channels based on the Non-Equilibrium Green's Function (NEGF) approach. The behavior of the entire network is then simulated by coupling a SPICE program with an iterative algorithm that calculates self-consistently the electrostatic potential and the current flow in each node of the network. The validation of the model has been performed by comparing the simulations with measurements of different kind of devices, such as simple resistive films, sensors and finally with more complicate thin-film transistors structures.

Kurzfassung

In den letzten zehn Jahren hat das Interesse an neuartigen elektronischen Materialien stark zugenommen. Dabei werden ungeahnte Möglichkeiten eröffnet und spannende Perspektiven geboten, die so bisher nur als reine wissenschaftliche Neugierde abgetan wurden. Terminologien wie etwa „Flexible Elektronik“ und „Organische Elektronik“ bekommen von Tag zu Tag mehr Anziehungskraft und treiben nicht nur die Grundlagenforschung, sondern vielmehr auch umfangreiche Ressourcen in weltweit führenden Unternehmen an. Unter den zahlreichen aufstrebenden Technologien können dünne Schichten aus Kohlenstoffnanoröhrchen (Carbon Nanotubes, CNTs) aus anwendungsorientierter Sicht bestimmt zu den Interessantesten gezählt werden. Dieses Interesse erhöht die Nachfrage nach einem vertieften Verständnis der zugrundeliegenden physikalischen Phänomene, welche den Ladungstransport durch diese Bauelemente dominieren. Aus diesem Grund tragen theoretische Arbeiten basierend auf numerischen Lösungswegen wesentlich zum Design und der Entwicklung dieser Hochleistungsbauelemente bei.

In diesem Zusammenhang konzentriert sich die vorliegende Arbeit auf die Entwicklung einer Software für die Multiskalensimulation mit dem Ziel das Design von CNT-Dünnschichtbauelementen für verschiedenste Anwendungen zu erleichtern. Das Model basiert auf einem stochastischen Algorithmus der es erlaubt nicht-starre Festkörper im dreidimensionalen Raum zu generieren und dabei die typischen beteiligten Herstellungsprozesse mit einer hohen Genauigkeit nachbildet. Die Transportmechanismen werden unter Berücksichtigung der Theorie eines ballistischen Transports in eindimensionalen Kanälen basierend auf einem NEGF-Formalismus modelliert. Das Verhalten des gesamten Netzwerkes wird durch Kopplung mit einem SPICE-Programm mit Hilfe eines iterativen Algorithmus, der selbstkonsistent das elektrostatische Potential und den Stromfluss in jedem Knoten des Netzwerks berechnet, simuliert. Das zugrundeliegende Model wurde durch Vergleich der erlangten Simulationsergebnisse mit Messergebnissen

verschiedener Bauelemente, wie etwa einfachen resistiven Filmen, Sensoren und abschließend auch mit komplexen Dünnschichttransistorstrukturen, validiert.

Contents

Chapter 1

Introduction

> "It is a staggeringly small world that is below. In the year 2000, when they look back at this age, they will wonder why it was not until the year 1960 that anybody began seriously to move in this direction."

It was back in the 1959 when Richard Feynman gave his lecture *"There's Plenty of Room at the Bottom"* at the American Physical Society meeting at Caltech [1]. In this groundbreaking speech, Feynman considered the possibility of direct manipulation of the matter on an atomic scale. Although the term "nanotechnology" would have been coined many years later, Feynman's talk inspired the conceptual foundations of this field.

The emergence of nanotechnologies was promoted in the early 1980s after the invention of the scanning tunneling microscope (STM), which allows the imaging and manipulation of individual atoms within materials. The experimental advances of the last three decades and some revolutionary discoveries such as the one of fullerenes, boosted the interest in the field of nanomaterials and nanoelectronics. Because of the variety of potential applications, governments have invested billions of dollars in nanotechnology research. According to estimates, governments around the world have invested over USD 67 billion in nanotechnology research since 2000 [2]. The research interest in the field of nanoscience and nanotechnology has been confirmed also in the last decade. To cite an example, the European Commission (EC) has explicitly included nanotechnology as a fundamental theme in its research funding programmes; through the Seventh Framework Programme (FP7) the EC has supported institutions and researchers with a funding initiative of EUR 2.5 billion [3].

By convention, nanotechnology is taken as the scale range which goes approximately from 1 to 100 nm, as stated by the National Nanotechnology Initiative (NNI) [4]. While the lower limit is set by the size of atoms, the upper limit is more or less arbitrary but is around the size that phenomena not observed in larger structures start to become influential. Any material which satisfies such conditions is referred to as nanomaterial, and it has often unique optical, electronic and mechanical properties. Historically the first observed nanomaterial was the fullerene, a class of allotropes of carbon which is conceptually graphene sheets rolled into tubes or spheres. The first fullerene molecule to be discovered, the buckminsterfullerene (C_{60}), was prepared in 1985 by Richard Smalley, Robert Curl, James Heath, Sean O'Brien, and Harold Kroto at Rice University. The importance of this discovery was acknowledged 11 years after, when Kroto, Curl and Smalley were awarded the 1996 Nobel Prize in Chemistry for their role in this discovery [5].

From the family of fullerenes, a particular type of cylindrical nanostructure known as carbon nanotube (CNT), has attracted a lot of attention in the scientific community. Due to their unusual properties, CNTs have been object of extensive research studies in the field of nanoelectronics, in the attempt of realizing electronic devices that could one they substitute the current silicon-based technologies. However, while some applications are still far away to become a reality, in other cases the extraordinary properties of the nanotubes have been exploited in a different way. In this regard, one could distinguish the so-called nanodevices from devices based on nanomaterials. In the former case, the nanomaterial constitutes basically the whole device; an example is a Field-Effect Transistor (FET) based on a single nanotube. In the latter case, the nanomaterial is included in a much bigger domain, often as an additive to various material; this is the case for example of carbon fibers.

In this regard, according to this distinction, the work here presented can be considered in the field of devices based on nanomaterials. Carbon nanotube networks are indeed composed by a mixture of nanotubes interconnected between each other, forming macro and micro-devices based on nanomaterials. While the entire devices have dimensions in which phenomena relevant to the nanoelectronics are not evident, the fact that they are composed by objects with a diameter in the order of 1 nm, makes these effects not negligible. It is for this reason that this project aimed to develop a multi-scale simulation tool

capable of treating effects relevant to the nano-scale world and extend them to dimensions several order of magnitude higher. The main motivation behind the need of numerical simulations is that a new technology has always to face some design problems. Simulations can in principle better elucidate some of the most unclear aspects of a new technology and help in finding a way towards an optimum design. Furthermore, once the technology reaches a satisfactory level of maturity, simulations are a powerful mean to assist mass production and application-oriented designs.

The thesis is divided into 7 chapters including this introduction and the final conclusions. The first two chapters describe the state-of-the-art and the theoretical background on which this work is based.

Chapter 2 introduces the reader to the world of carbon nanotubes. Without claiming to be exhaustive, the basics on the different carbon nanotubes technologies are given both from a theoretical and an experimental point of view. More detailed information can be found in highly specialized books, on which chapter 2 takes some cues from [6]. The topic is addressed starting from a single nanotube and ending to a carbon nanotube network, aiming to explain the motivations behind this particular technology and the possible applications. In the conclusive part of the chapter, a brief bibliographic review on the simulation techniques for this specif problem is presented, with a special focus on the flaws of the state-of-the-art simulations of carbon nanotube networks.

In Chapter 3 a comprehensive description of the numerical methods used for the modeling of carbon nanotube networks is given. The simulations are performed with an in-house software developed during the period of this project. The code, completely written in MATLAB language, can be conceptually divided into three sub-programs interconnected between each other. The electrical solver is an external freeware SPICE software, which is embedded in the developed program. Together with the software, all the implemented theoretical models are presented, in the hope of successfully explain the multi-scale approach here adopted.

After these two chapters, the second part of the thesis deals with the results obtained from the simulations. Each chapters is focused on a particular analysis of the networks, thus is based on different models and levels of approximations. The choice of the chapters' sequence aims to introduce the different models in a increasing level of complexity, starting from a purely resistive model and

finishing with a more elaborate transistor model.

In particular, Chapter 4 is focused on the resistive behavior of the CNT films. Important aspects related to the design of the device are numerical studied in details. First of all, some considerations on the stochastic nature of the percolative transport are reported, highlighting critical concepts such as the border effects and the percolation threshold. Moreover, the basic resistive model is extended to include the reactive properties of the nanotubes in the attempt of simulating the frequency behavior of the networks.

Chapter 5, further extends the models of the single nanotubes, including the effects of temperature variations and molecules absorption on the transport properties of the networks. The two phenomena, which are intimately dependent on each other, are the basic working principle for sensors based on CNT films. Once again, in order to optimize the performance of the sensors, the device must be thoroughly designed.

A whole different story is described in Chapter 6. An additional contact, acting as a gate electrode, is added to the architecture of the device. In this configuration, the film behaves as a thin-film transistor in which the gate modulates the transport between the two contacts of source and drain. The resistive model is therefore substituted with a more complicate one where every single nanotube in the network is treated as a small transistor.

Finally, in Chapter 7, conclusions and outlooks are presented together with a brief summary on the main findings.

Chapter 2

Carbon Nanotubes Networks

A random carbon nanotube (CNT) network, is an aggregate of nanotubes with different properties, which is randomly deposited over a certain substrate. These networks are nowadays of great interest thanks to their versatility in a broad range of application in science and engineering. This prefatory chapter gives an extensive overview on their properties, practical applications and possible simulation methodologies. Prior to this, it is however necessary to introduce some of the physical properties of carbon nanotubes, especially from the electronic point of view. This will help in better understanding the motivations behind the development of CNT-based thin films. Furthermore, particular emphasis is given to the fabrication processes involved in the realization of these networks, which represent one of the key strengths of this technology. The last part of the chapter is dedicated to the possible simulation methodologies, with special attention on the so-called *percolation theory*. By exploring the theory and its limitations, some specific modeling challenges will emerge. The chapter is finally concluded with the introduction of the proposed modeling approach, which aims to overcome some of the flaws in the current state of the art.

2.1 From the Single Nanotube to the Network

Since their discovery in 1991 [7], carbon nanotubes have been extensively studied due to their unique properties and potential applications. Field-effect transistors based on individual semiconducting CNTs have been successfully demonstrated, as well as interconnects made by metallic nanotubes [8]. Perhaps the most interesting property of single-wall carbon nanotubes (SWNTs) is their incredibly

high carrier mobility, which is more than an order of magnitude larger than the one of crystalline silicon [9, 10]. Almost after a decade, in the early 2000, new devices based on carbon nanotubes arose, gaining more and more attention by the research community. Among them, randomly aligned network of CNTs are promising candidates for many emerging applications. In the last few years these films have shown remarkable properties, a good processability and relatively low cost [11]. However, these films are not intended to replace devices based on single nanotubes, but rather to cover a different share of the market. Also from the simulation point of view, new techniques must be adopted in order to proper model these devices. The fact that the technology is promising and, at the same time, relatively recent, encourages researcher all over the world to study it also numerically, in the attempt of finding all its potentials, and of course, its limitations.

2.1.1 Electronic Properties of Carbon Nanotubes

Carbon nanotubes are probably the most explored one-dimensional nanostructures. This fact is the result of two rising needs in the world of the electronic devices. From one side, the approaching end of the silicon era, as expected by the trend of Moore's law, has pushed the researchers to find alternatives to traditional semiconductors like silicon and III-V semiconductors. On the other side, the uprising interest in nanostructures like quantum dots and nanowires, has driven the attention to new architectures. However, to truly exploit the potentiality of these new technologies, it is essential to understand that all the concepts learned from bulk device physics are not applicable to carbon nanotubes devices.

A CNT is nothing else than a rolled-up graphene strip which forms a closed cylinder. The graphene lattice is generated by the following basis vectors:

$$\vec{a_1} = \frac{a}{2}\left(\sqrt{3}, 1\right), \tag{2.1}$$

$$\vec{a_2} = \frac{a}{2}\left(\sqrt{3}, -1\right), \tag{2.2}$$

where $a = \sqrt{3}\, a_{C-C}$ ($a_{C-C} = 0.142$ nm is the carbon-carbon distance in graphene). It is worth to mention that the choice of the basis and the atoms of the unit cell

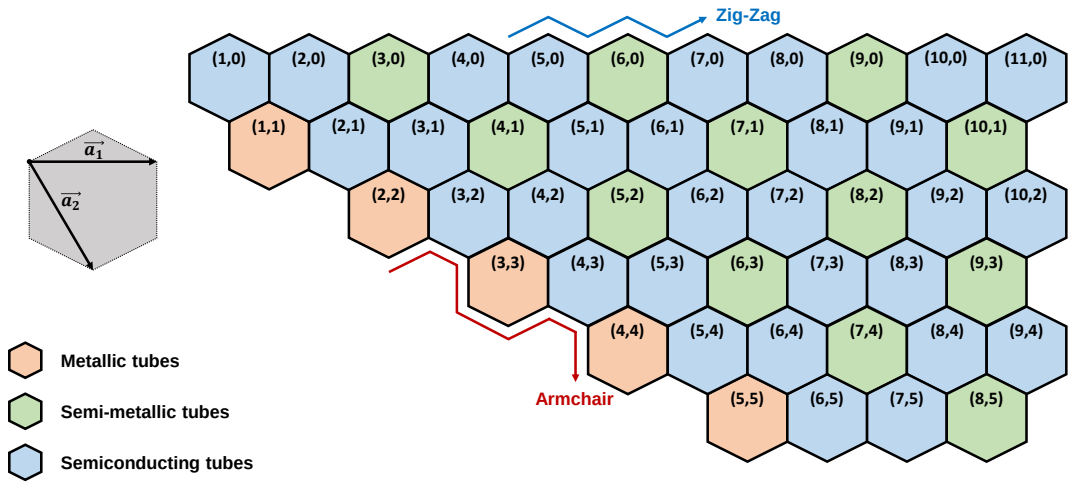

Figure 2.1: Schematic representation of a graphene layer and the classification of the different nanotubes species according to their chiral vector.

is not unique. By cutting rectangular stripes from the graphene layer, one can define a circumferential vector:

$$\vec{C} = n\vec{a_1} + m\vec{a_2}, \tag{2.3}$$

where n and m are the index of the so-called *chiral vector*. The CNT radius is obtained with a simple geometrical calculation in the following way:

$$r = \frac{|\vec{C}|}{2\pi} = \frac{\sqrt{3}}{2\pi} a\sqrt{n^2 + m^2 + nm}. \tag{2.4}$$

According to their chiral vector, CNTs can be divided into three main categories:

- **Armchair CNTs:** A nanotube with the circumferential vector along the direction exactly between the two basis vector ($n = m$).
- **Zig-Zag CNTs:** A nanotube with the circumferential vector that lies purely along one of the two basis vector (n,0).
- **Chiral CNTs:** Generic nomenclature for nanotubes that are not included in any of the two previous classes.

A schematic picture of the different types of CNTs is presented in Figure 2.1. After this classification, one is naturally led to wonder what are the differences between these classes. Indeed, the three classes (and more in general, every chiral vector) present very different electrical properties, that can vary from a

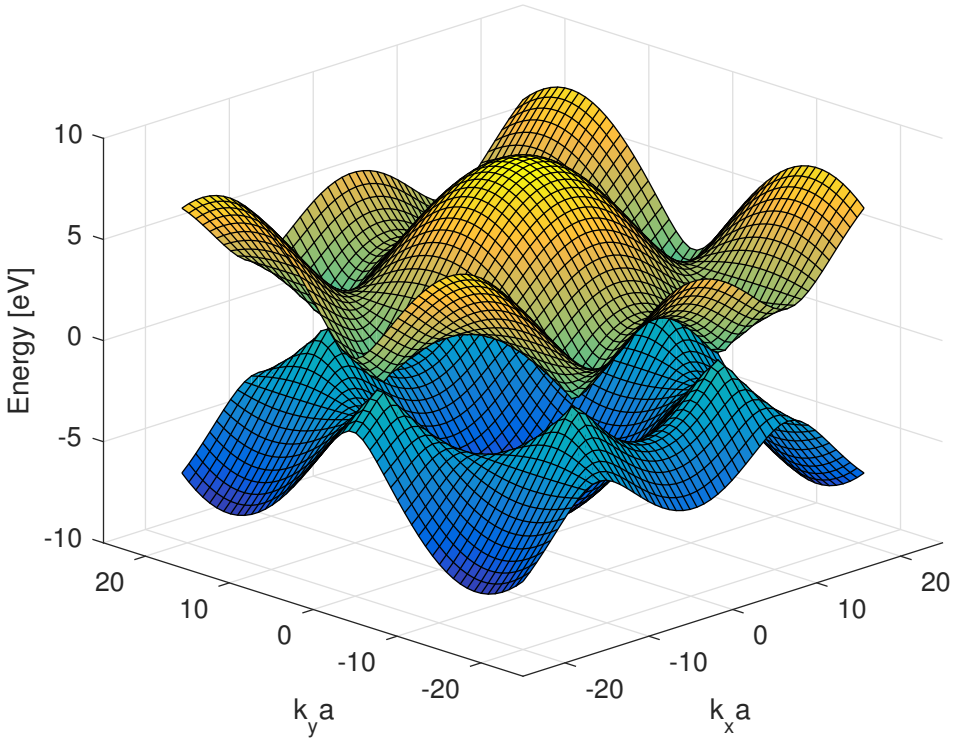

Figure 2.2: Electronic band-structure of graphene computed with a tight-binding model.

semiconducting behavior to a metallic one. The reasons behind, are to be found in the electronic band structure of the nanotubes, which, in a simplistic model, can be directly derived by the one of the graphene.

In a graphene layer, each carbon atom of the lattice possesses six electrons. According to the sp^2 hybridization of the carbon, typical in graphite compounds, the graphene will have two $1s$ electrons, three $2sp^2$ electrons and one $2p$ electron. The three $2sp^2$ form three bonds in the plane of the graphene sheet, giving the mechanical stability to the structure, while the $2p$ electron is left in an unsaturated π orbital. This π orbital, perpendicular to the graphene layer (and as a consequence to the surface of the nanotube), forms a delocalized π cloud, which is responsible for the electronic properties of the structure.

The electronic structure of graphene can be reasonably well described using a rather simple tight-binding Hamiltonian, leading to analytical solutions for their energy dispersion and related eigenstates. Without entering into the details of the mathematical derivation, which can found elsewhere [12, 6], the final expression of the graphene band-structure is here reported:

$$E^{\pm}(k_x, k_y) = \pm\gamma_0\sqrt{1 + 4\cos\left(\frac{\sqrt{3}k_x a}{2}\right)\cos\left(\frac{k_y a}{2}\right) + 4\cos^2\left(\frac{k_y a}{2}\right)}, \tag{2.5}$$

where γ_0 is the transfer integral between first-neighbors π orbitals (typical values for γ_0 are $2.9 - 3.1$ eV. This band-structure is plotted in Figure 2.2 as a function of k_x and k_y. The valence and conduction bands meet at six points, exactly at the corner of the Brillouin zone. In a way, graphene can be thus described as a semi-metal (or zero-gap semiconducting character), with a non-zero density of states at the Fermi level, but with the Fermi surface consisting only of points.

To electronic structure of the CNTs is obtained starting from the one from the graphene. The accepted idea is to quantize the wavevector in the circumferential direction:

$$\vec{k} \cdot \vec{C} = k_x C_x + k_y C_y = 2\pi p, \tag{2.6}$$

where p is an integer. The parametric Equation (2.6) gives a relation between k_x and k_y and it defines lines in the (k_x, k_y) plane. Each line gives a one-dimensional energy band by slicing the two-dimensional band-structure of the graphene. The particular values of C_x, C_y and p determine where the lines intersect the graphene band-structure. This is probably the most important aspect of the CNTs, which can be either metallic or semiconducting, depending on whether or not the lines pass through the graphene Fermi points. When the lines do not intersect the Fermi points the CNT is semiconducting, with a band gap determined by the two lines that come closer to the Fermi points. These concepts are schematically illustrated in Figure 2.3. On the other hand, if the lines intersect the Fermi points, the CNT has crossing bands and thus a metallic character.

This can be seen also mathematically by combining Equation (2.5) and Equation (2.6), leading to the condition

$$|n - m| = 3\,d, \tag{2.7}$$

where d is an integer number. When the indexes of the chiral vector follow the relation expressed in Equation (2.7), the nanotube is said to be metallic. Nanotubes for which this condition does not hold are semiconducting.

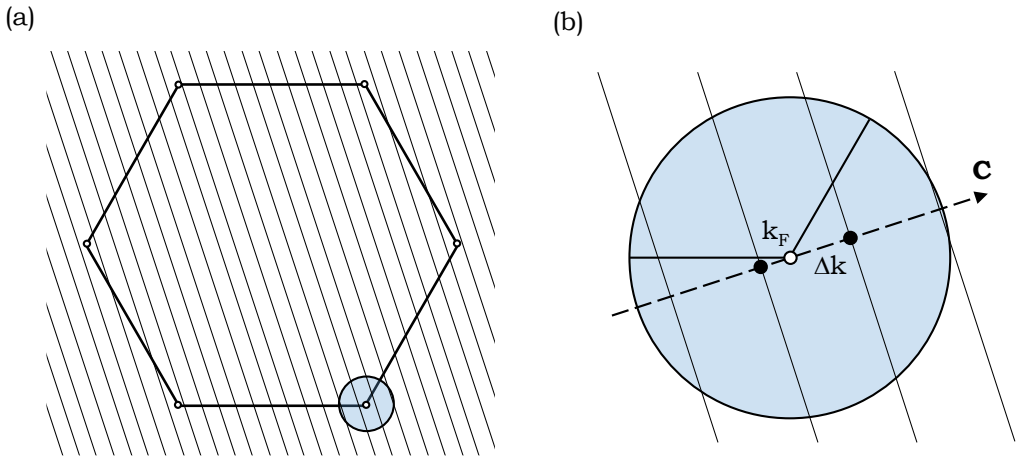

Figure 2.3: (a) Brillouin zone of graphene. The parallel lines represent the allowed states for a semiconducting nanotube. The circle at the bottom-right corner delimits the region of the states near one of the Fermi points. (b) Expanded illustration of the allowed states near the Fermi point k_F. **C** represents the roll-up vector of the nanotube. Figure redrawn from [13].

It is worth to mention that this methodology for the derivation of the band-structure of the nanotubes, which goes under the name of *zone-folding approximation*, has some flaws when treating small-diameter nanotubes. The main reason is related to the curvature of the nanotube, which increases with decreasing the nanotube diameter. As a result of curvature, some of the main assumptions of the previously mentioned tight-binding construction of the Hamiltonian is no longer valid. First of all, the integrals describing the three bonds between nearest neighbors are not identical anymore. Secondly, with small diameters, a $\sigma - \pi$ hybridization of the orbitals can appear, which is instead absent in a simple graphene layer. This effects, have been instead included in more sophisticated numerical techniques, such as in the density functional theory with the local-density approximation (DFT-LDA) method [14, 15]. Among the differences between the two levels of approximation, it is worth to mention the presence of a small gap (in the order of tens of meV) for nanotubes that the zone-folding approximation had predicted as metallic. Interestingly, this does not hold for armchair nanotubes, which show always a metallic behavior no matter how small the diameter is. However, it has been demonstrated that folding the electronic structure of graphene to describe the band structure of CNTs produces accurate results for tubes with diameters larger than 0.8 nm [16, 17].

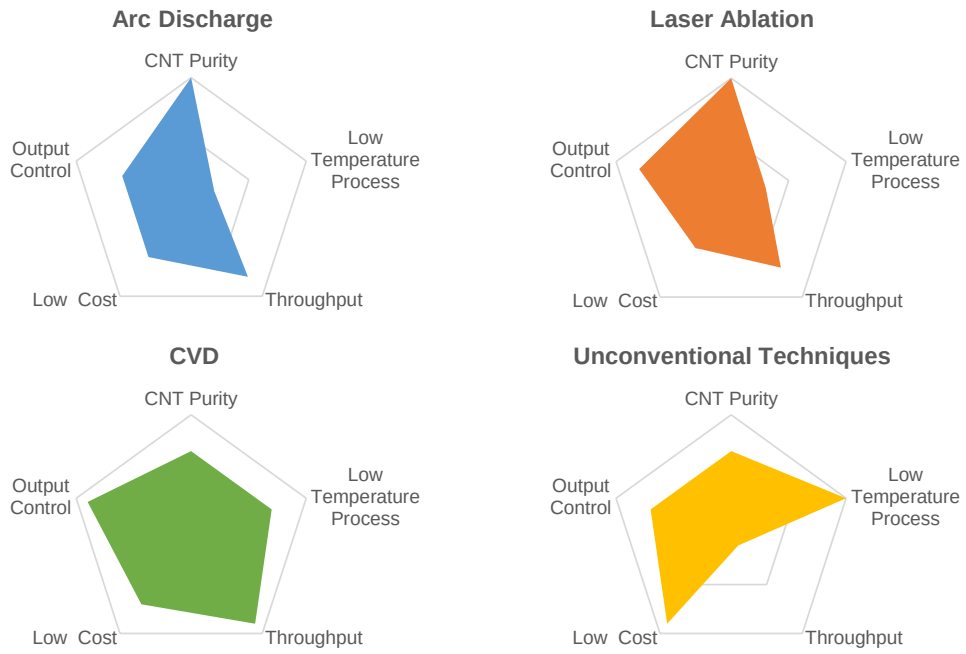

Figure 2.4: Radar charts showing a comparison between the common techniques for the synthesis of CNTs. The evaluation criteria are based on the discussion presented here in this section.

2.1.2 Synthesis of Carbon Nanotubes

CNTs can be constructed in two basic forms, the already discussed single-walled carbon nanotubes (SWCNTs) and the multi-walled carbon nanotubes (MWCNTs). MWCNTs, which are composed of several concentric tubes of graphene fitted one inside the other, are not considered in this work. There are three principal techniques to produce high quality SWCNTs: laser ablation [18], electric arc discharge [19, 20] and Chemical Vapor Deposition (CVD) [21, 22]. In the last few years other less conventional techniques, like the liquid pyrolysis and the bottom-up organic approach, have been developed in the field of CNT synthesis [23]. A summary of the currently used methods for CNTs synthesis is presented in Figure 2.4.

The arc discharge belongs to the high-temperature techniques (above 1700 °C), which usually causes the growth of CNTs with fewer structural defects in comparisons with other techniques. From the pioneering work of Iijima and Ichihashi in 1993 [24], this method has been constantly improved over the years and can now guarantee the synthesis of CNTs with a purity higher then 90% [25, 26].

Another technique that requires high temperatures (above 1000 °C) is the laser

ablation. The quality of the CNTs is strongly dependent on many parameters, such as the laser properties, the structural and chemical composition of the target material, the chamber pressure, the gas composition, the substrate and the distance between the target and the substrate. Laser ablation, which was first demonstrated in 1995 [27], achieved great results in terms of quality and purity of the synthesized nanotubes. The mechanisms are similar to the ones of the arc discharge, with the difference that the source power is a laser (usually Nd:YAG or CO_2) hitting a graphite pellet containing the catalyst materials [28].

The last of the standard techniques is the CVD, which allows the production of large amounts of CNTs with a reasonable level of purity, therefore becoming the most important commercial approach for manufacturing carbon nanotubes. The catalytic chemical deposition is often thermal or plasma enhanced, but recently other techniques have been employed as well. The main advantage is that it does not require the very high temperature of the previous two methods. CVD is known as an irreversible deposition of a solid from a gas or a mixture of gases through a heterogeneous chemical reaction. The size, the shape and the alignment of the nanotubes can be controlled by carefully designing the patterning of the catalysts on the surface of the substrate [22].

Regardless the preparation method, the nanotubes are always produced with a certain amount of impurities. Most of the already mentioned techniques produce powders which contain only a small fraction of CNTs and also other carbonaceous particles such as nano-crystalline graphite, amorphous carbon and different metals that were introduced as catalysts during the process. These impurities must be removed from the final product, hence one of the most important challenges in CNTs synthesis is the development of an efficient purification methods [29], which nowadays are mostly based on acid treatments [30].

2.1.3 Comparison among CNT-based technologies

As already briefly mentioned, the unique structure of CNTs gives them impressive properties. Their high electron mobility makes them ideal candidates for electronic device applications (e.g. field-effect transistors) while their surface-to-volume ratio offers remarkable sensitivity for chemical and biological sensor applications. Furthermore, CNTs have demonstrated outstanding mechanical properties, with fracture strains up to 30% [31]. However, the fabrication of

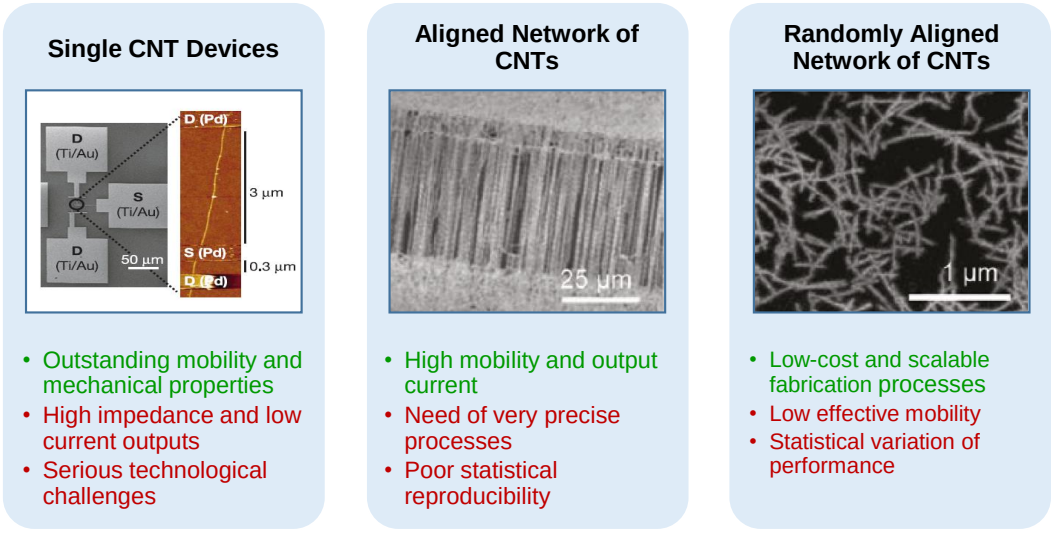

Figure 2.5: Comparison between different CNT-based technologies. Single CNT device: figure reproduced from [33]. Networks of aligned and randomly aligned CNTs: figure reproduced from [34].

devices based on single CNTs has to face some serious challenges [32]. First of all, the electrical heterogeneity of as-synthesized CNTs, which gives different electrical and mechanical properties depending on the structure and diameter of the nanotube. Second of all, the high impedence and low current outputs associated with a single nanotube device. Ultimately, the difficulty of assembling and integrating the single nanotube device into circuits. Until these obstacles are bypassed, single CNT devices will be purely a research subject, without real-world applications.

One mean to solve some of the aforementioned challenges is the use of effective thin films consisting of large numbers of CNTs. With such an approach, it is possible to minimize the effects of the statistical heterogeneity of the single CNTs, have large area active devices with high output currents and relax the requirements of precise spatial positioning of the individual nanotubes in the device.

The most attractive device in terms of performance would be a network of aligned nanotubes between the two electrodes. In a first approximation, such a device could be seen as the parallel of many single CNT devices; this device would conserve the high mobility of the single CNTs, and at the same time, increase the output current. However, an approach like this would also conserve one of the major drawbacks of CNTs technology, namely the need of a very

precise (and expensive) positioning and a poor statistical reproducibility.

In order to avoid the assembly problems associated with the fabrication of the two previously mentioned technologies, one could exploit the interface properties of the CNTs to build a new class of device. It has been shown that crossed nanotubes have a high inter-tube tunneling probability due to strong van der Waals interactions [35]. This distinctive feature can be used to form a new electronic material that is composed of an electrically interconnected network of CNTs [36]. In this way, the assembly problems are bypassed as well as the heterogeneity of the individual properties, which are averaged by the ensemble of the many nanotubes in the network [37]. These randomly-aligned networks have a low mobility in comparison to the other two technologies, but still higher than many other organic-based devices, making them suitable also for thin-film transistors applications. What makes expressly interesting these films, is the low-cost fabrication process, a key point that is discussed in detail in Section 2.2. Figure 2.5 summarizes the earlier mentioned technologies, comparing their strengths and major drawbacks.

2.2 Fabrication of CNT Thin Films

A straightforward method for the synthesis and fabrication of CNT thin films is represented by the chemical vapor deposition. During the CVD process, catalyst nanoparticles are employed as seeds for the growth of the nanotubes. This method has the capability of producing the films either randomly distributed or aligned. The latter case requires a fine control over the process parameters (e.g. directional gas flow) and some further expedients, like the use of patterned catalysts or through high electric fields [38, 39]. Although, the CVD process allows a better control on the positioning of the nanotubes and better inter-tube junctions, there are some major drawbacks. The most critical is that CVD is a high vacuum, high temperature process, thus incompatible with most of the new emerging fields of low-cost and flexible electronics.

A significant step towards the commercialization of novel CNT electronics has been done after the development of large-area and high-throughput processes for the fabrication of CNT films. The so-called, solution-based techniques have several advantages:

- **Compatible with low temperatures:** Deposition over plastic, flexible substrates, with temperatures lower than 100 °C.
- **Compatible with normal atmosphere environment:** No need of high-vacuum systems, which reduces costs significantly.
- **Compatible with roll-to-roll techniques:** High-speed depositions.

A successful strategy usually involves the usage of a wrapping surfactant, which enable the formation of solution with a reduced number of CNT-bundles; the fabrication process is terminated once all these surfactants are removed by the solution, through, for example, the evaporation of the solvents [40, 41]. Since in this work the experimental samples used for the validation of the simulations have been fabricated with spray-coating deposition, it is necessary to introduce some of the key aspects of this particular technology.

2.2.1 Spray Coating Deposition

Among all the different fabrication techniques available, spray coating deposition is considered to be one of the most competitive in terms of cost-performance ratio. It offers the means for depositing CNT films with high uniformity and low roughness over large areas in a high-throughput (inline) process. The successful adoption of this technique to CNT film fabrication for various applications has been previously reported in literature [42, 43].

The spray coating deposition is part of a broad family of techniques in which a certain material is uniformly deposited over a target surface. Each application area requires different spray nozzles to fulfill the specified criteria for the coating thickness and roughness. Currently, in the field of flexible electronic, two are the types of nozzle which guarantee highly uniform films: the air atomizing nozzle [44, 45] and the ultrasonic spray nozzle [46].

The parameters to be adjusted for obtaining the desired spray characteristics are the material flow rate, the atomizing gas (N_2) pressure, nozzle-to-sample distance and substrate temperature. Figure 2.6 shows a schematic drawing of the test setup, indicating the vertical arrangement of nozzle and substrate.

In order to disperse CNTs in an aqueous solution, which can be subsequently sprayed, a certain dispersant is needed. One of the most widely used in the literature, is the sodium carboxymethyl cellulose (CMC), a high molecular weight

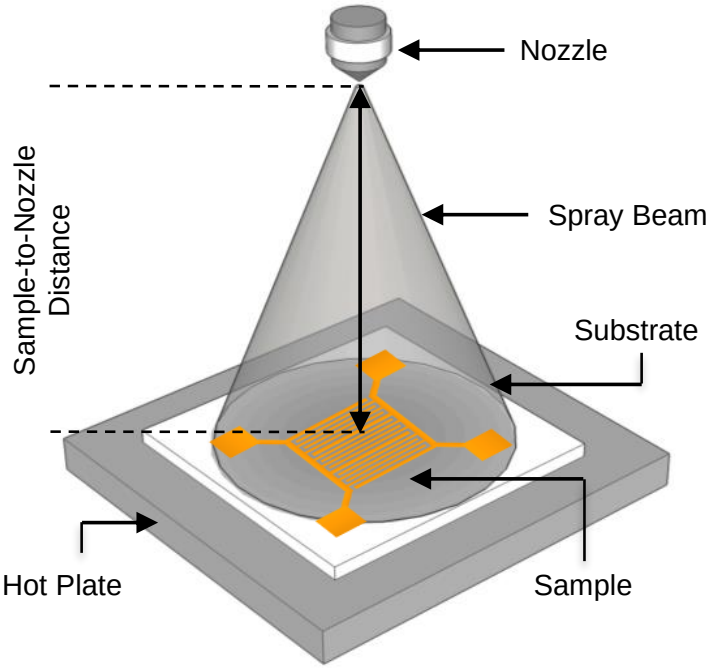

Figure 2.6: A schematic drawing of a spray-coating setup indicating the most important spray parameters.

cellulose derivative [47]. The primary reason is to prevent the nanotubes to aggregate in bundles. During the first step of the solution preparation, a certain amount of CMC, typically around 0.5wt%, is added to DI water; the resulting solution must be then stirred to uniformly dissolve the surfactanct in water. In a second step, the CNTs are added into the solution. Typical concentrations vary between 0.03wt% and 0.05wt% [48]. The solution with completely dispersed CNTs is achieved after a sonication and a consecutive centrifuge (few hours at a speed typically around 15000 rpm). The final solution that will be sprayed, is finally obtained by decanting the top part of the supernatant, to avoid the presence of some residuals.

Prior to the film deposition, it is necessary to apply a surface treatment to the substrate, to increase the wettability of the surface and to obtain a uniform surface coating during the spray deposition. As an example, has been reported that a plasma treatment greatly improve the uniformity films spray coated over glass surfaces [45]. Furthermore, a chemical post-deposition treatment is necessary to remove the CMC-matrix embedding the nanotubes. If this step is neglected, the film would contain a huge amount of CMC particles with a completely insulating behavior. The sample are thus left overnight in diluted HNO_3 (13-23%)

and finally rinsed in DI water. It is worth to mention, that every step of the process is done in ambient condition.

Before moving forward, it is important to clarify some aspects of the fabrication process, and how some of the required steps affect the resulting network. In particular, two steps have a strong impact on the outcome from the stochastic point of view. The first one is the sonication, combined with the centrifuge. During this procedure, the original nanotubes provided by the supplier, are fragmented in smaller nanotubes with a length that follows a certain statistical distribution [49]. The second one, regards the removal of the CMC particles via HNO_3 bath. Indeed, it has been demonstrated that the HNO_3 alters considerably the electronic properties of the nanotubes, with a sort of doping effect (p-type) [50, 51]. Furthermore, since everything is processed under normal ambient condition, also the oxygen content in the air (as well as minor interaction with the substrate) has an effect on the electrical behavior of the nanotubes [52, 53]. This combination of geometrical and electrical variations in the nanotubes properties, leads to some statistical variations on the properties of the network itself, which must be taken into account during the design of a certain device, as it will be explained into details in Section 4.2.

2.3 Properties of Carbon Nanotube Thin Films

In the recent years, the electric arc discharge technique (EA) demonstrated to be one of the best candidate for the large-scale production of highly-pure single walled nanotubes [20]. However, the currently available techniques for the synthesis of nanotube powders cannot guarantee a precise control over the chiralities and, at the same time, over the diameters [54]. As a direct consequence, a nanotube powder for solution-based techniques contains a mixture of metallic and semiconducting CNTs. In the so-called as-prepared solution, where there is no sorting of the different species of nanotubes, statistically, 1/3 of the total number of nanotubes will be metallic, while the remaining 2/3 will be semiconducting. The reason behind can be found in the already introduced Equation (2.7), which establishes the condition of metallicity, based on the indexes of the chiral vector

The main point here, is that the nanotubes in a CNT film have different electronic properties due to the different chiralities. The analysis of the transport in the network, is thus not trivial; the transport along metallic and semicon-

ducting nanotubes is dramatically different. For example, semiconducting CNTs show a modulation of their transport upon an appropriate gate voltage, whereas metallic CNTs are pretty insensitive to the modulation (at least for small biases). Semiconducting CNTs show also a stronger temperature dependence in the conductivity. An even more interesting aspect is related to the inter-tube junctions between nanotubes of different species. While, with a good approximation, nanotubes of the same species show an ohmic contacting between them, semiconducting-metallic junctions show a Schottky behavior [55, 35, 56]. This particular phenomenon will be discussed in more details in Section 3.6.

However, many efforts have been made in the attempt of sorting the different species of nanotubes. A technique worthy of be mentioned is certainly the destruction of metallic CNTs via Xenon-lamp irradiation [57]. With this approach, it has been demonstrated the possibility to increase the percentage of semiconducting nanotubes up to the 95% of the overall amount of CNTs.

In addition to some interesting electrical properties, CNT films have shown a superior mechanical flexibility. Their unique structure is responsible of a peculiar insensitivity to strain and bending stresses. The strong binding energy with the substrate allows the realization of devices over flexible substrates which are capable to maintain their electrical properties up to large strains and small bending radii [11].

2.4 Applications

Random carbon nanotube (CNT) networks have raised a continuously increasing interest among a broad and multidisciplinary community of researchers throughout the last decade. The remarkable and concurrently diverse properties of such networks have rendered them suitable for a wide range of applications in science and engineering. Among the most promising applications are transparent conductive electrodes [58, 59], thin-film transistors and circuits [60, 61], mechanical and chemical sensors [62, 63, 64]. The desired functionality of the CNT films produced for different applications depends primarily on the choice of the appropriate raw material. Nevertheless, it is strongly influenced by major process specific aspects.

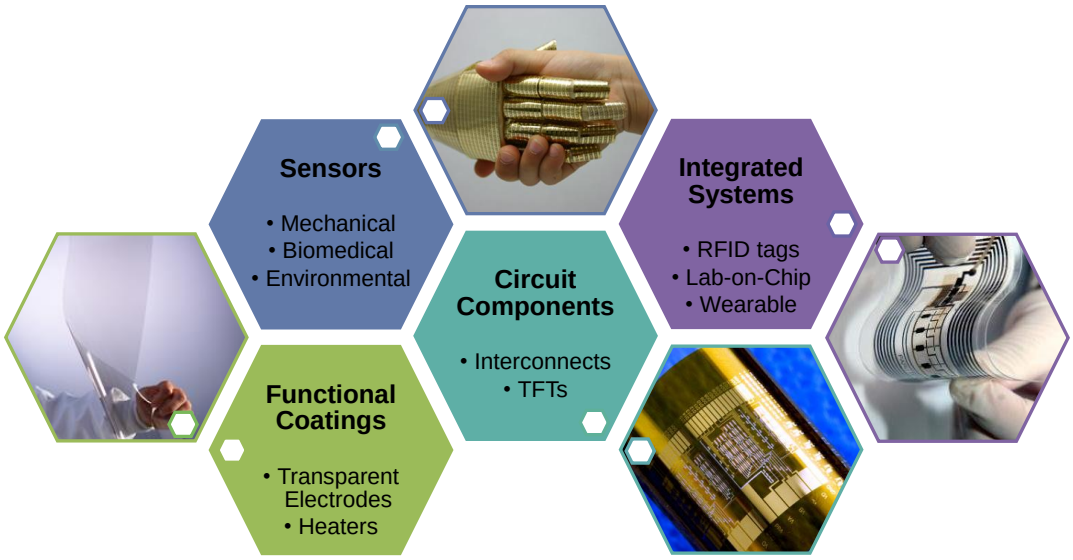

Figure 2.7: Summary of the main applications in which CNT films have been investigated as active material.

2.4.1 Transparent Electrodes

Indium-Thin-Oxide (ITO) is still the prevailing Transparent Conductive Electrode (TCE) material leading to an annual worldwide indium consumption of 1.5 ktons that is mostly used for flat-panel displays and has led to a huge price increase of indium from 94 $kg^{-}1$ in 2002 up to 745 $kg^{-}1$ in 2015 [65]. Beside the increased indium price and its accompanied increasing scarcity, ITO faces a number of additional drawbacks such as:

- Requirement for expensive vacuum and sputtering technology at substrate temperatures as high as 400 °C prohibiting the use of most polymer substrates [66].
- Strong optical absorption in the near-infrared window [67].
- Low flexibility [68, 69].

These drawbacks have pushed the research on alternative materials, such as CNTs, and silver nanowires (AgNWs) [70]. In particular, CNT thin films offer remarkable electrical, mechanical and optical properties in a cost-efficient way [71, 72].

Although the idea behind the exploitation of CNT films as conductive materials is rather simple, the overall properties of the film depend on many parameters,

Table 2.1: Guidelines for an optimum design of a conductive film.

Parameter	Optimum Design
Tube length	Long tubes, to reduce the number of inter-tube junctions and as a consequence the resistivity of the film.
Tube diameter	Relatively large diameters, to minimize the band-gap of the nanotubes.
Tube density	Trade-off between resistivity (high-density films) and transparency (low-density films).
Deposition method	Solution-based techniques, to have large-area, low-cost and uniform films.
Content of impurities	Low content, to reduce the resistivity and increase the transparency.
Chirality	Metallic nanotubes, to increase the conductivity.
Doping level	High concentration of dopants, to increase the conductivity of the semiconducting nanotubes.

such as the average tube length, the tube diameter, the density of the nanotubes per unit of area, the deposition method, the content of impurities, the ratio between metallic and semiconducting CNTs and the level of doping induced by the ambient conditions [73, 74]. The parameters that leads to an optimum design of a conductive film are summarized in Table 2.1

These films have shown very promising results, almost comparable with the ITO standards. Films made by unsorted CNTs have reached sheet resistances lower than 100 Ω sq^{-}1 and transmittance greater than 70% over the entire visible range [75, 76]. Moreover, films with an higher content of m-CNTs, which have been collected through ultra-centrifugation, have shown sheet resistance as much as 10 times smaller than the unsorted CNT films [77].

2.4.2 Sensors

In the last few years, a tremendous interest has grown toward sensing devices based on nanoscale materials. The major advantage in using these materials, is their high sensitivity to environmental changes due to their huge surface area. Another interesting aspect is the low dimensionality of the materials. For example, a carbon nanotube has a typical diameter in the nm range, which is similar to the DNA diameter and one order of magnitude smaller than a protein. It has been shown that the particular dimensions of the nanotubes guarantee an high

sensitivity toward these objects [71]. Although sensors based on single CNTs have the potential of an extremely high sensitivity, the difficult reproducibility and manufacturability renders the technology too far to be exploited in commercial applications. On the contrary, the great advantage of CNT films is that the network averages out the variations in the properties of the individual CNTs, making the devices more robust respect to manufacturing process variations.

The device structure for sensing applications can be either a simple two-terminal device or a three-terminal transistor. In the former case, the sensing is monitored by checking the resistance variation (or sometimes the capacity variation) between the two electrodes; in the latter case the sensing is often checked by measuring the variations in the threshold voltage of the transistor. The CNT film can be used as a bare material or it can be functionalized with some chemical groups, a solution often adopted in biological applications [78, 79]. Applications of CNT network-based TFTs in the detection of proteins [80] and glucose [81] have been successfully demonstrated. Furthermore, CNT films have shown a great sensitivity towards pH variations in solutions [82] and selective sensing towards different ions [83, 84].

The electronic properties of the CNTs, which are basically based on the arrangement of surface atoms, are very sensitive to adsorbents [85, 86]. Out of this reason, CNT films can be used as sensing devices for various molecules of interest, like CO, CO_2, NH_3, and ethanol. Furthermore, the presence of a significant amount of semiconducting nanotubes can be exploited in the realization of temperature sensors [87, 88].

In this work, the sensing properties of the CNT films are studied through these last two typologies of sensing devices, namely the temperature and gas sensors. The main mechanisms behind the operating principles of such devices will be discussed into details in Chapter 5.

2.4.3 Thin Film Transistors

CNT networks have been extensively explored as semiconducting material for thin film field effect transistors. One of the main reason is the intrinsically high mobility of the single nanotubes in the network that guarantees an overall interesting mobility of the entire film, a primary requirement for high-speed electronics. While the most common organic semiconductors seem to have reached a

technological maturity in terms of performance, field-effect transistors based on CNT films have shown still a positive trend in the increase of performance [89]. Several groups have presented also hybrid solutions, with a mixture of organic materials and dispersed CNTs. These FETs have shown a very high on/off ratio, mainly due to the organic materials, and a surprisingly high mobility, reached with the aid of the nanotubes in the film [90]. The key parameters in the description of a thin film TFT are especially the mobility, the on/off ratio, the sub-threshold swing and the high frequency response. It is important to notice that in the current state of the art, these FETs show a significant hysteresis in their I-V characteristics.

This technology has inherited a lot of know-how from the organic thin film FETs, especially regarding the architecture of the device. The choice of the most suitable architecture is often related to the material used for the fabrication of the device. A standard bottom-gate architecture is used when the film is deposited over a SiO_2 layer which separates the film itself from a gate contact (i.e. either a heavily doped silicon layer or a metal). In other applications, an electrolyte gated transistor can be used in top-gate configuration [91, 92]. Regardless the architecture, a fine design is needed to guarantee acceptable performance. Many parameters have a huge effect on the transistor behavior, like the oxide material, the oxide thickness and the materials used for the contacts. Concerning the active part of the device, one must be particularly careful to the density of the nanotubes and the type of solution. Has it has been already mentioned, the CNT solution contains a certain amount of metallic nanotubes, which are pretty insensitive to the gate voltage. When the content of these metallic nanotubes is higher than a certain threshold, the current in the off-state is not negligible anymore. In the literature a huge span of on/off ratios has been reported, ranging from 1 to 10^5.

More details, together with a comparative theoretical-experimental analysis on the transistors behavior, will be given in Chapter 6.

2.5 Simulation of CNT Networks

Since the late 1960s, the evolution of technology computer-aided design (TCAD) has been strictly connected to the advances in devices fabrication. The possibility of predicting in a reliable way the behavior of a device, is one of the

main factor that led to the mass production of device components and electronic circuits, and the reason why the TCAD products are part of a profitable market. The Electronic Design Automation Consortium (EDAC), an international association of companies developing EDA tools and services, has reported a constantly increasing yearly revenue in the time lapse from 1996 and 2015 [93]. The helpfulness of TCAD products has been exploited in a wide range of applications, ranging from process simulations to circuit level simulations, and not only in the industrial world. As a matter of fact, in the field of academic research, the usage of simulations has widely spread with the goal of studying and developing new technologies that can replace more traditional devices (i.e. conventional semiconductors-based devices). It is exactly in this context, that researchers have been studied the theory of more exotic technologies, like, to cite an example, organic electronics.

TCAD design has found a breeding ground also in carbon-based materials, especially in the study of CNTs and graphene. While for single CNT-based devices there have been already several simulation studies, not so much has been done regarding the CNT networks. In Section 2.3, while highlighting the the major properties of CNT films, some problems concerning the design of the devices emerged. The aim of this project is indeed to develop a simulation tool that could help in the design of CNT films devices, and reducing the gap with the know-how of other competing technologies.

As already showed in Section 2.1.3, CNT-based technologies can be very dissimilar from each other. It is intuitive to imagine that devices with huge differences in fabrication processes and performance, require different approaches for the modeling and simulation. An explanatory example, relative to this particular work, is the difference between the approaches that can be used for the simulation of devices based on single CNT and the one suitable for the simulation of CNT networks. Neglecting process simulations, which constitute a separate case, the TCAD design can be divided in several families, depending on the level of approximation of the problem. In Figure 2.8 a schematic representation of the various levels of simulations is depicted. Each simulation level is restricted to a particular time and length frame, where the reliability of the results is guaranteed in a reasonable simulation time. Simulations on the bottom of the scales are more detailed, and at the same time more computational demanding; their usefulness is thus restricted to small structures where the interesting physical

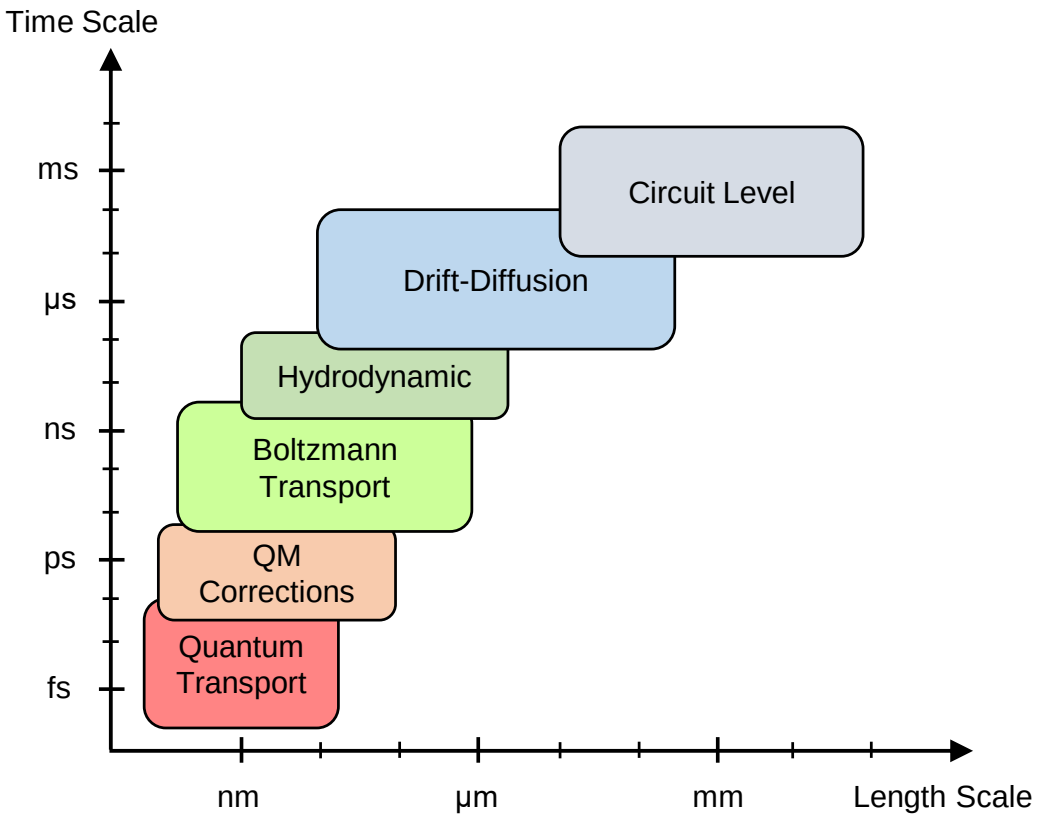

Figure 2.8: Classification of the different simulation methodologies according to the time and length scale of interest. From the bottom to the top, the simulation suitability goes from the physics world to the engineering one.

phenomena occurs in a small time frame. On the other hand, simulations on top of the scales are less detailed, and can treat easily bigger structures (e.g. entire circuits).

It is then of a fundamental importance to find the right trade-off between simulation complexity and computational demands. In other words, the device under exam must be collocated somewhere in the graph of Figure 2.8. For single CNT devices, the problem of finding the appropriate time and length scale is not very complicate, since the device is mostly composed by an entity with well defined dimensions.[1] On the other hand, CNT networks are macroscopic objects composed by the integration of a huge number of microscopic objects. In this case, some precautions must be taken in pursuit the right trade-off. To better give an idea of the complexity of the problem, one has to consider the size of a nanotube respect to the whole film. A nanotube can be thought as a

[1] While the definition of the time and length scale is quite straightforward, what is less trivial is the choice of a proper simulation method.

cylinder with a diameter of few nm (in same cases even less) and a length that can vary from hundreds of nm, to several μm; on the other hand, the film can even reach few cm^2 of area. The choice of the trade-off is basically focused on how to represent the single nanotubes in the network. The easier the model, the greater the number of nanotubes that can be treated. As an example, it would be practically impossible to simulate an entire film with an approach based on a Finite Element Method (FEM). The problem in this case lies in the tricky aspect-ratio of the nanotubes (that can be in the order of $10^3 - 10^4$) which makes the generation of a proper mesh computationally too expensive.

In the next few sections, a review on the state-of-the-art for the simulation of CNT networks will be given, with special emphasis on the strengths and weaknesses of the different models. In particular, this review will introduce the percolation theory and the most common percolative models treated in the literature. The chapter will be then concluded with the model proposed in this work, which is intended to overcome some of the flaws of the state-of-the-art models.

2.5.1 Percolation Theory

The electrical conductivity behavior of a CNT network has been commonly described by the semi-empirical *percolation theory* [94]. According to the theory, the conductivity of a random network is highly non-linear and it has a strong dependence on the density of the nanotubes. When the density of the nanotubes is lower than the so-called percolation threshold, the film has an insulating behavior, since there are no direct paths between the two electrodes. On the other hand, if the percolation threshold has been reached, current can flow between the two contacts, and a certain conductivity can be measured. Figure 2.9 shows schematically the two different behaviors of a network, depending on whether or not the percolation threshold has been reached.

The value of the conductivity abruptly increases after the percolation threshold, and can be semi-empirically described by the power law

$$\sigma = \sigma_0 (v - v_c)^t \tag{2.8}$$

where σ is the electrical conductivity, σ_0 a scaling factor, v the volume fraction

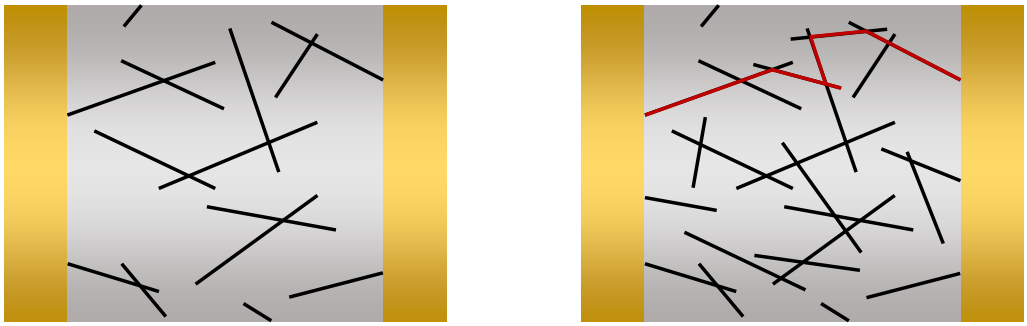

Figure 2.9: Illustration of the percolative conduction mechanism. (Left) A network of nanotubes with a density below the percolation threshold. (Right) A network with a density greater than the percolation threshold. In red, the percolation path is highlighted.

of the material, v_c the percolation threshold and t an empirical exponent which depends on the dimensionality of the system. However, Equation 2.8 tries to simplify a rather complex problem with the use of highly arbitrary empirical parameters. It is worth to mention that although some theoretical studies have been made for the estimation of the percolation threshold values [95, 96], not so much has been done regarding the other parameters that complete the equation. The biggest problem of Equation 2.8 is a lack of generality, due especially to the impossibility to estimate the value of σ_0 a priori. This parameter depends greatly on the conductivity of the single objects in the network and on the way these objects are coupled among them. In a sense, this formalism could give reliable results in the unlikely case where all the objects (and all the coupling mechanisms) have the same conductivity.

A similar problem arises with the prediction of the parameter v_c, which is reliable in the special case where all the objects have the same geometrical properties. Due to statistical fluctuations, this formalism could produce reasonable results also when the objects have some small variations in their dimensions. However, this is not the case in CNT networks, where the length of the nanotubes is characterized by a relative broad distribution function.

Finally, the evaluation of the exponent t has a substantial dependency on the number of dimension of the system. The accepted values vary between 1 and 1.3 for a 2D system and between 1.5 and 2 for a 3D system [97, 98]. The parameters of the percolation theory formalism and their dependencies are summarized in Table 2.2.

Table 2.2: Parameters and their dependencies in the percolation theory formalism.

Parameter	Dependencies
σ_0	Conductivity of the single objects Conductivity of the connections between the objects.
v_c	Density of objects in the volume Arrangement of the objects Statistical distribution of the objects geometrical properties Dimensions of the device.
t	Dimensionality of the system.

2.5.2 Percolative Modeling and its Challenges

The classical percolation theory outlined in the previous section only addresses homogeneous and infinite networks. For some applications, especially in transistors, the electronic heterogeneity of the CNTs, their anisotropic alignment, and the finite extent of the film make it necessary to develop nonlinear, finite-size percolation models, for a predictive assessment of the electronic properties.

The first numerical analyses on CNT films were mainly focused on predicting the conductance of the networks as function of the tube densities and channel lengths [99]. The models proposed in the literature were based on the semi-classical transport theory, by coupling the Poisson equation with a drift-diffusion model, under the assumption that the channel of the device was much longer than the mean-free path [100, 101]. However, due the advances in the fabrication of short-channel devices, these assumptions over the diffusive nature of the electronic transport may fail [36]. Moreover, even with long channel lengths, there is no evidence of how the transport happens locally in the single nanotubes. Other groups have adopted a semi-empirical approach to describe the local transport in the nanotubes, obtaining results in good agreement with the experiments [102, 103, 104, 105, 106]. Nevertheless, these models suffer of a lack of generality, and have a strict dependence on the fabrication process. Although they can be opportunely tuned and used as designing tools, their predictability cannot always be taken for granted.

The need of a more general framework, which can be used for several applications, is certainly one important aspect which should be addressed, but it is not the only one. In fact, all the works presented in the last decade are based on 2-D models for the representation of the CNT networks; the reasons why this

approximation could led to inaccurate results are given in Section 2.5.3. Indeed, the work here presented is intended to overcome some of the flaws regarding the modeling of randomly aligned network of CNTs. First of all, a full three-dimensional model for the generation of the network has been implemented, to better describe the percolative nature of the problem. Additionally, an appropriate formalism for the transport mechanisms has been introduced, together with an iterative algorithm that calculates self-consistently all the electrical quantities in every node of the network. In other words, the transport is described within a multi-scale approach, in which the macroscopic quantities of the entire network are derived from the evaluation of the microscopic quantities of the single elements constituting the network itself.

2.5.3 Three-Dimensional Modeling

As already introduced, one of the most important missing aspects, which affects all the presented works in the literature, is the lack of a three-dimensional model that could be able to capture the real morphology of these networks. The generation of a realistic morphology is a crucial problem. Since the transport is imposed by the percolation paths, it is mandatory to represent the network in a three-dimensional space. A two-dimensional model, would indeed overestimate the number of percolation paths, by including many fictitious junctions (i.e. all the projections on the substrate plane) in the network. The network in a two-dimensional space is much more connected, and this leads to a current flow that can be very different respect to the real behavior. On the other hand, in a 3-D model, the number of the junctions between different CNTs is much closer to the reality, and the current flow distribution in the network is more reliable as well.

Figure 3.5 shows a schematic representation of two identical network represented with a 2-D and a 3-D model. As it stands out, even if the number of CNTs is very low, with a 2-D model the number of junctions is overestimated. In the simple case shown in Figure 3.5, the network in a 3-D space has 8 junctions between the nanotubes; a 2-D model, instead, will count a total of 10 junctions, by considering the real junctions plus two fictitious connections that result from the projection of the network into the 2-D plane. This artifact has a dramatic effect on the reliability of the simulation, especially for dense films. The first effect is that in a 2-D model the network is more connected, since more percolation

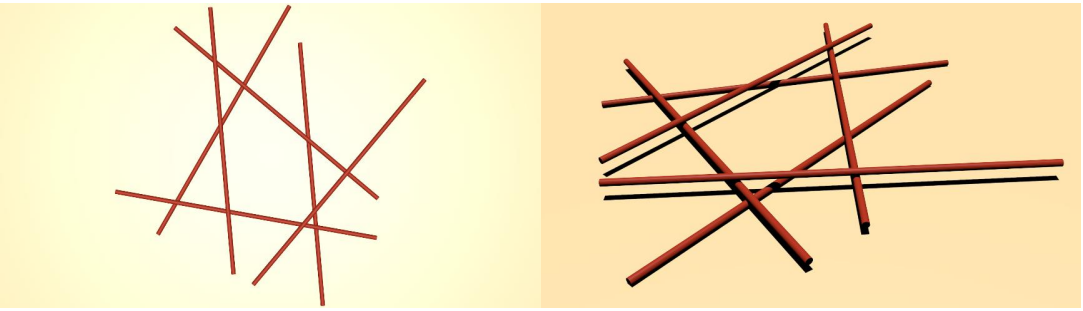

Figure 2.10: Schematic comparison between a 2-D (left) and a 3-D (right) rigid-stick model; with the 2-D model the number of the actual junctions is overestimated by counting all the projections on the plane. In this particular example the 2-D model considers 10 junctions, whereas the 3-D model only 8.

paths are introduced. Furthermore, since the junctions actually represent one of the major contributions to the resistance of the film [35], it is clear how a 2-D model fails in capturing the real electrical behavior of the network.

Further quantitative details will be given in Section 3.2.3, together with a comparative study on the differences between 2-D and 3-D models.

2.5.4 Towards a Multi-Scale Approach

Multi-scale modeling is essential when dealing with problems which have important features at multiple scales of time and/or space. A detailed treatment of carbon nanotube requires an atomistic description of the nanotube along with a quantum mechanical treatment of electron transport, both ballistic and with the effects of dissipative scattering included. Even for simple systems (e.g. a single nanotube), multi-scale methods are unavoidable. Metal/nanotube contacts, nanotube/dielectric interfaces, and defects require a rigorous, ab-initio treatment, whereas to treat an entire device, simpler descriptions must be used.

For this reason, the approach here proposed, tends to go in the direction of a multi-scale modeling system, where different levels of the simulation are treated with different degrees of approximation. The idea, which is schematically represented in Figure 2.11, is to divide the whole problem into three different hierarchical sub-problems. Starting from the bottom, a semi-empirical atomistic model based on the Non-Equilibrium Green's Function (NEGF) Formalism is used to calculate the electronic transport in the coherent regime for a small section of a single nanotube. The results of this first step are then coupled with

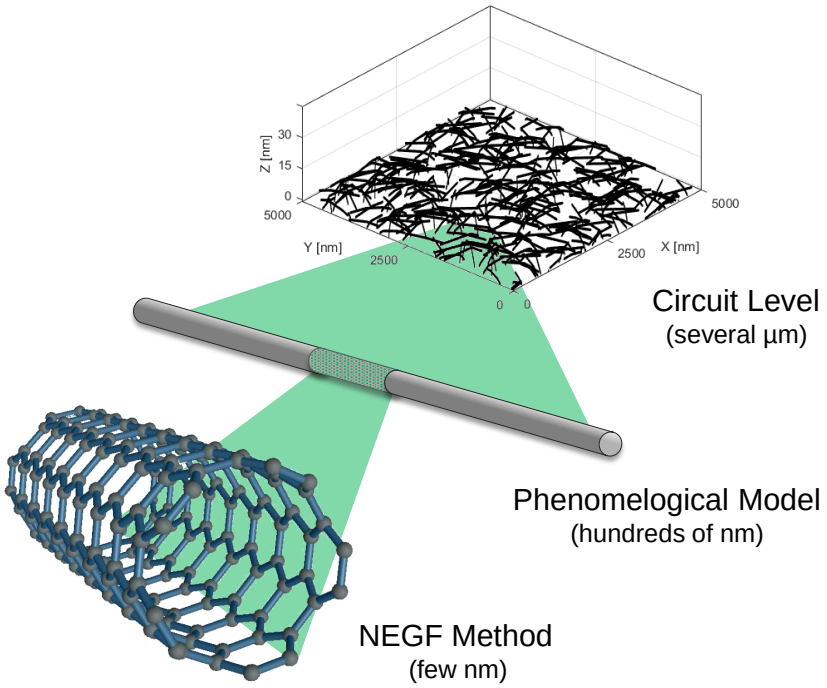

Figure 2.11: Illustration of the multi-scale approach implemented in this work. From the bottom to the top, the complexity of the simulation is gradually reduced. Results extracted from a simulation level are then given as input the the next one.

a phenomenological model that treats the scattering phenomena, which once again, occurs in a single nanotube. Finally, the outcomes of this second step are given to a circuit-level model, which simulates the behavior of the entire network. The theory and the implementation of the different modeling levels, is the core subject of the next chapter.

Chapter 3

Modeling of CNT Networks

This chapter, which may be considered the core part of this project, gives a comprehensive description of the implemented simulation tool, as well as of the theoretical models on which the simulations are based. The purpose of the program is to numerically simulate the electrical behavior of randomly aligned network of carbon nanotubes. The electrical quantities, such as the current that flows through a nanotube or the potentials in every node of the network, are computed based on a set of physical equations that describe the conduction mechanisms. As briefly mentioned already in the conclusive part of the previous chapter, the simulations are based on a multi-scale approach in which the results from hybrid atomistic-phenomenological models are coupled with a high-level circuit simulation. In order to fully understand the electrical behavior of the networks, it is important to grasp the theory behind the numerical models, and explore their validity and limitations. Therefore, a significant part of the chapter is dedicated to the theoretical bases and the explanation of all the employed approximations.

Furthermore, in addition to the theoretical background, the working principle of the software will be thoroughly examined. The code, which is entirely written in MATLAB language, can be run on a normal desktop PC or high to mid-range laptops. The simulation time is strictly dependent on the number of generated nanotube, and can vary from few minutes to several hours according to the complexity of the network. During the simulation process, the program will call several time the freeware software LTspice IV [107], which solves the electrical problem in background. Although the user has not interaction with the SPICE software, the properties of the electrical solver can be adjusted via GUI at the beginning of the simulation.

3.1 Overview on the Simulation Tool

The program is divided into three main blocks, plus a visualization tool. The tool flow is schematically depicted in Figure 3.1. At the beginning the program creates the structure of the device to be simulated and stores the information related to the geometry in an external file. Before the actual simulation starts, there is an intermediate step where the software pre-computes the IV characteristic of all the species of nanotubes (i.e. all the introduced chiralities) and store them into another external file. This step is the most time-consuming process during the whole simulation, and must be repeated every time something changes in the electrical properties of the nanotubes. This can happen, for instance, during a temperature, gas or gate voltage sweep. The reasons behind the pre-computation, as well as the theory behind it, are discussed in details in Section 3.3.1.

The third and last block is the core of the program, which reads all the input files given by the two previous blocks, solves the network and gives the results to the visualization tool. This is done through several steps, where the program converts the set of nanotubes in a suitable netlist that can be read by LTspice. After the electrical simulation has been successfully performed, the program must interpret the results from LTspice and convert them back for the analysis of the network. The solution of the problem is obtained self-consistently through consecutive iterations, as it will be further explain in Section 3.8. The software calls each time the SPICE solver, reads the outputs and processes them, until some convergence criteria are fulfilled.

3.2 Network Generation

In a typical simulation workflow, the first task is the structural representation of the device under investigation. Depending on the problem, different approaches can be used for the discretization of the geometry. In this work, the so-called stick-percolation theory [94] has been extended by including the 3D structure of the nanotubes.

The network generator is based on a stochastic algorithm that can generate non-rigid solid objects in a three-dimensional space, emulating with high fidelity the typical fabrication processes involved. Although the code can be adapted to

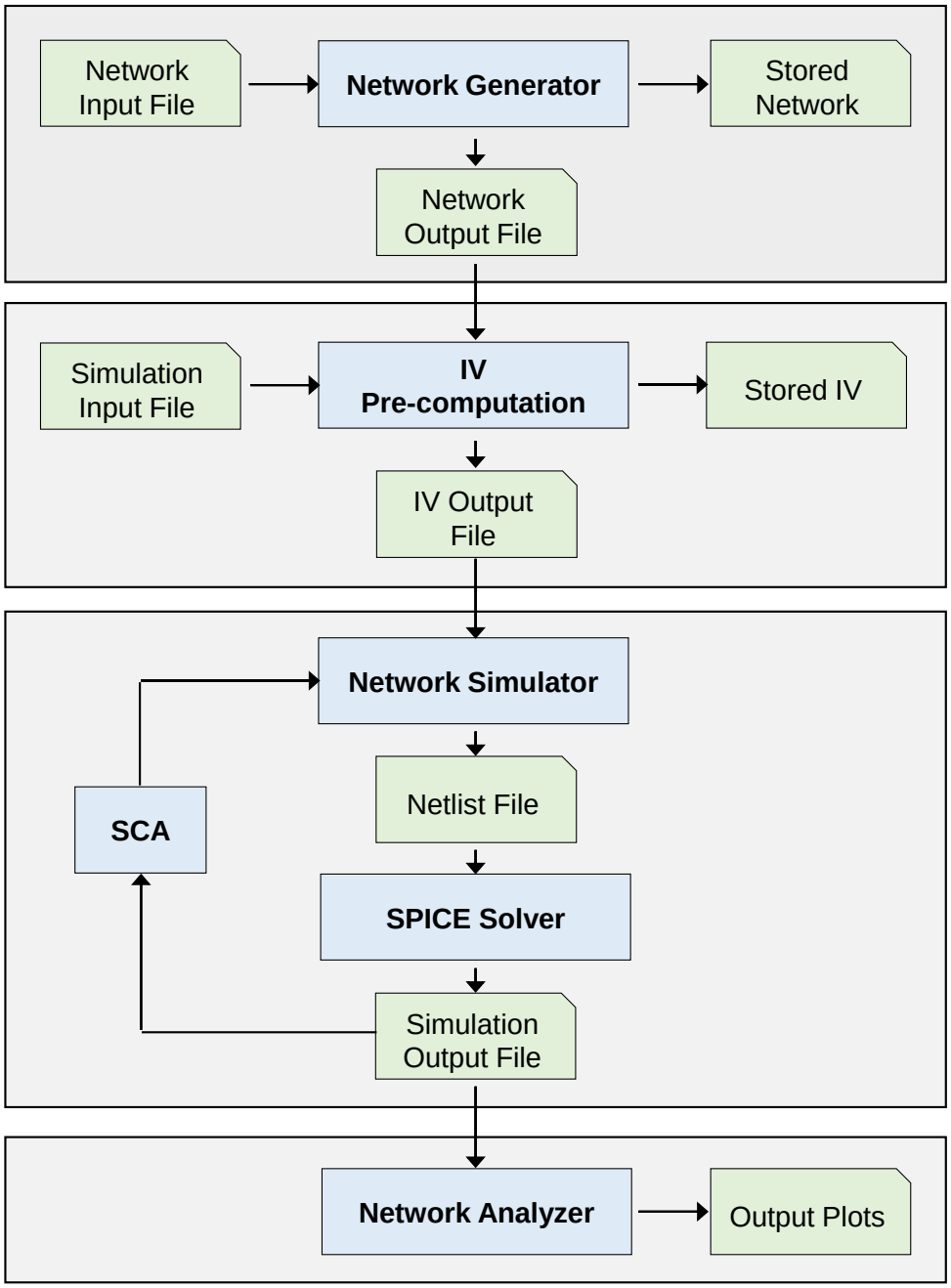

Figure 3.1: Schematic working principle of the proposed program. In evidence the main blocks: the network generator, the IV pre-computer, the network simulator and the network analyzer.

different processes, this work has been done in analogy with the spray coating technique. The geometrical properties of the nanotubes (i.e. length and radius), as well as the density of nanotubes of the film, are extracted according to some probability distributions inferred from experimental measurements.

During this step the program stores all the information of the network in an external file, which can be used afterwards as an input for the simulator. This file contains the three coordinates of every node, the information on the connections between the nodes and the class of the object. An object can be either a nanotube (two connected nodes that share the same physical properties) or a junction between two nanotubes (two connected nodes with no constraints on the physical properties). The class of the object contains the information on the properties of the object, which are dependent on the chiral vector. A nanotube is specified by a single chiral vector, whereas a junction has the two chiral vectors of the two connected nanotubes. The generation of the network can be divided into two consecutive operations, namely the extraction and the placement of the nanotubes.

3.2.1 Extraction of the Device Properties

The first step in the generation of the randomly aligned network is the extraction of the device properties. In analogy with the experimental setup, the user can specify the dimensions of the device, the properties of the solution and the parameters of the deposition. The geometry of the device can only be rectangular or square-shaped and defines the area where the nanotubes are allowed to be deposited during the placement procedure.

Regarding the solution, the user can set the length distribution of the nanotubes and the physical properties of the nanotubes, through the chiral vector distribution. There are several possibilities to set the length distribution for the nanotubes, which can also be given manually by the user. The most reliable way, however, is to analyze the length distribution extracted from AFM images of real samples, calculate the probability density function and then give it as input to the simulation software. Figure 3.2 shows an example of the length distribution for one of the networks under analysis.

After the lengths have been extracted, the next step is the extraction of the radii of the nanotubes. This is a delicate problem since, as already discussed

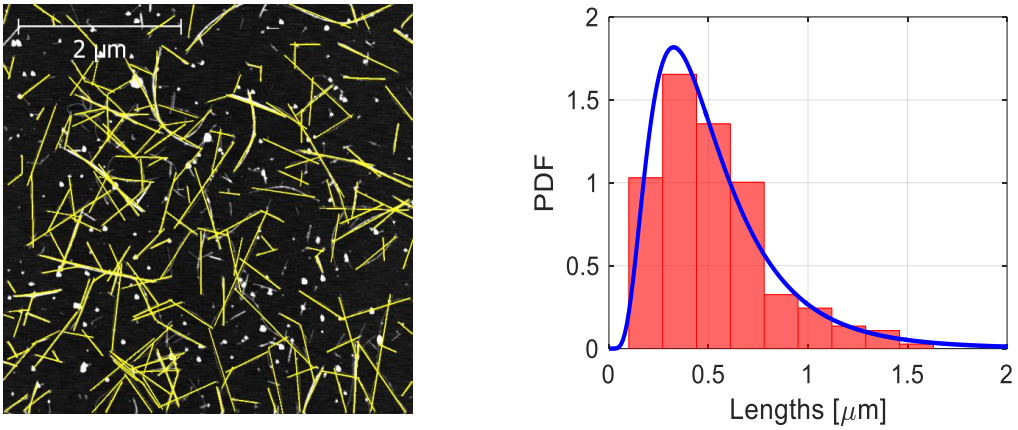

Figure 3.2: (Left) Extraction of the nanotubes lengths from the AFM image of a sample under investigation. (Right) Corresponding estimated probability density function (PDF) for the nanotubes length distribution. The area of each bar is the relative number of observations. The sum of the bar areas is 1. The blue curve represents the fitting of the distribution and the input for the network generator.

in Section 2.1.1, the radius of a nanotube is strictly related to its chiral vector according to (2.4). What must be taken into account, is that generating several radii means introducing many chiral vectors in the network. As already mentioned, the program will afterwards pre-compute the IV characteristics for all the species in the network. This process is very slow, and the time needed is linearly dependent on the number of different chiralities. A reasonable approach is to analyze the nanotubes in the network (e.g. through AFM pictures) and include few chiralities compatible with the observed radii. The outcome of the optical observations is a very narrow distribution of radii, centered around 0.6 nm, which reduces drastically the number of possible chiralities. This findings are in good agreement with what declared by the solution supplier. Furthermore, the variation of the nanotubes conductivity due to different diameter is expected to be smaller than the one connected to the length distribution.

Another crucial point is to consider the right ratio of semiconducting to metallic nanotubes; this information is usually provided by the solution suppliers. In this work mainly two types of solution have been studied, with a semiconducting nanotubes concentration of 66% (as-prepared solution), and one of 90% (semiconducting solution). Considering all these assumptions, reasonable results can be achieved with two different chiralities (one for semiconducting nanotubes and one for the metallic ones), which are extracted together with the lengths.

The last important part in the extraction of the device properties is to set the

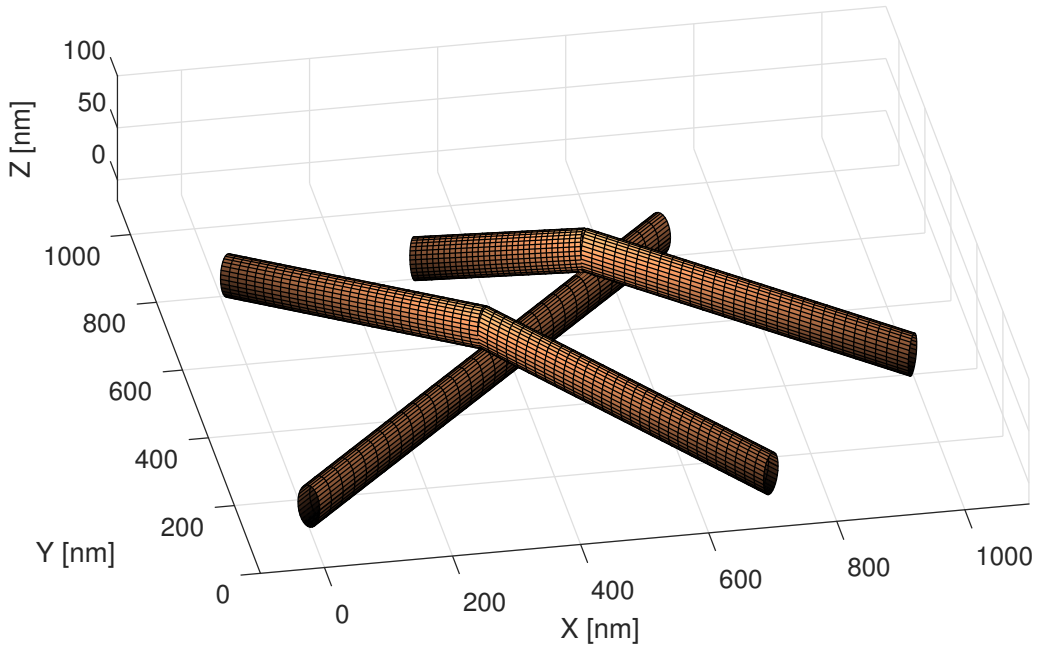

Figure 3.3: Schematic representation of three intersecting nanotubes. The aspect ratio of the nanotubes has been changed to help in the visualization.

number of nanotubes to be generated. This is done once again through the use of AFM images of real samples. From these images, a density of nanotubes per unit of area (μm^{-2}) can be extracted and given to the simulator as input.

During this process, in addition to the aforementioned properties, also the orientation angle in the XY plane for each nanotube is extracted. For completely randomly aligned network, there are no constraints on the orientation of the nanotubes, which are free to be oriented in any direction respect to the substrate plane. However, if needed, the user can also specify a preferred angle of orientation for the nanotubes.

3.2.2 Placement of the Nanotubes

The placement procedure starts only once every property of every nanotube has been chosen and stored. Nanotubes that are outside the length-boundaries (along the direction of the source and drain contacts, by default the x-direction) are rejected, whereas nanotubes that exceed the boundaries along the transverse direction (by default the y-direction) are accepted if at least one of the two nodes is inside the simulation domain. This is because usually the simulated device has smaller size than the real device; in this case cutting all the nanotubes on

the external edges could reduce consistently the number of percolation paths between source and drain.

In the proposed approach, CNTs are placed sequentially one after the other, controlling each time if there are any intersections between the incoming nanotube and the already existing ones. The nanotubes are coming from the top, parallel to the substrate. For each single nanotube, the program will use the extracted length and the orientation respect to the XY plane to calculate the (x, y) coordinates of the two ending points of the tube itself. Once the coordinates are obtained, the algorithm will look for all possible intersections with the existing nanotubes. A list of all such intersection points is generated and among them the one with the highest vertical coordinate is picked as the first intersection point. This is a crucial point and is the most expensive from the computational point of view. After this step, the original single nanotube is split in two sub-segments, which are allowed to bend in the z-direction. The algorithm will once again compile a list of possible intersection points and pick the one with the highest z-coordinate.

There are three main constraints that the algorithm must respect:

- Maximum bending angle, which is chosen to be less than 10°.
- Length of the nanotube, which is kept constant during the bending procedure.
- Resting point, which has to be either on the substrate or over another nanotube. No floating CNTs are allowed; in case a CNT is not able to touch a proper resting point, the CNT will be force to slide until a satisfactory condition is fulfilled.

The process of bending is repeated every time the nanotube finds a new resting point on the network; this happens especially with high-density films. Figure 3.3 shows the schematic representation of three intersecting nanotubes.

At the end of this step, the program saves two different files. The first one is a matrix of N rows, the number of nodes, and 5 columns, which represent respectively the index of the node, the three spatial coordinates, and an identifier that contains the information on the chirality of the nanotube. The second file is a list of M couples of nodes which are connected among each other in the network.

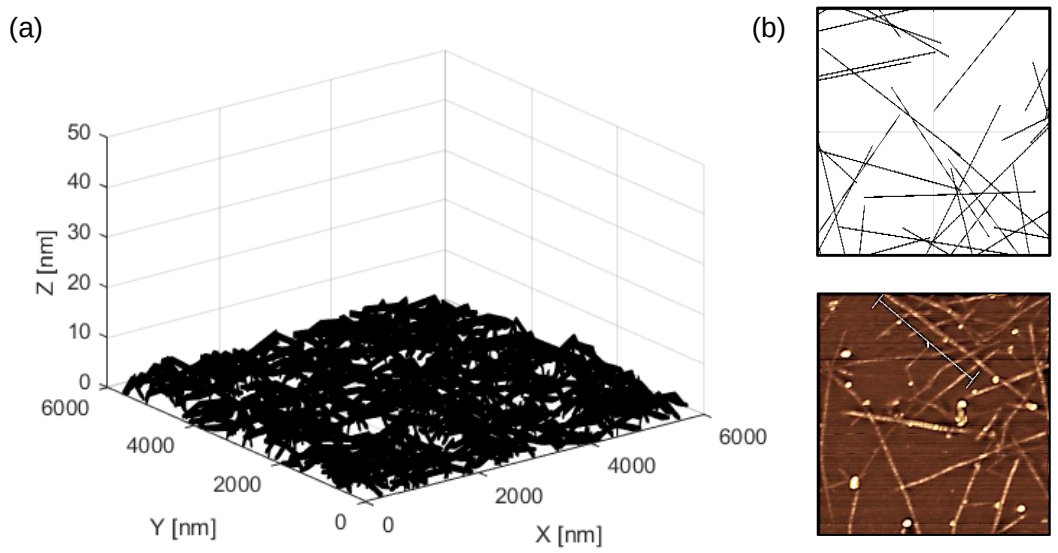

Figure 3.4: (a) Three dimensional representation of a generated network with a density of 18 CNT/μm^2. The simulation domain is a square region of 36 μm^2. (b) Comparison between a generated network and an AFM picture of a real fabricated device (area of 1 μm^2).

To validate the model for the device generation, some comparisons with real networks under AFM have been made, as it is shown in Figure 3.4. The generated networks showed a good agreement with the observed samples, both in terms of coverage of the surface and thickness of the film.

3.2.3 2D vs 3D Model

As already stated in Section 2.5.3, the generation of a realistic morphology is a crucial problem. Since the transport is imposed by the percolation paths, it is mandatory to represent the network in a three-dimensional space. A two-dimensional model, would indeed overestimate the number of percolation paths, by including many fictitious junctions (i.e. all the projections on the substrate plane) in the network. The network in a two-dimensional space is much more connected, and this leads to a current flow that can be very different respect to the real behavior.

With the presented method, the number of the junctions between different nanotubes is much closer to the reality, and the current flow distribution in the network is more reliable as well. Figure 3.5 gives an estimation on the effect of

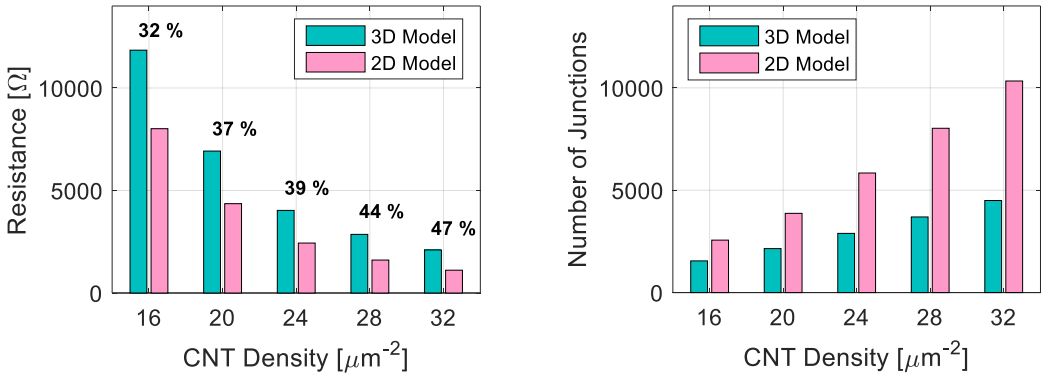

Figure 3.5: (Left) Resistance versus CNT density for the 3D and the 2D model. The numbers in percentage represent the relative variation, which appears to be higher for denser networks. (Right) Same graph showing the number of junctions instead. The 2D model shows a higher number of junctions by counting all the projections on the plane.

this artifact for networks with different densities, for a 3D and a 2D model. As expected, the difference between the models is higher with higher densities. In fact, when the thickness of the network increases, the nanotubes that are on the top of the film are not actually in contact with the nanotubes that lie on the substrate.

3.3 The Simulation Setup

Before performing a simulation, the program needs to know which device must be simulated and what kind of simulation must be carried out. The first task is done by reading the already mentioned input file, that is the one containing the coordinates of all the nodes, the properties of the nanotubes and the connections between all the nodes in the network. For the second task instead, the program has to read a list of directives, which contains all the information relative to the geometry of the device (e.g. dimensions of the active area and of the contacts), the information on the boundary conditions, and the parameter that must be swept from an initial value to a certain goal value. Regardless of which kind of simulation has been selected, the program will follow a standard routine for the conversion of the morphology file to a proper netlist. Following the schematic of Figure 3.1, the remaining part of the chapter will go through all the consecutive steps of the algorithm, starting with the precomputation of the I-V characteristics and the theory behind it.

3.3.1 Precomputation of the I-V Characteristics

In algorithms theory, the precomputation is the act of performing an initial computation before run-time, in order to generate a lookup table that can be used by an algorithm to avoid repeated computation each time it is executed. The generated lookup table, which is nothing else than a matrix with stored data, replaces some run-time computation with a simpler array indexing operation. The savings in terms of processing time is enormous, since since retrieving a value from the memory is significantly faster than undergoing expensive computation operations each time the needed function is called. The reason why this approach is essential, is related to the long computational time needed for the calculation of the transport through a single nanotube. Such an operation, cannot be performed several thousand times, which would be the case if it is called for each nanotube in the network.

In fact, the transport mechanisms are here modeled according to the theory of one-dimensional ballistic channels based on the NEGF formalism. The current through a single nanotube is computed on the base of the *coherent transport* formalism (see Section 3.4.3) with the addition of a phenomenological model to include the scattering events. This choice is driven by computational constraints, which make impossible the use of a full atomistic approach based on the NEGF. As already mentioned in Section 2.5.4, an interesting way to solve the problem is to simulate the entire network within a multi-scale framework, where an atomistic model for the single nanotube is coupled to a circuital model for the whole network.

However, also this approach has several constrains dictated by the computational time needed for the simulation. In a typical network simulation, the number of nanotubes can easily be in the order of $10^3 - 10^4$. For this reason is impracticable to apply an atomistic model to each nanotube; in such case, a single simulation cycle would run for an estimated time of around 20000 hours.

In the proposed work, the main idea is to group the nanotubes in classes, according to their chiral vector. The number of possible classes can vary a lot depending on the typology of network that must be evaluated. Also in this case some precautions must be taken, with the aim of reducing as much as possible the number of classes. To achieve this goal, the specification from the supplier of the nanotube solution and a study of AFM images of deposited films can be

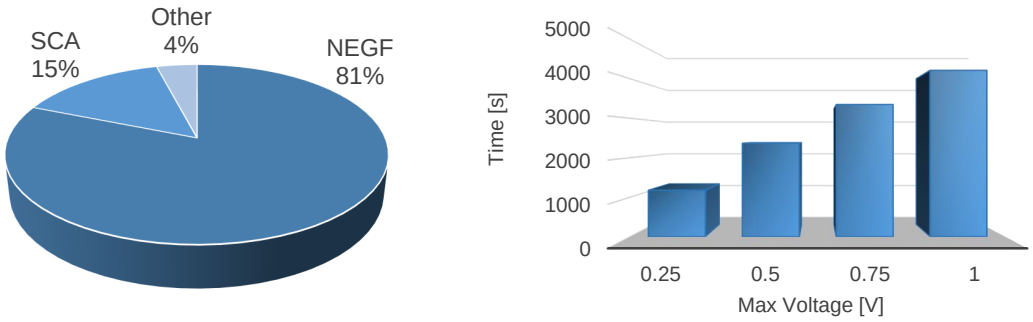

Figure 3.6: (Left) Pie chart on the time required for the functions in a simulation cycle. (Right) Plot of the time required by the NEGF function for the pre-computation of different biases with a constant voltage discretization. The charts are referred to a PC with an Intel® Core™ i5-2500 CPU @ 3.30 GHz with 12 GB of RAM.

combined together, in order to have a comprehensive statistic of the possible classes. The specifications of the supplier give two important parameters: the estimated diameter of the nanotubes (which is verified also through the AFM images) and the concentration of metallic nanotubes in the solution. With this two information, and by knowing the relation between the diameter of a nanotube and its chirality (see Section 2.1.1), the number of classes can be narrowed down usually to 2 or 3.

However, grouping the nanotube is not enough to reduce the complexity of the problem to something practically solvable. In each of these classes, all the nanotubes have different lengths, thus different conductivity. The simulation through the NEGF approach of all these nanotubes is still something not feasible. The idea is then to have one single NEGF simulation for each of the classes, and afterwards to distinguish the different nanotubes with some phenomenological model that takes into account their lengths.

The pre-computation of the IV characteristic constitutes anyway the most time consuming step in a typical network simulation. In the left panel of Figure 3.6 the different time contributions are shown. The total time for the pre-computation depends mainly on the dimension of the Hamiltonian, which however cannot be adjusted without taking in consideration some precautions. The first important parameter is the discretization in energy on which the program will build the Green's function. If the discretization is not fine enough, numerical problems relative to the inversion of the Green's function matrix will arise, causing inaccuracy and in the worst case impossibility to solve the prob-

lem. The discretization depends strictly on the considered energy range, which is also related to the bias condition of the device. The applied bias has a fundamental influence also on the second important parameter, which is the number of biases precomputed by the NEGF function. As already mentioned, the program has to assign a resistance value to a certain nanotube according to its potential by reading the pre-computed look-up table. This is done in two steps: firstly, the difference of potential between the two nodes of a nanotube is compared to every value in the look-up table; secondly, the program assigns a value of the resistance by considering the closest value of potential in the look-up table respect to the real potential of the nanotube. The main implication is that the look-up table must be fine enough in order to guarantee a certain accuracy in reading the potentials and assigning the proper resistance values. This is based on a comparison with a certain ΔV

$$\Delta V = \frac{V_{max}}{2p-1}, \tag{3.1}$$

where V_{max} is the maximum voltage pre-computed, and p the number of points in the look-up table. When the voltage increases, the number of points must increase in order to keep ΔV small enough. The effect on the simulation time can be seen in the right panel of Figure 3.6, where the V_{max} has been increased and the ΔV has been kept constant.

3.4 The Non-Equilibrium Green's Function (NEGF) Formalism

The non-equilibrium Greens function (NEGF) formalism provides a powerful conceptual and computational framework for the analysis of quantum transport in nanodevices. [108]. This method is based on the solution of the Schrödinger equation under non-equilibrium conditions and can rigorously treat the coupling between the active device and the contacts, which is one of the most critical aspects in the simulation of nanoscale devices. This approach has been regularly used in the past few years to calculate currents and charge densities in several types of nanoscale conductors under bias, both in the coherent and incoherent regime. Among the many applications, from conventional semiconductor MOSFETs [109, 110], to molecular transistors [111], the NEGF method has been

successfully implemented in the simulation of CNTs-based Field-Effect Transistors (CNTFETs) [112].

A brief summary of the NEGF simulation procedure, and its application in the simulation of ballistic CNTFETs by self-consistently solving the Poisson and Schrödinger equations is reported in this section. More comprehensive descriptions of the technique are widely available in the literature [113, 114].

The standard procedure to obtain the solution for a device under equilibrium is to calculate self-consistently the potential profile $U(x)$ and the charge density $\rho(x)$ with the so-called Schrödinger–Poisson solver [115]. The first step is to identify a suitable Hamiltonian H that provides an adequate description of the isolated device. When the device is connected to the contacts, some charges are transferred into or out of the device, giving rise to a potential $U(x)$ that must be calculated self-consistently. In thermal equilibrium, the electron and hole densities $n(x)$ and $p(x)$ are calculated from the quantum states $\{E_\alpha, \psi_\alpha\}$ through the law of equilibrium statistical mechanics, by filling up the eigenstates $\Psi_\alpha(r)$ of the Schrödinger equation according to the Fermi function:

$$n(x) = 2\sum_\alpha |\psi_\alpha^e(x)|^2 \, F\left(\frac{E_\alpha^e - E_F}{k_B T}\right), \tag{3.2}$$

$$p(x) = 2\sum_\alpha |\psi_\alpha^h(x)|^2 \, F\left(\frac{E_F - E_\alpha^h}{k_B T}\right). \tag{3.3}$$

To complete the picture of the charges, also the space charges due to the presence of dopants must be included

$$N_D^+(x) = N_D^+ \left[E_C(x)\right], \qquad N_A^-(x) = N_A^- \left[E_V(x)\right]. \tag{3.4}$$

The total charge density is obtained by adding up all these contributions:

$$\rho(x) = q\left[p(x) - n(x) + N_D^+(x) - N_A^-(x)\right]. \tag{3.5}$$

Through the Poisson equation

$$\nabla \cdot [\varepsilon(x)\nabla U(x)] = -\rho(x), \tag{3.6}$$

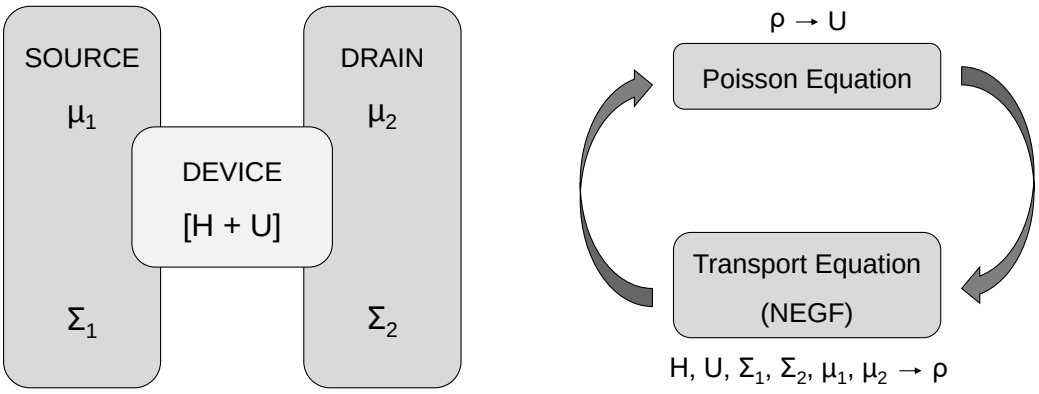

Figure 3.7: (Left) A device driven out of equilibrium by two contacts with different Fermi levels μ_1 and μ_2. (Right) Self-consistent procedure for determining the density matrix ρ from which all quantities of interest can be calculated.

the electrical potential $U(x)$ can be evaluated. An important aspect is that this potential modify the band edges E_C and E_V according to

$$E_C(x,U) = E_C(x) - qU(x), \qquad E_V(x,U) = E_V(x) - qU(x). \tag{3.7}$$

As consequence, the charge density $\rho(x)$ becomes potential-dependent, and the Poisson equation non-linear in $U(x)$. The Schrödinger equation and the non-linear Poisson equation form a coupled system of differential equation that must be solved self-consistently. The solution to this problem is usually computationally demanding. Indeed, it has been demonstrated that calculate the Green's function is much faster than solve the whole eigenvalue problem [114]. Furthermore, the extension to a device out of equilibrium is straightforward, as well as the introduction of scattering events for the analysis of incoherent transport.

The Green's function basically gives the response of a system to a constant perturbation in the Schrödinger equation. Figure 3.7 shows a generic device channel connected between two contacts and the self-consistent procedure with the NEGF approach.

The first step in the NEGF approach, consists in the identification of a suitable Hamiltonian matrix for the isolated channel. The self-consistent potential, which is a part of the Hamiltonian matrix, is included in this step.

The second step is to compute the self-energy matrices, Σ_1 and Σ_2, which describe how the ballistic channel couples to the source/drain contacts. A rigorous treatment for the more general case of incoherent transport should include also

Σ_S, the scattering matrix, which describes the scattering processes in the channel. The work here presented is based on the more approximate case of coherent transport, with the addition of scattering events through a phenomenological model which is not part of the NEGF formalism. The reason behind this approach is discussed in details is Section 3.5.

After identifying the Hamiltonian matrix and the self-energies, the third step is to compute the retarded Green's function

$$G(E) = [(E + i0^+)I - H - \Sigma_1 - \Sigma_2]^{-1}. \tag{3.8}$$

The fourth step is to determine the physical quantities of interest from the Green's function. In the ballistic limit, states within the device can be divided into two parts: 1) states filled by carriers from the source according to the source Fermi level, and 2) states filled by the drain according to the drain Fermi level. Within the device, the source and drain Local Density of States (LDOS) are

$$D_S = G\,\Gamma_S\,G^\dagger, \qquad\qquad D_D = G\,\Gamma_D\,G^\dagger, \tag{3.9}$$

where

$$\Gamma_S = i(\Sigma_1 - \Sigma_1^\dagger), \qquad\qquad \Gamma_D = i(\Sigma_2 - \Sigma_2^\dagger). \tag{3.10}$$

is the energy level broadening related to the source and drain contact respectively. The total charge density is obtained by summing up the contributions of the two contacts (or in a more general case, the i contacts), appropriately weighted with their Fermi levels

$$\rho = \frac{2\,(\text{for spin})}{2\pi} \int_{-\infty}^{\infty} dE \sum_i f(E, \mu_i)\, G\,\Gamma_i\,G^\dagger. \tag{3.11}$$

Also in this case the system is non-linear, hence the NEGF transport equation must be solved self-consistently together with the Poisson equation.

The computationally expensive part of the NEGF simulation is finding the retarded Green's function, according to (3.8), which requires the inversion of a matrix for each energy grid point. The straightforward way is to explicitly in-

vert the matrix, whose size is the size of the basis set. In the ballistic limit, the problem is simplified because only a few columns of the Green's function are needed. However, the reduction of the size of the Hamiltonian matrix is a very crucial aspect in atomistic simulations, especially in the incoherent transport regime.

3.4.1 The Hamiltionian

The first step in the NEGF approach, is to identify a set of atomistic orbitals adequate to describe the essential physics for carrier transport and then to write down the Hamiltonian matrix for the isolated channel in that basis. At this point several possibilities are available regarding the choice of representation. This work is based on a real space approach. Although other methods might be more suitable for the simulation of entire devices (e.g. the mode space approach[116]), especially in the incoherent transport regime, the simulation of entire nanotubes with the NEGF formalism is out of the scope of this project (and for the reasons explained in Section 3.3.1, practically impossible to implement).

Although the carbon nanotubes properties have been already introduced in Section 2.1.1, some of the main concepts will be here repeated for a better understanding of the Hamiltonian structure. Each carbon atom in the hexagonal cell has six electrons; since carbon hybridize sp^2 forming the graphene structure, two electrons will be $1s$, three $2sp^2$ and one $2p$. The three $2sp^2$ are responsible of the bonds on the graphene sheet plane, leaving an unsaturated p orbital (conventionally p_z orbital) with a single electron, which then forms delocalized π bonds responsible for its transport properties. With one orbital per carbon atom, as the basis set, the size of the Hamiltonian matrix is the number of carbon atoms in the device. It is worth mentioning that, even after this simplification, simulating an entire carbon nanotube it is computationally highly demanding. The size of the Hamiltonian is NxN, where N, the number of atoms in the nanotube, could be several thousand.

A tight-binding approximation has been used to describe the interaction between carbon atoms, and only nearest neighbor coupling is considered. A coupling parameter of $t = 3eV$ was assumed. The method is here applied to the specific structure of carbon nanotubes; the more general approach with a generic discretization of a device can be found in literature [117, 118]. In the following

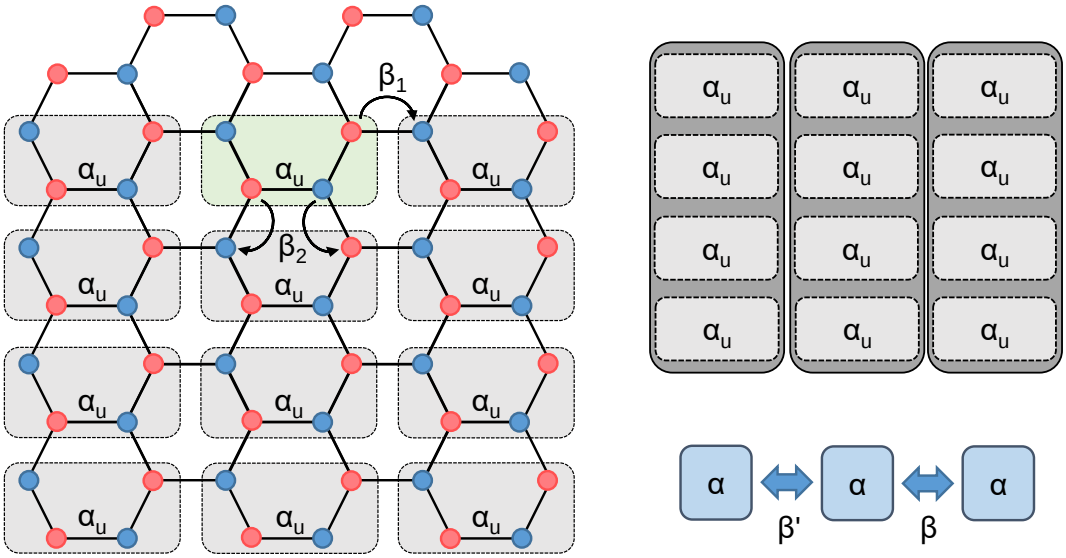

Figure 3.8: Definition of unit cells (left) and macro-unit cells (right) for the construction of the Hamiltonian.

example, a 4-atom unit cell is defined, on the basis of which the Hamiltonian will be construct. For the sake of brevity, here only the case of a zig-zag nanotube is presented. The method is easily extendable to armchair and chiral nanotubes in a straightforward manner.

The matrix related to each individual unit cell:

$$\alpha_u = \begin{bmatrix} 0 & t & 0 & 0 \\ t & 0 & t & 0 \\ 0 & t & 0 & t \\ 0 & 0 & t & 0 \end{bmatrix}$$

A unit cell is connected to the surrounding unit cells by two coupling matrices. The matrix β_1 establishes a connection between two atoms of two consecutive unit cells along the longitudinal direction, whereas the matrix β_2 connects two pairs of atoms of two different unit cells along the transversal direction. All the matrices are nxn, where n is the number of atoms in the unit cell. A schematic representation of the unit cells and their connections is shown in Figure 3.8.

$$\beta_1 = \begin{bmatrix} 0 & 0 & 0 & 0 \\ 0 & 0 & 0 & 0 \\ 0 & 0 & 0 & 0 \\ t & 0 & 0 & 0 \end{bmatrix} \qquad \beta_2 = \begin{bmatrix} 0 & 0 & 0 & 0 \\ t & 0 & 0 & 0 \\ 0 & 0 & 0 & t \\ 0 & 0 & 0 & 0 \end{bmatrix}$$

It is worth mentioning that the procedure shown until here is not dependent on the chirality but solely on the choice of the unit cell representation. Depending on the structure of the nanotube, the choice of which connections are parallel or orthogonal to the propagation direction can be made after this step. In order to have a one-dimensional problem, multiple unit cells can be grouped into a single macro-unit cell, as shown in Figure 3.8. The matrix of the macro-unit cell become then:

$$\alpha = \begin{bmatrix} \alpha_u & \beta_2 & 0 & \dots \\ \beta_2' & \alpha_u & \beta_2 & \\ 0 & \beta_2' & \alpha_u & \ddots \\ \vdots & & \ddots & \ddots \end{bmatrix}$$

The connections between the macro-unit cells are given by the matrix β

$$\beta = \begin{bmatrix} \beta_1 & 0 & 0 & \dots \\ 0 & \beta_1 & 0 & \dots \\ 0 & 0 & \beta_1 & 0 \\ \vdots & \vdots & 0 & \ddots \end{bmatrix}$$

The dimensions of the matrices α and β depends on the structure of the nanotube (i.e. on the chirality). The complete Hamiltonian can be written as:

$$H = \begin{bmatrix} \alpha & \beta & 0 & \dots \\ \beta' & \alpha & \beta & \\ 0 & \beta' & \alpha & \ddots \\ \vdots & & \ddots & \ddots \end{bmatrix}$$

After all these quantities are computed, it is straightforward to calculate the band structure of a nanotube. In general the band structure of a certain device can be calculated by solving a matrix eigenvalue equation of the form

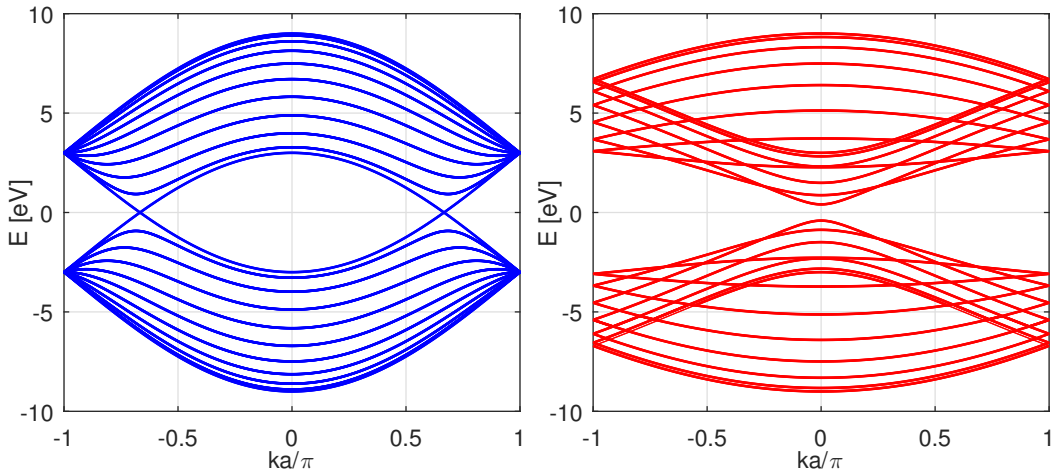

Figure 3.9: (Left) Computed band structure for an armchair (10,10) nanotube. (Right) Computed band structure for a zig-zag (13,0) nanotube.

$$E(\phi_0) = [h(\vec{k})]\,(\phi_0), \tag{3.12}$$

where

$$[h(\vec{k})] = \sum_m [H_{nm}] e^{i\vec{k}\cdot(\vec{u_m}-\vec{u_n})}. \tag{3.13}$$

The size of the matrix $h(\vec{k})$ is bxb, being b the number of basis per unit cell. Following the procedure previously applied, the modified set of basis with the macro-unit cell can be used. The sum must be evaluated considering all the neighboring macro-unit cells (including the macro-unit cell itself). The choice of the macro-unit cell is irrelevant since the structure is assumed periodic. Equation (3.13) is reduced then to the form

$$[h(\vec{k})] = \alpha + \beta' e^{-ika} + \beta e^{ika}. \tag{3.14}$$

The sub-bands can be plotted by finding the eigenvalues of the matrix in Eq. (3.14), for each value of $\vec{k}$, and it has n branches, one for each eigenvalue.

As already introduced in Section 2.1.1, a nanotube can show different band structures according to its chiral vector. In Figure 3.9 the sub-bands of an armchair (10,10) and a zig-zag (13,0) nanotube are presented. In the left panel of the figure, the lines of the quantized wavevectors intersect for a specific value

of the wavevector, leading to crossing bands and thus to a metallic character. In the right panel, there are not intersections for any value of the wavevector; in this case the nanotube has a semiconducting behavior, with a bandgap determined by the two lines that come closer. In both cases the band structures show various sub-bands, arising from the quantization of the wavevector around the circumference of the nanotube.

3.4.2 Self-Energy Matrices

After the Hamiltonian of the device has been specified, the next step is the computation of the NxN self-energy matrices for the two contacts. The concept of self-energy is widely used in many-body physics to describe electron-electron and electron-phonon interactions. However, the concept can be easily extended to describe the effect of a semi-infinite contact on a device by an opportune modification of the Hamiltonian [119]. In this context, the self-energies describe the open boundary conditions for the Schrödinger equation. Since only the first and the last unit cells are coupled with the contacts, the self-energy matrices are highly sparse.

$$\Sigma_1 = \begin{bmatrix} \Sigma_{11} & 0 & \dots & 0 \\ 0 & 0 & \dots & 0 \\ \vdots & \vdots & \ddots & \vdots \\ 0 & 0 & \dots & 0 \end{bmatrix} \qquad \Sigma_2 = \begin{bmatrix} 0 & \dots & 0 & 0 \\ \vdots & \ddots & \vdots & \vdots \\ 0 & \dots & 0 & 0 \\ 0 & \dots & 0 & \Sigma_{m2} \end{bmatrix}$$

In Σ_1 the only non-zero element is the submatrix Σ_{11}, which connects the first unit cell with the first contact; similarly, in Σ_2, the only non-zero element is the submatrix Σ_{m2} that connects the last unit cell with the second contact. The rigorous derivation of the submatrices can be be found in [116]. The non-zero element are computed through an iterative evaluation of the *surface Green's functions* $g_{1,2}$, which is simply a subset of the full Green's function of the contact $G_{1,2}$

$$g_1 = [(E + i0^+)I - \alpha - \beta' \, g_1 \, \beta]^{-1}, \qquad g_2 = [(E + i0^+)I - \alpha - \beta \, g_2 \, \beta']^{-1} \, . \quad (3.15)$$

The self-energy matrices are then

$$\Sigma_1 = \beta' \, g_1 \, \beta \,, \qquad \Sigma_2 = \beta \, g_2 \, \beta' \,. \tag{3.16}$$

The self-energy method is computationally intensive, since it requires an integration over energy, but it offers a formally correct way to treat properly the open boundary conditions. The need of this method is more evident when the device is under a certain bias, a problem that cannot be treated with simpler assumptions, such as, for instance, the periodic boundary conditions.

Furthermore, the introduction of the self-energy matrices has two implications on the system. These matrices are slight different from the canonical Hamiltonian, since they are energy dependent and not Hermitian. The first property has the effect of changing the Hamiltonian of the system, thus the eigenstates and their energies. The second property, which appears less evident, has however important conceptual implications, since the total system becomes non-Hermitian. This introduces an imaginary part to the energy, which give rise to the already introduced *broadening functions* (3.10). While the real part of the self-energy causes just a shift in the device energy levels, the imaginary part has the effect of giving the eigenstates a finite lifetime [119], implying that the wavefunctions and the associated probability decay with time.

3.4.3 The Coherent Transport

Once the device Hamiltonian and the self-energy matrices are known, the calculation of the current that flow through the device is straightforward. Fundamentally, there are two ways to simulate such a system, which make use of two different levels of approximation, namely the *coherent* and *incoherent* transport approximation. The propagation of electrons in a device is considered coherent if it does not suffer of the so-called *phase-breaking* scattering events, which cause a change in the state of an external object. If a certain event occurs, where an electron interacts with an external object without changing its states, the transport is still considered coherent, and the effect of the event can be incorporated with an appropriate potential in the Hamiltonian of the system. An example is the scattering with an impurity, where an electron interacts with a rigid defect (i.e. the impurity does not vibrate or get deflected). However, if the electron manages to transfer some energy to the atomic lattice, the transport is not considered coherent anymore, and the effect of the event cannot be incorporated in

the Hamiltonian. This is the case of the phase-breaking processes, which arise from the interaction of one electron with the surrounding ensemble of phonons, photons and other electrons. In other words, in the case of incoherent interactions, the state of the system changes as the result of transport.

The question now concerns whether the transport in a carbon nanotube is coherent or incoherent. The answer to this question is not unique: the nature of the transport depends on the structure of the nanotube. In fact, the structure of the nanotube dictates how the electrons travel along it, and how many interactions they have during their motion. In this context, the so-called *mean-free-path* (MFP), which is the average length a carrier will travel between two collision events, can be introduced. CNTs have shown amazingly long MFPs, of several hundreds nm [120]. This means that the electrons travel without any interactions along those lengths, in a way that could be considered coherent. On the other hand, for long nanotubes the assumption of coherent transport is not valid anymore. Furthermore, the MFP is dependent on the applied electric field, as it will be explained in details in Section 3.5.

However, the idea of using the more general incoherent model is practically not applicable. As already explained in Section 3.3.1, the only way to apply a multiscale approach to the film is to calculate the IV characteristics not for every nanotube in the network, but only for some classes. Since the incoherent transport formalism requires the calculation of an additional matrix (i.e. the scattering matrix), which depends on the length of the nanotube, the precomputation of only few classes would not be possible anymore. Furthermore, the calculations of the incoherent transport are intrinsically very demanding in terms of computational power. For this reason, this work has been based on coherent transport processes combined with phenomenological models for the treatment of the scattering events.

A comprehensive description on the assumptions behind this theory can be found elsewhere [119]. Here, only the main results and their application to the carbon nanotubes are reported.

The current I_i at a terminal i can be written as follows:

$$I_i = (-\frac{q}{h}) \int_{-\infty}^{\infty} dE\, \tilde{I}_i(E), \tag{3.17}$$

with

$$\tilde{I}_i(E) = \text{Trace}[\Gamma_i A]\, f_i - \text{Trace}[\Gamma_i G^n], \tag{3.18}$$

being a dimensionless current per unit of energy. In (3.18), the matrix A is the so-called *spectral function*

$$A \equiv i[G - G^\dagger] = A_1 + A_2\,. \tag{3.19}$$

where

$$A_1 = G\,\Gamma_1\,G^\dagger\,, \qquad A_2 = G\,\Gamma_2\,G^\dagger\,. \tag{3.20}$$

The current between two contacts can be also rewritten according to the *Landauer formalism*

$$I_i = (-\frac{q}{h}) \int_{-\infty}^{\infty} T(E)(f_1(E) - f_2(E))\, dE\,. \tag{3.21}$$

where the so-called *transmission function* $T(E)$ represents the rate at which electrons are transmitted from a source to a drain contact.

$$T(E) \equiv \text{Trace}[\Gamma_1 A_2] = \text{Trace}[\Gamma_2 A_1]\,. \tag{3.22}$$

As it has been already introduced in Section 3.3.1, the calculation of the transmission functions for the different nanotube species is a central aspect in the simulation tool.

As an example, the plot of the transmission function for two different species of nanotubes is shown in Figure 3.10. Once T(E) is known in the energy range of interest (which is variable depending on the bias conditions of the device), the current of the nanotube is computed through Equation (3.21) for different values of the applied potential in order to build up the IV characteristic of the nanotube.

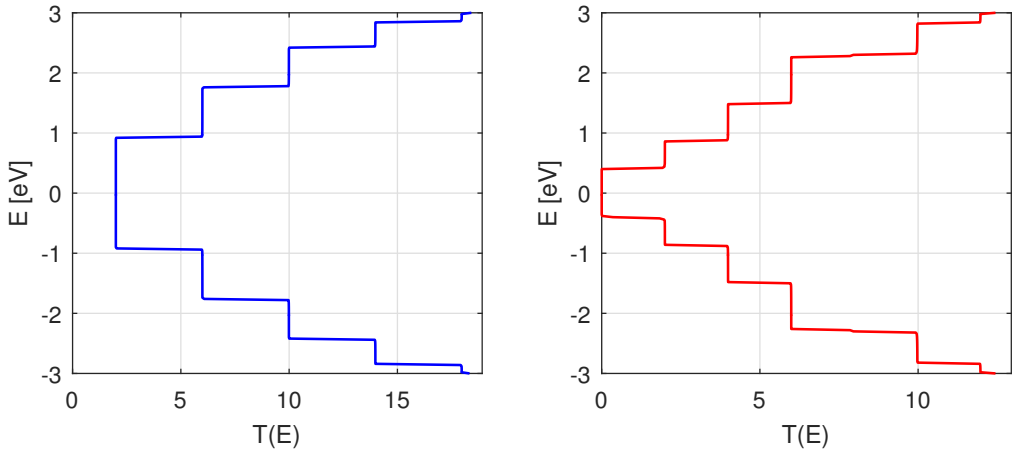

Figure 3.10: (Left) Transmission rate of an armchair (10,10) nanotube. (Right) Transmission rate of a zig-zag (13,0) nanotube.

3.5 Phenomenological Model for Scattering

The calculation of the IV through the coherent transport formalism covers only a part of the whole story. By assuming the transport to be coherent, all the intrinsic scattering mechanisms (e.g. scattering with phonons) are neglected. This is definitely a too optimistic view of the transport through the CNT networks studied in this work. Due to the impossibility of applying a fully-incoherent calculation to every nanotube, a phenomenological model for the different scattering events has been implemented with the following formulation:

$$R_{TOT} = R_{coh}\left(1 + \frac{L}{\lambda_{TOT}}\right), \tag{3.23}$$

where R_{coh} is the resistance calculated with the coherent transport formalism, as the result of the ration between the applied voltage and the pre-computed current. L is the length of the tube, whereas λ_{TOT} is the mean-free-path, which is, in turn, calculated as:

$$\lambda_{TOT} = (\lambda_{AC}^{-1} + \lambda_{OP,ems}^{-1} + \lambda_{OP,abs}^{-1})^{-1}. \tag{3.24}$$

In Equation (3.24), the total mean-free-path λ_{TOT} is obtained from Matthiessen's approximation [121] as the sum of the contributions of different scattering events. The included events are elastic scattering with acoustic phonons (λ_{AC}), and inelastic electron scattering by optical emission ($\lambda_{OP,ems}$) and absorption ($\lambda_{OP,abs}$).

Around room temperature and above, the acoustic phonons modes are thermally occupied ($k_BT \gg \hbar\omega_{AC}$), and their scattering rate is linearly proportional with temperature [122]. The adopted formulation is the following:

$$\lambda_{AC} = \lambda_{AC,300}\left(\frac{300}{T}\right), \tag{3.25}$$

where $\lambda_{AC,300}$ is approximately equal to 1600 nm (for metallic tubes) [123].

For OP phonons the problem must be handled more carefully. It is worth noting that this contribution has been often neglected at room temperature, due to the large OP phonons energy ($\hbar\omega_{OP} \approx 0.16 - 0.20eV$) [124, 125]. The electron scattering rate with the OP phonons can be directly derived from the Fermi's Golden Rule [126]:

$$\frac{1}{\tau_{OP}} = \left(N_{OP} + \frac{1}{2} \mp \frac{1}{2}\right) D(E \pm \hbar\omega_{OP}), \tag{3.26}$$

where the upper and lower signs correspond respectively to OP absorption and emission, and N_{OP} is the optical phonon occupation, which follows Equation (3.27).

$$N_{OP} = \frac{1}{[\exp(\hbar\omega_{OP}/k_BT) - 1]}, \tag{3.27}$$

The OP absorption length can be finally written as

$$\lambda_{OP,abs}(T) = \lambda_{OP,300}\left(\frac{N_{OP,300} + 1}{N_{OP}(T)}\right), \tag{3.28}$$

where $\lambda_{OP,300}$ is the spontaneous OP emission length at 300 K and it is approximately equal to 15 nm [127]. Such a short distance however, is not the average OP emission length, which is much longer since that not all the electron energies reach the OP threshold. Most of the electrons in the system have to somehow gain this energy (e.g through an electric field).

The last phenomenon included is the emission of an optical phonon after a scattering event. Such an event is possible when the electron gain enough energy through an electric field or after an OP absorption event. The total mean-free-path for this event is once again calculated from the Matthiessen's approxima-

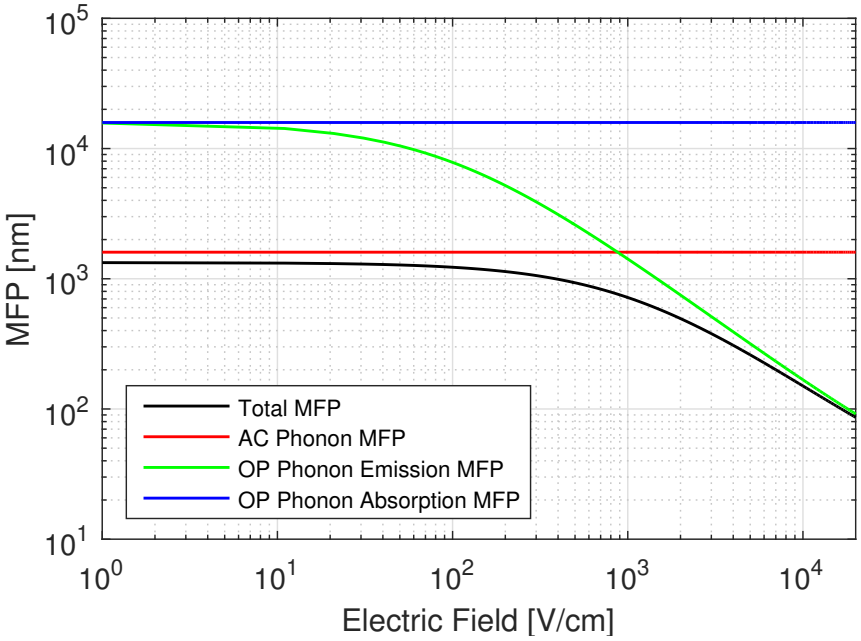

Figure 3.11: Plot of the mean-free-path versus the electric field. The total mean-free-path (black curve) is the result of all the contributions summed up through the Matthiessen's rule.

tion, as the sum of two contributions:

$$\lambda_{OP,ems} = (\lambda^{-1}_{OP,ems-field} + \lambda^{-1}_{OP,ems-abs})^{-1}. \tag{3.29}$$

The term related to the electric field can can be written as

$$\lambda_{OP,ems-field}(T) = \frac{(\hbar\omega_{OP} - k_B T)}{qF} + \frac{N_{OP,300}+1}{N_{OP}(T)+1}\lambda_{OP,300}, \tag{3.30}$$

where F is the applied electric field. The second term instead, the one related to the OP emission after an absorption event, has a similar formulation, in which the first term of Equation (3.31) is replaced with the OP absorption length of Equation (3.28):

$$\lambda_{OP,ems-abs} = \lambda_{OP,ems-abs}(T) + \frac{N_{OP,300}+1}{N_{OP}(T)+1}\,\lambda_{OP,300}, \tag{3.31}$$

The overall results for the mean-free-path are reported in Figure 3.11 as a function of the applied electric field. Similar results have been already obtained in the literature [128, 123].

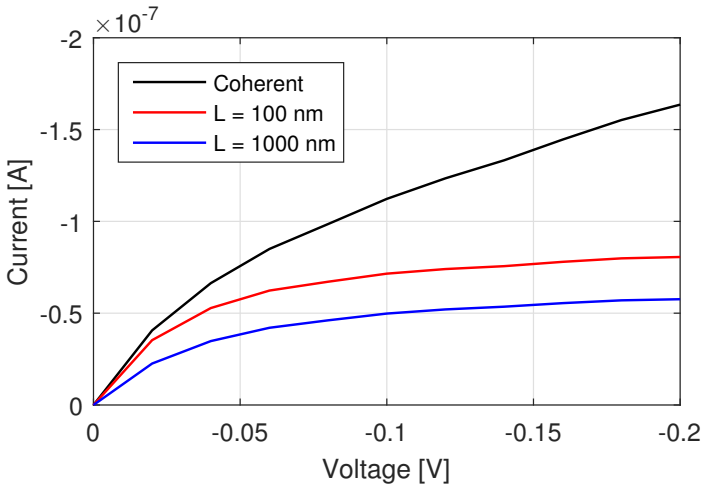

Figure 3.12: Current versus voltage in nanotubes with different length. The variation in the curves is due to the aforementioned scattering events.

It is worth noting that this approach is quite rigorous only for metallic CNTs, whose density of states is nearly constant in the considered energy range. This is also a good approximation for gated semiconducting tubes, when strongly biased away from the band gap.

With this approach, IV table of the pre-computed characteristics is extended to a wide range of lengths, by combining the results of the coherent calculations and the mean-free-paths of different scattering events. This allow to have a fairly accurate model for the transport in the nanotubes in a reasonable amount of time. In Figure 3.12, the effect of the mean-free-path on the IV of nanotubes with different length is showed. Results are in good agreement with works previously done by other groups [122].

3.6 Junctions Model

CNT films are composed by an ensemble of nanotubes, interconnected to each other by inter-tube junctions. Until this point, only the transport through the individual nanotubes has been described. However, nothing has been said regarding the transport in these inter-tube junctions.

Before the advent of the randomly aligned network of CNTs, researchers have been studying the transport properties of junctions between tubes precisely positioned on substrates [129]. These kind of studies have been done both experimentally [55, 35] and theoretically [56, 130]. In the first experiments, single-

walled CNTs were seamlessly joined together by introducing topological defects (pentagon-heptagon pairs) into the hexagonal graphene structure [131]. Electronic properties of such junctions, which generically have the shape of a kink, have been also investigated theoretically [132, 133].

Another interesting configuration, which is more related to the case presented in this work, is the study of crossed nanotube junctions [35]. In this context, junctions consisting of two crossed single-walled CNTs were fabricated with electrical contacts at each end of each nanotube. The measurements presented by Fuhrer et al. (two-terminals and four-terminals measurements) showed a different behavior depending on the chirality of the two nanotubes forming the junctions. For instance, a junction formed by two metallic CNTs (MM-junction) has shown a conductance comparable to the one of the individual nanotubes. The IV characteristics of the junctions showed a linear behavior, indicating a resistive behavior. The values of the resistance of the junctions, which were extracted from the slope of the curves, were of the order of few hundreds of $k\Omega$. Similar results were obtained from the measurements of junctions formed by two semiconducting CNTs (SS-junction). The values of the resistances were two or three times higher than the ones of MM-junctions, but they have still shown a resistive behavior. The physical explanation that has been given, is that these kind of junctions form a relatively good tunnel contact due to the finite density of states available for tunneling on either side of the junction.

The case of junctions made by contacting a metallic and a semiconducting nanotube (MS-junctions) is qualitatively different from the MM and SS cases. The charge transfer at such a junction is expected to form a Schottky barrier [56]. In fact, the two nanotubes share the same graphene band structure, hence the should have nearly the same work function. As a consequence, the Fermi level E_F of the metallic nanotube should align within the band gap of the semiconducting one at the junction. For this reason, in addition to the tunnel barrier, there is also a Schottky barrier with a height approximately equal to half the band gap of the semiconducting CNT. The result is a rectifying behavior with a non-linear IV characteristic.

It is worth noting, that although this method gives reasonable results when applied to an entire network with thousands of junctions, at the same time it simplifies a problem that under some circumstances could need a more sophisticated approach. In order to explore the details of the inter-tube junctions,

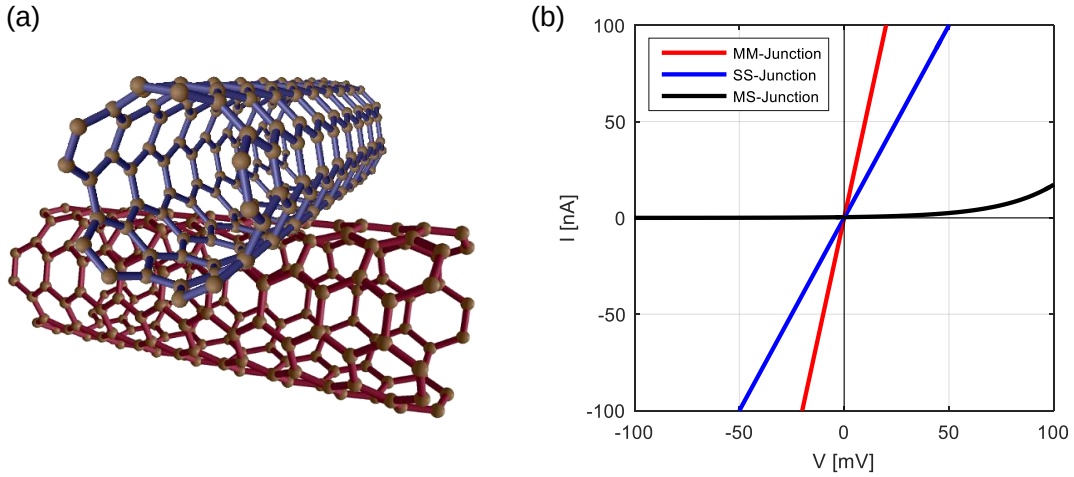

Figure 3.13: (a) Two intersecting nanotubes forming a junction. (b) I-V characteristic of the three different typologies of junctions.

more advance techniques are needed, as for example, the NEGF approach. The correct representation of the Hamiltonian of the junction, by the tight-binding theory, is a crucial aspect. Buldum et al. [130] have reported interesting phenomena such as a negative differential resistance and non-linear variation of the resistance with the contact area. Indeed, the junction behavior can be really peculiar, depending on how the atoms are arranged to form the junction. For instance, two semi-infinite nanotubes connected end-to-end in parallel showed a resonance in the electron transmission, due to quantum-interference effects. Other junctions showed different behaviors depending on whether or not the atoms forming the junction were in registry (i.e. aligned along a specific direction). Furthermore, when the junctions are placed on a substrate, the electronic contact is actually changed by the structural relaxation of the tubes and by the adhesion forces between the tubes and the substrate. In order to investigate these effects, other approaches must be used, such as molecular dynamics [134].

However, such detailed models could not be implemented in the simulation of an entire network. The strength of these models is to correctly represent the transport properties of the inter-tube junction, which are dependent on the angle between the tubes, the overlap between the nanotubes, the chiral vector of the nanotubes and many other parameters. For the same reasons given in 3.4.3, would not be possible to pre-compute all the possible cases of junctions. Certainly, such a simplified model could not be used for a device composed by two single nanotubes opportunely positioned over a substrate. The argument on the validity of the model follows exactly the motivation that pushed researchers

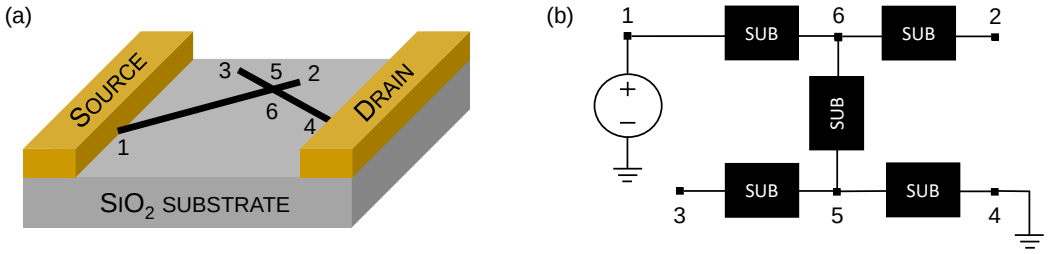

Figure 3.14: (a) Schematic representation of a network with only two nanotubes deposited between a source and a drain electrode. (b) Corresponding representation in terms of electrical components. The possible sub-circuits are the subjects of the next chapters.

to fabricate randomly aligned networks of CNTs. As already mentioned in the prefatory chapter, the difficulty in the fabrication processes of individual CNT devices, has made necessary to develop new solutions in which the positioning of the nanotubes was not so critical anymore. At the same time, also the numerical models have to scale up of one level, renouncing to the atomic details, but making the simulation of entire networks possible.

3.7 Creation of the SPICE Netlist

After the network generation and the pre-computation steps, the program must convert the resulting set of tube segments and tube junctions into a netlist that can be read by the SPICE program. In the netlist a node represents either an ending point of a nanotube or of a junction. Between every pair of nodes, the program assigns a certain block, as schematically depicted in Figure 3.14. Each block contains an equivalent circuit for the electrical representation of the component. The description of these blocks will be given in the next three chapters, together with the motivation behind their electrical representation.

The conversion from the generated network to the SPICE netlist is done through two consecutive steps. During the first attempt to create the netlist, the program receives several errors and warnings from SPICE, due to two possible reasons.

The first one, which results into an error from SPICE, is that some of the nanotubes are not connected to the rest of the network, thus to one of the two contacts. Electrically, this means that these resistances are floating and prevent SPICE to successfully solve the problem. This problem occurs especially

for sparse networks, where it is very likely to have individual unconnected nanotubes. After this first failed attempt, the program receives back a text file containing all the floating nodes, and modifies the netlist by putting to ground all this nodes. This expedient does not affect the result of the simulation, but allows SPICE to complete the simulation.

The second one, which results into a warning from SPICE, happens when a segment of a nanotube has an unconnected node. In Figure 3.14 for example, is the case of the segments (3-6) and (5-2), where the nodes 3 and 2 are connected to less than two nodes. This situation does not prevent SPICE to complete the simulation. However, since these nodes do not contributes to the percolation paths, they can be neglected in the electrical simulation. The idea is to save them into an external file, and list them as nodes on which the program has not to spend further time during the self consistent calculation. Considering that the number of these nodes is usually significant, the simulation can be much faster by not including them in all the calculations.

3.8 The Self-Consistent Algorithm (SCA)

As already stated, the netlist is composed by blocks, which contain a certain equivalent circuit. Regardless the content of the ”black-box”, it is important to point out that the electrical behavior is dependent on the potential applied to the two external nodes. Hence, in order to find the solution to the problem, an iterative procedure is required. The network is thus solved self-consistently through consecutive iterations.

During the first step, the algorithm makes a guess on the value of the electrical components, and writes the netlist. The netlist is then given to SPICE, which solves the electrical problem and saves all the currents between the nodes and all the potential in the nodes. These data are sent back to the program, which converts them and store all the information in external files. These information can be further analyzed and plotted; an example is represented by Figure 3.15, where the potential map of a network is shown.

After the initial step, the program has to read from the pre-computed tables the corresponding value for the electrical component with respect to the difference of potentials between the nodes. Once it finds the proper value of the component,

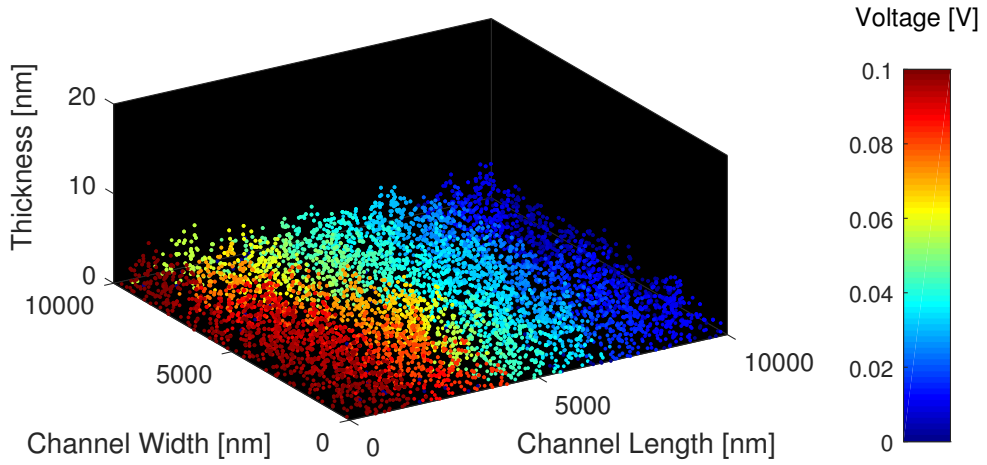

Figure 3.15: Example of the three dimensional representation of the potential distribution in a network.

it writes a new netlist and a new cycle starts. This procedure is repeated until the variation of potential between two consecutive iterations, in each node of the network, is less than a certain tolerance (e.g. 5 mV). Once the convergence criteria are fulfilled, the program saves all the results, which can be afterwards print through the visualization tool.

Chapter 4

Percolative Transport

This chapter is focused on the conduction in CNT networks. Particular attention is dedicated to the percolative nature of the transport by investigating the effects of different macroscopic variables such as, for example, the density of nanotubes in the film and the area of the devices. These kind of simulations, which have been validated against experimental measurements of several type of devices, provide useful insights on the transport through the networks and guarantee the design of reproducible devices in terms of performance. The benefits of having a reliable way to predict the behavior of the networks are more evident after introducing the concept of the *percolation threshold*. In many applications, the films are indeed designed to be close to this percolation threshold, in order to form sort of mono-layers with interesting transport properties.

After the study of the DC conductivity, in the last part of the chapter, the model is extended to introduce the reactive behavior of the nanotubes. The purely resistive model for the single nanotubes is thus substituted with a more general equivalent circuit, which takes into account the capacitive and inductive components as well, allowing the analysis of the networks under AC stimulation.

4.1 DC Conductivity of the Network

Due to its particular morphology, a CNT network presents a peculiar conductivity in comparison to other commonly used electronic materials. To understand these dissimilarities, it is important to have a clear view on what conductivity means for traditional semiconductors, and to analyze the differences that arise when the same definition of conductivity is applied to a CNT network.

Table 4.1: Conductivity of various materials at $T = 293$ K.

Species	**Material**	**Conductivity [S/m]**
Metal	Silver	6.3 x 10^7
	Gold	4.1 x 10^7
	Copper	5.9 x 10^7
Semiconductor	Gallium Arsenide	10^{-8} to 10^3
	Germanium	2.2
	Silicon	1.6 x 10^{-3}
Insulator	Air	10^{-15}
	Fused Quartz	10^{-18}
	PET	10^{-21}

Definition 1. The electrical conductivity is an *intrinsic property* that quantifies the ability of a material to conduct an electrical current.

Although the qualitative definition is general and it is valid for every material, the step of making this definition quantitative must be taken carefully. The reason lies in the causes that make a material able to conduct current, which can be really different. As an example, for metals, semiconductors and insulators, the reasons can be found in the band-theory, which explains how the energy bands are filled by electrons. On the other hand, in ionic liquids and electrolytes, the electron conduction does not happen due to the particular band structure, but by the motion of the ions in the medium. Examples of other different mechanisms of conduction include plasma and superconductors.

Even by staying on the topic of conventional electronic materials, the macroscopic quantitative description of the conductivity depends strictly on the microscopic property of the material under exam. It is fairly understandable that a material with a homogeneous and order crystalline structure can have a different capability of carrying current respect to a completely disordered material.

Without entering into many details, here the fundamental aspect that should be considered is that according to the previous definition, the conductivity is an intrinsic property of a certain material. For a fixed value of temperature, a ordered, homogeneous material presents the same conductivity, expressed in S/m. In Table 4.1 the conductivity of some common materials are presented [135].

Concerning the CNT films, a question that could arise is where to position them in Table 4.1. The answer is not trivial, since a random network of nanotubes

is practically a mixture of different material. Furthermore, the current flow depends on how the nanotubes are arranged on the substrate. The models used for ordered materials fail in describing a percolative system like CNT networks, and the classical concept of conductivity loses its validity.[1]

The way the current flows is related to the number of *percolation paths*. For percolation paths are intended all the possible paths that connect the two electrodes of the device. The amount of these paths depends on several parameters, such as the amount of nanotubes in the film and the arrangement on the substrate. For these reasons, a CNT network can show very different electrical behaviors, from insulator to metallic, depending on how it has been designed.

4.1.1 Modeling of the Resistive Behavior of the Network

As already mentioned in the previous section, it is rather difficult to define rigorously the conductivity of a CNT film. Instead, when dealing with thin films, it is often convenient to work with the so-called sheet resistance. The utility of the sheet resistance is that it is invariable under scaling, and that it can be directly measured using a four-point probe technique. This is for example how CNT films used as transparent electrodes (and more in general TCO films) are characterized.

However, for most of the applications discussed in this work, it is better to refer directly to the resistance of the device. The main motivation lies in the architecture of the device. In fact, for transparent electrodes, the device is composed only by the CNT film, and the easiest way to characterize it is the four-point probe technique. In this specific application, the main goal is to have a film that is very thin (to have a good transparency) and very conductive (to have a low resistance). On the other hand, for other applications, such as sensors and TFTs, the main goal is to have a film of semiconducting nanotubes, as it will be explained in the next two chapters. The main implication is that the film is highly resistive, due to the significant resistance of the semiconducting nanotubes. Therefore, the architecture of the device must be designed in order to reduce the resistance of the film. The most common approach is to use an Inter-Digitated Electrod Structure (IDES), like the one depicted in Figure 4.1.

[1] The classical concept of conductivity actually fails in treating also many other type of devices, especially in mesoscale and nanoscale devices. One example is the case of ballistic conduction.

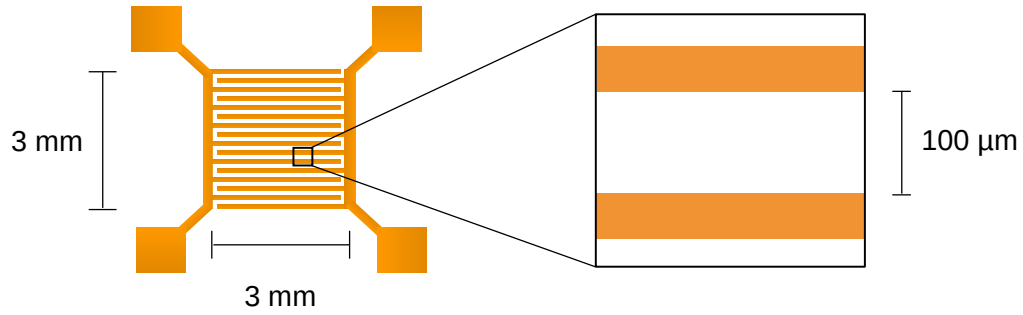

Figure 4.1: Schematic representation of the IDES structure of the real measured device.

Following what has been said in Section 3.7, in this case the equivalent circuit of nanotubes and junctions is composed by a simple resistance. The most important aspect that must be considered here is that in most of the applications, apart the transistors in Chapter 6, the networks are biased in the low-potential regime. Typically, during the measurements, these devices are biased with low voltages ($\sim$ 1-2 V). Keeping in mind the usual spacing between the fingers of the IDES, which is in the order of 100 μm, the drop of potential on a single nanotube on the network is very small. Therefore, it is possible to greatly simplify the problem, by referring to the initial region in the IV curves presented in Chapter 3.

4.2 Stochastic Nature of the Problem

From what has been said until now, it appears that a CNT network must be designed accordingly to the application target. A CNT film for sensing applications, for reasons that will be more clear in the next chapter, has for example a very low density of nanotubes respect to one designed as a transparent electrode. However, the need of a rational design is not a peculiarity of CNT films, but rather something associated to the development of every technology. A more distinguishing aspect is related to the stochastic nature of the problem. Due to the random alignment of the nanotubes over the substrate, there is an inherent aleatory in the morphology of the film, which turns out into a non-fully predictable electrical behavior. In other words, it is practically impossible to achieve the same film starting from the same initial conditions. The interesting question is by how much two nominal identical networks differ between each

other. In this regard, a combined theoretical and experimental study on the percolative transport could provide useful insights in the design of the device, by trying to take into account this distinctive feature of the CNT films. Before entering in the quantitative details, however, it is necessary to attribute the causes behind this behavior of the networks. The main cause is related to the fabrication process, which has been already introduced in Section 2.2.1. For fabrication process, here is now intended the full process flow, from the preparation of the solution to the spray deposition. Even assuming that all the nanotubes in the initial solution have the same identical geometrical properties, this is definitely not true after the solution has been processed. Moreover, the deposition on the substrate is done with a technique that does not allow the individual positioning of the nanotubes. The result is a network with a morphology that is, to all intents and purposes, completely random. The results of a comparative study between simulations and experiments are shown in the next sections.

4.2.1 Simulation domains

The first problem that arises when attempting to simulate a film of randomly aligned CNTs, is the need of finding a reasonable simulation domain. Like in any other simulation problem, one must consider the well-known trade-off between the computational demand and the required accuracy. For this particular issue, there is not a unique rule. However, some guidelines can often help in taking a proper choice, which guarantees results within a range of accuracy, in an acceptable amount of time. The time needed for a simulation is proportional to the applied discretization and to the number of equations in the system, which are calculated in every point of the discrete grid. The grid (often referred to as mesh), must be fine enough to guarantee that the smallest feature in the simulation domain is properly treated. To be more specific, one must always consider the smallest space in which a certain phenomenon can occur. A coarse mesh leads to an inaccuracy of the simulation, by neglecting the effect of some phenomena that manifest themselves in a space smaller than the space between two points in the grid. On the other hand, a fine mesh requires more computational resources.

Concerning the proposed approach (see Chapter 3), the required resources are proportional to the number of nodes in the network. Since it is computationally impossible to simulate the whole area of a real device (which can have an active

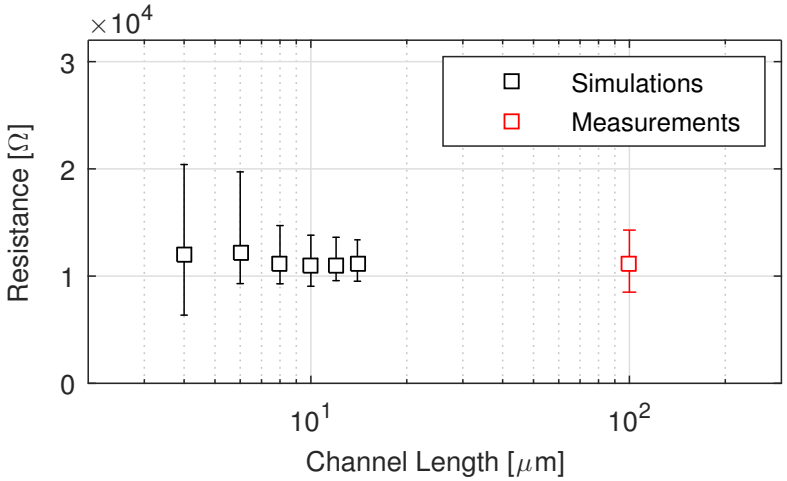

Figure 4.2: Comparison between the experimental data and the simulation of a low-density network. Red error bar: spread of the experimental results between nine different devices fabricated over the same wafer and with the same nominal properties. Each error bar from the simulation (in black) is calculated over 20 simulations.

area of few mm^2) some assumptions must be made.

The fabricated films are deposited by spray coating over a thermally grown SiO_2 substrate [44]. An interdigitated electrode structure (IDES) with 100 μm finger spacing, is evaporated on top of the substrate.

In order to have a comparison on the value of the resistance of the network, the idea is to simulate a smaller portion of the active area and then linearly scale the results up to the entire device area. However, this approach could lead to inaccurate results if the starting simulation domain is not large enough to guarantee a certain uniformity of the network. This is visible in Figure 4.2, where the comparison between some measured device and some networks generated over several simulation domains is shown.

To continue what has been previously said in Section 4.2, it is important to notice the inherent spread of the results from devices which are nominally identical. In order to validate the simulation, it is fundamental to replicate the same spread. As it turns out, if the simulation domain is too small, the variance of the results does not match the one presented by the measurements, even though the average value is the same.

For the sake of clarity, it is worth to mention that the big spread of the results on small areas is not simply an artifact of the simulations. In case the real

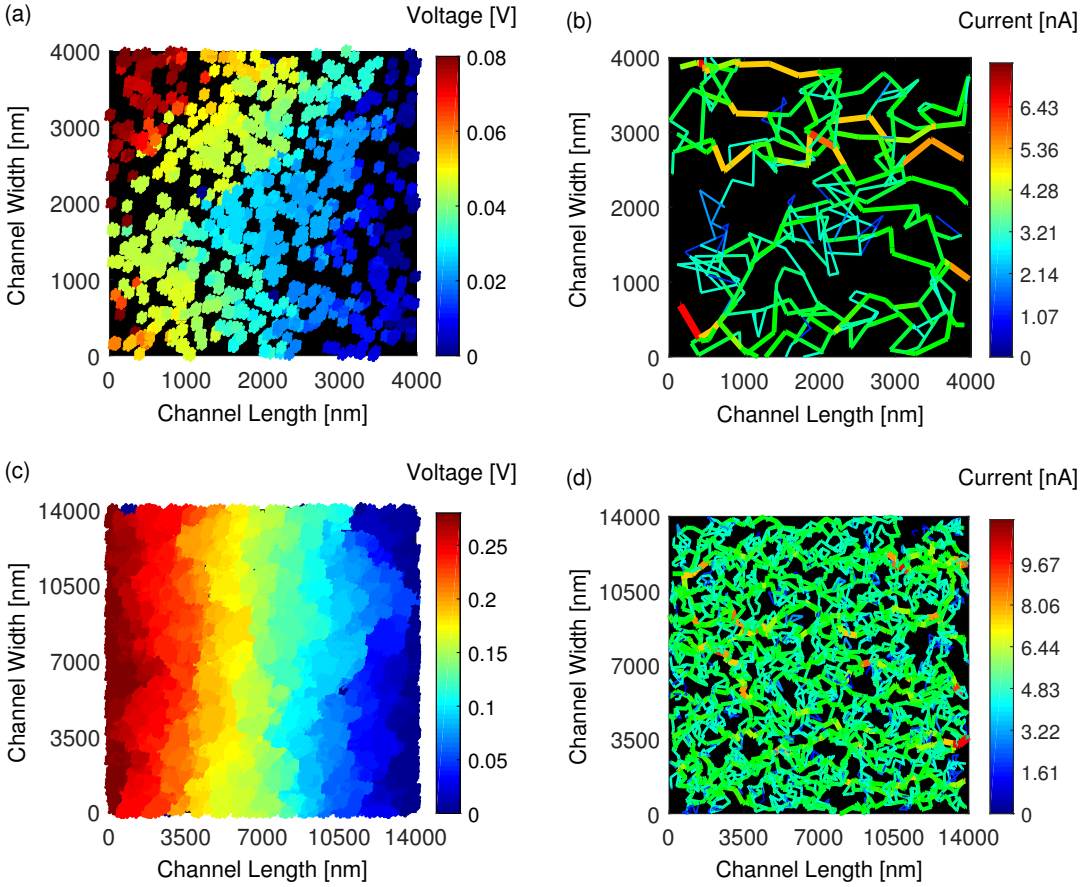

Figure 4.3: (a) Potential distribution of a network generated over a domain of 4x4 μm^2. (b) Current flow through the same device. (c) Potential distribution over an area of 14x14 μm^2. (d) Current flow through the same device. All the plots are top views of 3-D networks.

devices are fabricated over small areas, the resistance of different networks will presents the same variability predicted by the simulations. This effect is once again due to the percolative nature of the transport through the network and it can be further explained with the help of Figure 4.3. Figure 4.3(a) and (b) shows, respectively, the potential distribution and the current flow from a network randomly generated over a domain of 4x4 μm^2.

As it is clear from the plots, both the two quantities are not uniformly distributed over the surface. Moreover, if several networks are generated in that domain, the morphology and thus the electrical transport will be very different between each network. This is due to the presence of border effects, which are not negligible at all in the case of small area devices. This phenomenon is not just limited to the simulations; devices fabricated over such small areas will be also affected by a big variance of results.

When the domain reaches a certain threshold, the variance of the simulations tends to saturate to a value that is in good agreement with the one from the measured devices, as it is shown in Figure 4.2 for devices with an area greater than 10x10 μm^2. The reason can be found again by observing the potential a current distribution in the device. In Figure 4.3(c) and (d), these quantities are presented over a 14x14 μm^2 domain. Border effects are, here, much less influential on the behavior of the network, since many electrical paths contributing to the transport average them out. In this case, several nominal identical networks will show much smaller differences between them, granting a much smaller spread of the results.

The small differences in Figure 4.2 between the experiments and the simulations are most likely due to the fact that real devices, although they are on the same wafer and measured sequentially, experience different working conditions. It is well known that molecules in the atmosphere (especially oxygen) affect the behavior of the network in several ways [52, 53]. The amount of attached molecules reasonably depends on the morphology of the networks, which is different for every device. This phenomenon additionally increases the spread of the results. In the simulated devices in Figure 4.2, however, the networks are assumed to withstand the same amount of molecules, regardless their morphology.

4.2.2 Uniformity of the Film

The greatest influence on the conductive behavior of a CNT film is given by the density of nanotubes in the network. As already mentioned in Section 4.1, the amount of nanotubes greatly affects the number of percolation paths in the network, and consequently the capacity of carrying current between the two electrodes. If the density is not enough to guarantee at least one percolation path, the film is completely insulating. By increasing more and more the density, the connectivity of the network increases, and in turn, the conductive capability improves. The choice of the optimal density is subordinate to the application target. To cite an example, if the film is designed to be used as a transparent electrode for photovoltaic applications, the goal is to obtain a uniform, highly conductive and transparent film. Once again, as already explained in Section 2.4.1 there is a trade-off between the conductive property of the network and the transparency of the film. For other applications, where the resistance of the network is not the primary goal, it is often convenient to have

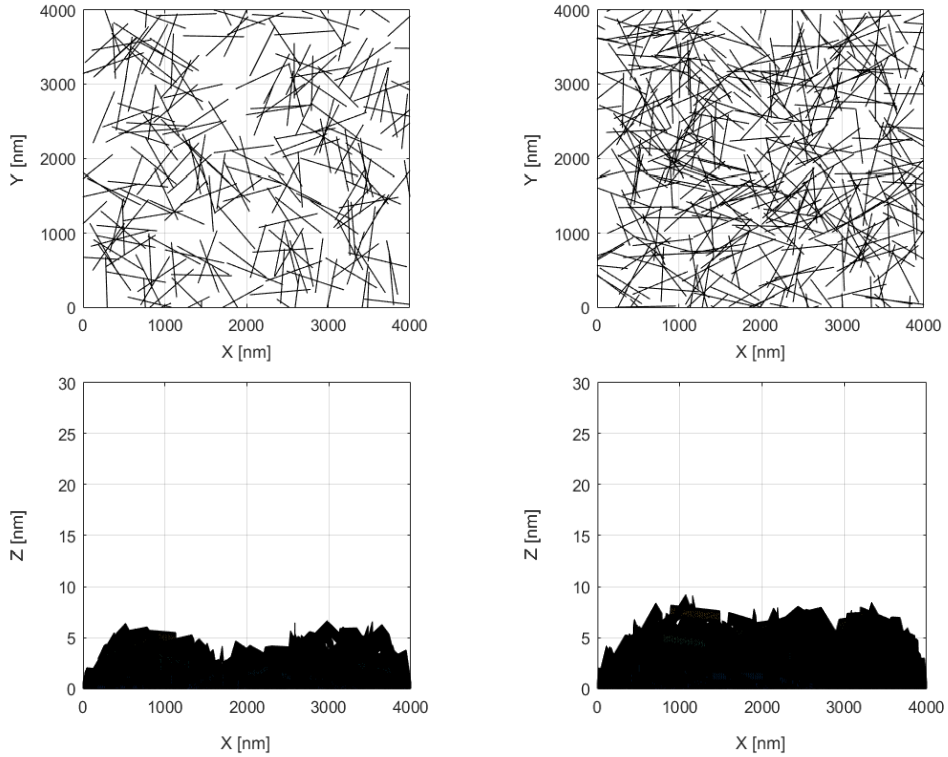

Figure 4.4: Plot of two different morphologies. On the left side a low density network (18 CNTs/μm^2) both from top and side view; on the right side the same plots for a network with higher density (30 CNTs/μm^2).

very thin and sparse networks, as it will be further explain in the next chapter.

The simulations can help in this case in the design of these films, by giving an estimation on the uniformity and thickness of the network. Figure 4.4 shows an example of two generated networks with different densities. The thin film has a low density of nanotubes per unit area (approximately around 18 CNTs/μm^2) whereas the thicker one has an higher density of approximately 30 CNTs/μm^2. In the side view pictures it is important to pay attention to the dimensions; in point of fact, the irregularity on the Z-axis is amplified by the scale compression along the X-axis. However, such a picture helps in visualizing the previously mentioned border effects, which are the main responsible for the broad results spread in films with a small area.

As previously stated, the increase in the nanotubes density leads to an improved conductive capacity of the network. There is also, however, a less evident effect of the density of nanotubes, which affects the aforementioned spread of the results. From a morphological point of view, a dense network is much more uniform than a sparse one. In a limit (but unrealistic case) a highly dense network

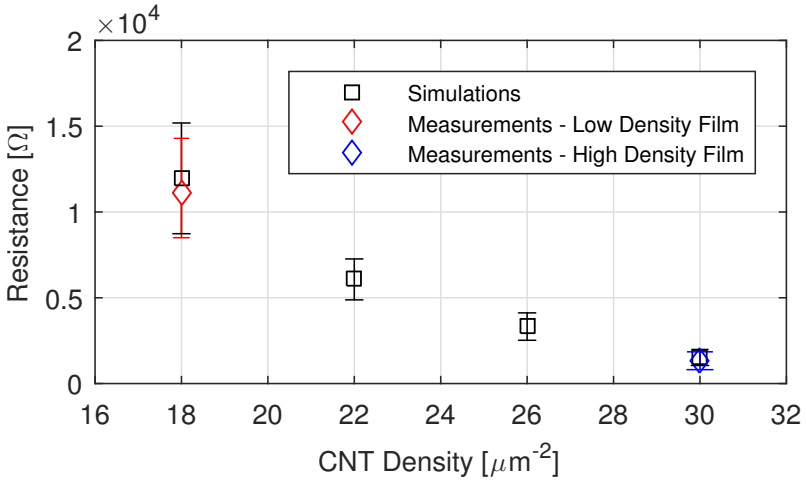

Figure 4.5: Plot of the resistance versus the CNT density of the film. Red error bar: spread of the results between nine devices with a nominal density of 18 CNTs/μm^2. Blue error bar: spread of the results between nine devices with a nominal density of 30 CNTs/μm^2.

has an electrical behavior that approaches the one of a uniform bulk material. At a first sight, without considering how the transport actually happens, it is reasonable to assume that different films would look much more equal to each other in the case of dense film rather than in sparse ones. In other words, dense networks have many more morphological similarities between each other. This is indeed reflected also on the transport properties; a huge number of percolation paths averages out the variability due to stochastic fluctuations. As an example, the resistance of a network with 100 possible percolation paths is almost identical to the one of a network with 95 paths. This is not applicable to a film with 10 possible paths, where even one or two paths more can make a huge difference. All these considerations are reflected in a smaller spread of the results in dense films, as it is shown by the comparative study in Figure 4.5.

In this particular analysis, two wafers of different densities with nine devices each have been studied both experimentally and simulated with the proposed tool. The low-density wafer has 18 CNTs/μm^2, while the second one has a higher density that is 30 CNTs/μm^2. As it stands out, the denser the film, the less pronounced the spread of the results. It is worth to notice that the aforementioned effect of the molecules on the film is less invasive in dense networks rather than sparse networks. This statement finds confirmation in some experiments that show how the sensitivity to molecules absorption changes with respect to the density of the film [136].

4.2.3 Striping, Changing Domains

Previously, in Section 4.1, the concept of conductivity in CNT networks has been discussed, highlighting the differences respect to conventional semiconductors. Since these films are really thin (in the nm range) it is not trivial to define a specific conductivity for the material. The conductivity, or its reciprocal, the resistivity, is a property of the material, which in principle, does not change depending on the amount of material considered. This is actually the difference between resistivity and resistance. As an example, a piece of silicon, with a specific volume, has a certain value of resistance, expressed in Ω and a certain value of resistivity, expressed in Ωm. The relation between the two quantities is the following:

$$R = \rho \frac{l}{\Sigma}, \tag{4.1}$$

where ρ is the resistivity, l the length of the material and Σ the cross-section where the current flows. Assuming a constant resistivity, if the cross-section of the material is for example reduced to half of its original value, the resistance would in turn be doubled. This is what, within certain limits, has been also experimentally observed. By measuring the resistance value of different volumes of the same material, the resistivity has always the same value. All these considerations are not valid anymore when considering CNT networks. If the cross-section of a CNT film is reduced to half of its original value, the resulting resistance is not simply doubled.

In order to prove that, a numerical experiment has been performed by altering the volume of some networks, as shown in Figure 4.6. In two different networks (the two pictures on the left) the volume has been changed by cutting half of the film in two different ways. The resulting resistance change, shows that the resistivity is not constant. The purpose of repeating the experiment on two differently dense networks, is to show that this phenomenon is much more evident for thin films. From the pictures it is clear how the effect is greater in less uniform films (i.e. thin films). In dense films, the behavior of the network is much closer to the one of a uniform material, thus the resistivity changes are reduced, for the same reasons previously discussed in Section 4.1.

More simulations have been performed by changing the aspect ratio of the net-

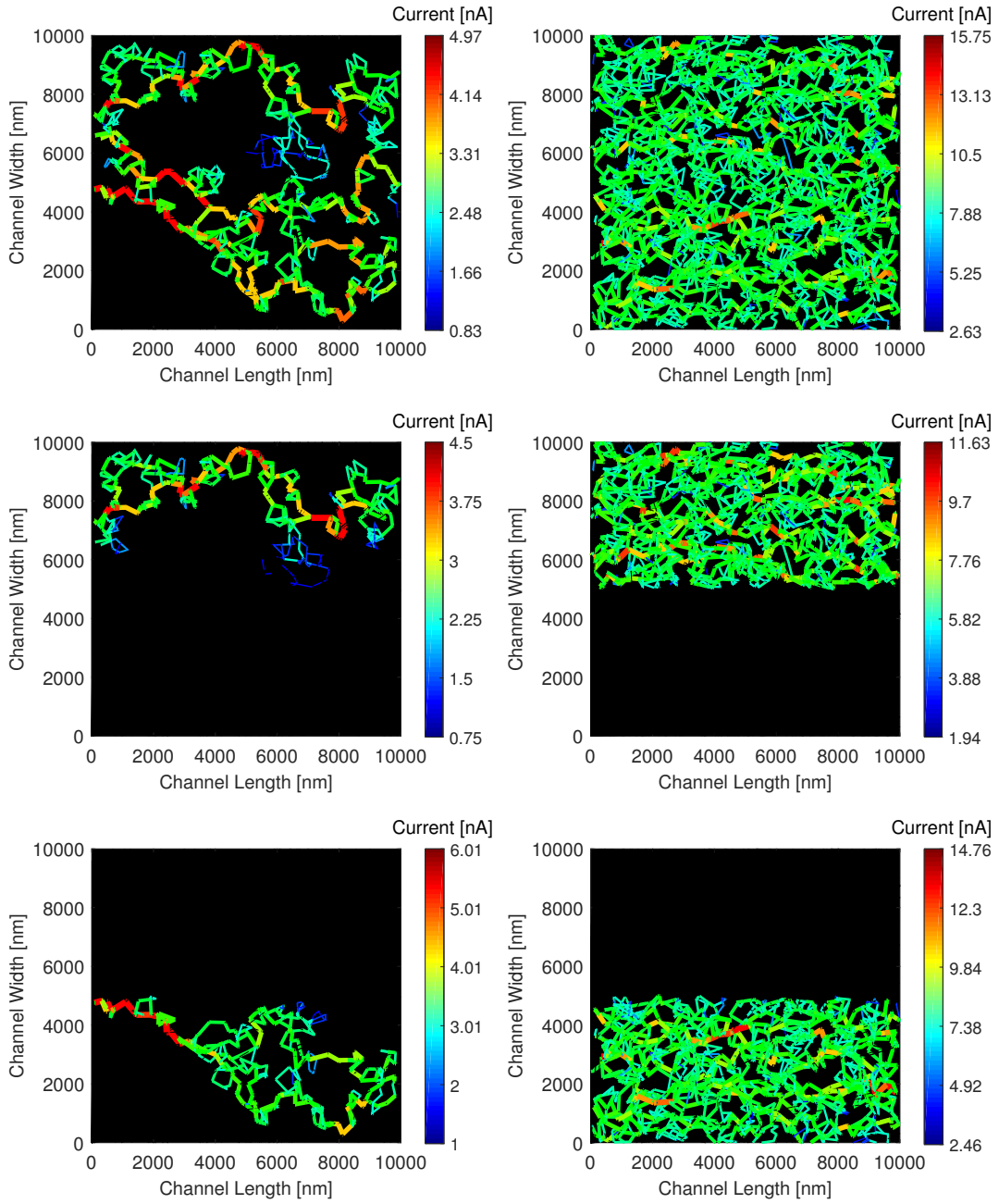

Figure 4.6: Plot of the current flow through a film of 12 CNTs/μm^2 (left) and a film of 24 CNTs/μm^2 (right). From top to bottom: the entire network, the network with the bottom half cut out and the network with the top half cut out.

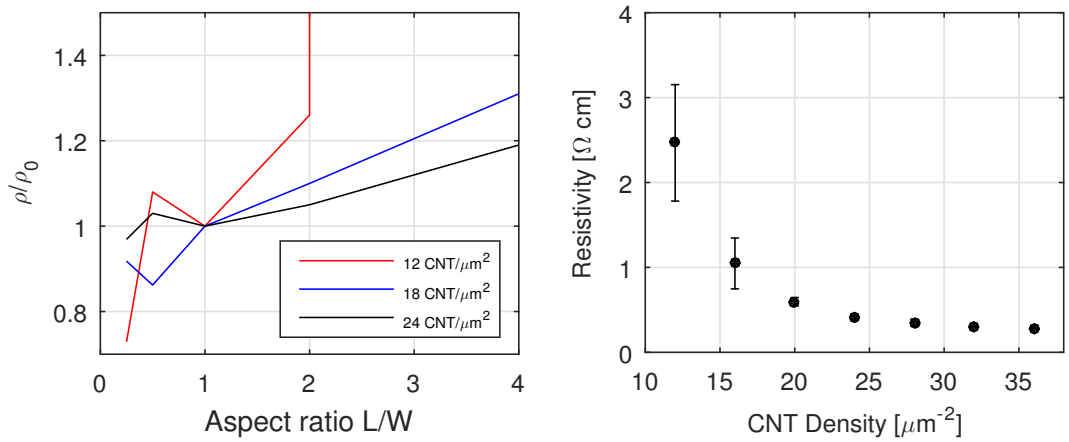

Figure 4.7: (Left) Normalized resistivity versus the aspect ratio of the simulated area for three different densities. (Right) Normalized resistivity versus the density of the nanotubes.

work, in particular by changing l and Σ of Equation 4.1. The results are presented in Figure 4.7(a) for three different densities. In one case the aspect ratio l/Σ is increased by keeping constant the cross section and increasing the length of the device. The resistivity, which has been normalized to the case where the aspect ratio is equal to one, increases, and the effect is much higher for low densities. The red curve is a limit case: with a double length, the film shows an infinite resistivity, which means that the film cannot reach the percolation threshold anymore.

It is important to specify that the cross-section, which has the dimension of a surface, depends on the width and the thickness of the device. Since the thickness is related to the density, in this experiment the cross-section is modified by changing only the width of the device. This means that, in the second case, where the aspect ratio is reduced, the width of the device has been changed, while the length has been kept fixed. The effect on the resistivity is now the opposite, since by increasing the cross section, the number of parallel percolation paths increases, and in turn, the resistivity is generally lower. The resistivity is here normalized respect to the initial network (CNT density around 12 CNTs/μm^2) and it is extrapolated by inverting Equation 4.1 once the simulation gives as output the value of the resistance, as well as an average value for the thickness of the film.

Furthermore, a similar analysis has been done on the resistivity of films with different densities, as it is shown in Figure 4.7(b). Consistently with the previous

findings, two different behaviors has been observed, depending on the density of the film. After a certain threshold, an increase of the density does not affect anymore the resistivity of the film, which tends to saturate to a certain value. As previously mentioned, when CNT networks are employed as transparent electrodes, it exists a trade-off between the resistivity and the transparency of the film. This analysis could be indeed useful for a proper design of the electrode; when the aforementioned threshold is reached, a further increase of the film thickness will not bring any appreciable benefit to the conductivity of the network, but it will drastically reduce the transparency of the film.

4.3 Percolation Threshold

So far, it has been showed that a CNT network can have different electrical behaviors according to how different parameters are related to each other. Among these parameters, the density of nanotubes per unit area and the device dimensions, are certainly the most important. It makes now sense to define a certain property of the CNT networks that connects these two parameters: the percolation threshold. As already briefly mentioned, a film below the percolation threshold does not have any path that connects the two electrodes, thus presenting an insulating behavior. The knowledge of this threshold is very important, since a lot of networks are usually designed to be very close to their percolation threshold. A film that has a density of nanotubes slightly above this threshold, forms a sort of mono-layer with some unique properties. The most important one, is that a small change in the environment causes a big change in the electrical properties of the network, making it very suitable for sensing applications (see Chapter 5). For similar reasons, a small change in the electrical boundary conditions, causes a big change in the electrical output, which is a primary criteria for the design of thin-film transistors (see Chapter 6). While designing such a network experimentally could be really time-demanding, with the help of the simulation this can be done after a statistical analysis of several samples.

In Figure 4.8 the percolation probability of films with different densities is presented. It is important to notice that the percolation threshold merely depends on the geometry of the network. The electrical properties of the single nanotubes have no impact on the threshold. The parameters that have a big impact are the following:

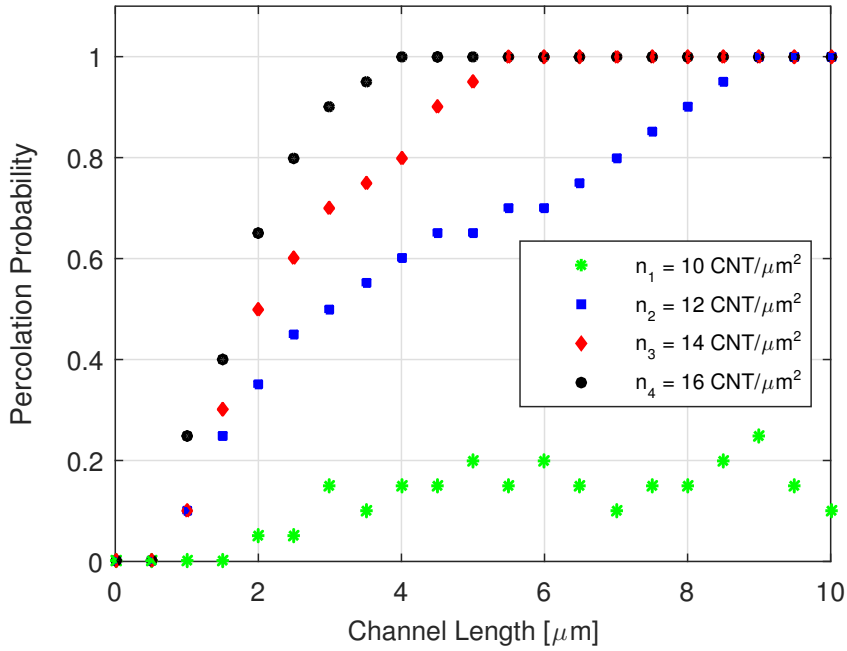

Figure 4.8: Plot of the percolation probability versus the simulation domain area. The multiple curves represent different CNT densities. Each point is the result of 20 different generated networks.

- **CNT density:** It dictates the probability of having percolation paths between the two electrodes. A linear increase of the density does not produce a linear increase of the number of paths, which is much higher. The effect of the density tends to saturate for really highly dense films;
- **Device domain:** It has a huge impact on the percolation probability. Wide and short devices have a higher probability to have paths between the electrodes, while in narrow and long devices the probability drops consistently. The choice of a proper device domain strictly depends on the CNT density of the film.
- **Nanotubes length distribution:** Not mentioned so far, it has a very important effect on the percolation probability. Since it contributes to the geometrical properties of the film, it must be taken into account together with the density of CNTs and the choice of the domain. Very short nanotubes (compared to the length of the device) drastically reduce the probability of having a direct path between the electrodes.

The plot of Figure 4.8 is the results of a statistical analysis, done for different films on different simulation domains. The aspect ratio of the domain is equal to one (the shape of the device is a square) and the lengths of the nanotubes

are described by a very narrow log-normal distribution centered around 744 nm, with a variance of 9.5 nm. As it turns out, if the density of nanotubes is not enough (green curve), the film will never reach the percolation threshold, no matter how big the domain is. Once again, this strictly depends on the distribution length; with very long nanotubes, the previous statement might not be true. By increasing the density of nanotubes, the film has a higher probability to have a direct connection between the electrodes. The percolation threshold for denser films is achieved with smaller domains.

The results of this analysis are in good agreement with some theoretical work presented in the literature [95], where the density of nanotubes necessary to reach the percolation threshold follows the expression:

$$n_{perc} = \frac{1}{\pi}\left(\frac{4.236}{L_{tube}}\right)^2 \tag{4.2}$$

where n_{perc} is the density limit and L_{tube} is the average length of nanotubes. By taking the average length at 744 nm, the minimum density to reach the threshold results to be $\sim$10 CNTs/μm^2, regardless the simulation domain area. However, depending on the area of the device, the threshold may or may not be reached, for the reasons discussed earlier about the border effects.

4.3.1 The Effect of the Length Distribution

Intuitively, the percolation threshold depends on the average length of the nanotubes. Having long nanotubes helps greatly to reach the percolation, since it increases the possibility that the nanotubes connect the two electrodes. Ideally, a very long nanotube, correctly positioned between two electrodes, is sufficient to reach the percolation threshold. This is confirmed also from Pike's theory; from Equation(4.2) it is clear that when the length increases, the minimum density of nanotubes necessary to reach the percolation threshold is reduced. Once again, it is important to highlight that the formula is somehow incomplete, since it does not take into account the shape of the simulation domain, which is considered as square-shaped. Furthermore, its predictability fails when treating very long nanotubes. In this regard, the numerical simulation can provide a more accurate statistical analysis of the influence of the length distribution function on the percolation threshold of differently shaped networks.

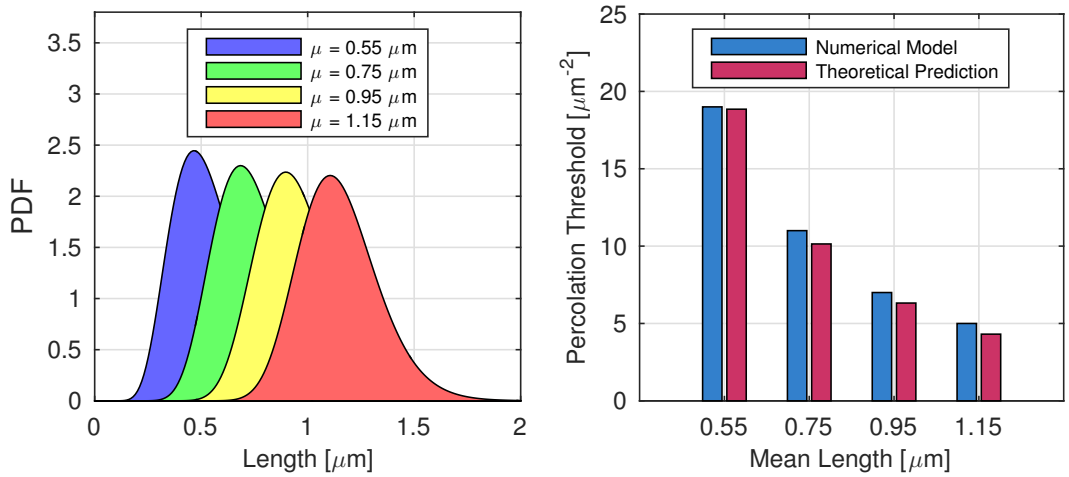

Figure 4.9: (Left) Plot of four different probability distribution functions for the lengths of the nanotubes. (Right) Comparison between the theoretical work from Pike and the numerical simulations performed during this work. The comparison is based on the probability distribution functions of the left figure.

In Figure 4.9, as an example, the percolation threshold of networks with different length distributions is represented and compared with the theoretical work of Pike. For square-shaped simulation domains, with lengths smaller than the device dimensions of at least one order of magnitude, the agreement between the model and the theory predictions is remarkable.

4.4 AC Conductivity

Until this point, the presented model has shown its validity in simulating the resistive behavior of the films, but its capabilities are still quite limited. Indeed, even a very complex network of resistances, can be eventually simplified to a unique equivalent resistance, which represents the overall behavior of the film. Such a simulation can only provide information about the resistance of the film.

However, in order to fully understand the electrical behavior of CNT thin-films, further analyses that go beyond what has been shown so far are needed. By changing opportunely the content of the blocks constituting the network, one can include additional physical models, and therefore increase the level of the simulations details.

One noteworthy analysis is certainly the AC conductivity study, in which the response of the film is given in terms of the complex impedence. The importance

of this analysis lies in the facts that the behavior of the film at high frequencies could be substantially different to the one in the DC regime. The reason is related to the presence of reactive elements in the system, namely capacitances and inductances, which modify the total impedence of the network depending on the frequency of the applied signal.

Quantifying the contribution of these elements, and understanding their derivation from physical phenomena, is an important aspect of the CNT films design. The frequency-dependent circuit model developed herein may have direct applications in determining the switching speed of a variety of nanotube based electronic devices.

4.4.1 Equivalent Circuit for the Single Nanotubes

The advent of deep-submicron semiconductor technology spotlighted the need of properly consider the parasitic effects introduced by wires in active circuits. The overly simplistic description in which interconnections are treated as simple ideal lines loses its validity under certain circumstances. To complete the whole picture, the contributions from the parasitic resistances, capacitances and inductances must be taken into account.

The level of expertise reached in the modeling of wires in integrated circuit can be exploited also in the simulation of networks of nanotubes. Under this approximation, the nanotubes constituting the network are thought as wires interconnected between each other. The choice of the level of details in representing the parasitic components is dictated as usual by the trade-off between complexity and computing-efficiency.

A conservative approach, in which all the possible parasitic effects are included, is simply unfeasible and only applicable to very small topologies. A more rational approach would be to establish from the beginning which are the most crucial phenomena, and describe them with few dominant parameters. This particularly applies when the number of nodes in the network is really high. To achieve a meaningful analysis of the context, the designer has to have a clear insight in the parasitic effects that can affect the nanotubes in the film.

The equivalent circuit for the single nanotubes is not well established experimentally. An interesting approach is to model the nanotubes with a trans-

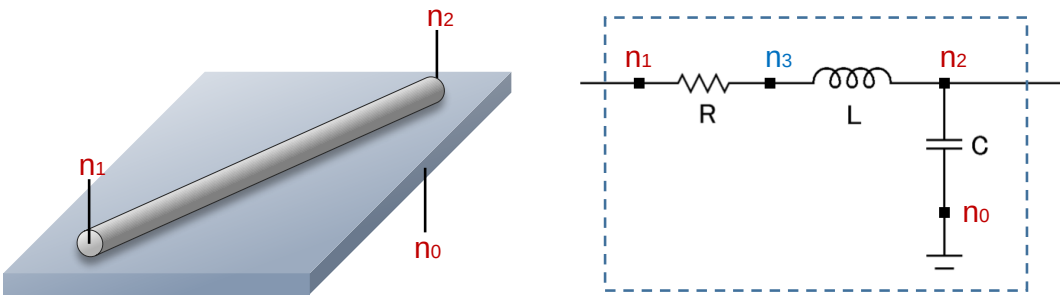

Figure 4.10: Frequency-dependent equivalent circuit for a nanotube. In red the external nodes of the sub-circuit (which are connected to the other sub-circuits of the network); in blue the only internal node.

mission line equivalent circuit that can be used to predict their dynamical impedance [137, 138]. The model proposed in this work, extends the transmission line formalism with the inclusion of the tube resistance, which is calculated according to the model presented at the beginning of the chapter. The equivalent circuit, whose diagram is illustrated in Figure 4.10, is essentially a RLC circuit.

Each component of the circuit is the result of different contributions, which will be discussed in details in the next sections.

4.4.2 The Inductive Contribution

The inductance is in general a property of an electrical conductor, by which a change in the flowing current induces an electromotive force in the conductor itself. The magnetic energy, however, is not the only energy that arises from the motion of charges. Another manifestation of energy is the kinetic energy of the electrons, which is essentially where the kinetic inductance originates according to the definition

$$E_k = \frac{1}{2} L_k I^2. \tag{4.3}$$

Indeed, the kinetic inductance can be seen in the earliest modern theory of conduction in metals by Drude [139], where the complex impedance has an imaginary term proportional to the frequency, reflecting an inductance.

The total energy arising from the motion of charges is the sum of the magnetic

and kinetic energies, which means that in circuits the kinetic inductance adds in series to the magnetic inductance.

A. Magnetic Inductance

When the distance between the nanotube and the ground plane is greater than the radius of the nanotube itself, the magnetic inductance can be simply calculated from the principles of electromagnetism [140]. The usual starting point is the current I that produces a certain magnetic field H around the tube. The two quantities are linked by Equation (4.4):

$$\oint \vec{H} \cdot d\vec{l} = I. \tag{4.4}$$

Since the boundary conditions are cylindrical, the integral can be evaluated over a circle of constant amplitude round the current. This leads to the following expression for the magnetic field as function of the current flowing through the tube:

$$\oint Hr\, d\theta = 2\pi r H = I\,. \tag{4.5}$$

Since $\mathbf{B}$ is proportional to $\mathbf{H}$ through the magnetic constant μ:

$$B = \frac{\mu I}{2\pi r}. \tag{4.6}$$

The total magnetic flux between the tube and the ground plane is thus:

$$\Phi_m = \int_d^h \frac{\mu I dr}{2\pi r} = \frac{\mu I}{2\pi} \ln\left(\frac{h}{d}\right). \tag{4.7}$$

Finally, the inductance per unit length is found from Equations (4.4) and (4.4) as

$$L_m = \frac{\mu}{2\pi} \ln\left(\frac{h}{d}\right), \tag{4.8}$$

which is expressed in Hm^{-1}. For the sake of simplicity, the situation is restricted to a nanotube over a ground-plane. However, in case there is no ground-plane,

the parameter h (the distance between the wire and the ground-plane) can be substituted with the length of the nanotube itself [138].

Since the typical oxide thickness in these applications is in the order of 100 nm, whereas a typical nanotube radius is around 1 nm, the value of the magnetic inductance per unit length is in the order of 1 pH/μm.

B. Kinetic Inductance

Kinetic inductance originates in the kinetic energy required by each electron that is contributing to a flow of current. In general the electrons in a solid are moving around continuously, evenly distributed among all the possible directions in the crystal. Thus they all possess kinetic energy even when no current flows. When a current flows the electric field adds a small drift velocity component to the whole electron distribution which requires the electron system to acquire kinetic energy:

In a normal or superconducting material this kinetic energy is equivalent mathematically to the energy invested in creating a magnetic field - the energy is effectively stored until the electrons decelerate again. This is often neglected in normal materials, where electrons scatter repeatedly, resulting in dissipation of the kinetic energy. In this respect, CNTs are interesting because, although they are not superconductors, they possess a very long mean-free-path. As a result, it is expected that the kinetic inductance in CNTs starts to play a role at frequencies around 100 GHz, which is potentially useful for high-frequency electronics [141].

The kinetic energy per unit length in a generical 1-D wire is the algebraic sum of the kinetic energies of the left-moving carriers and the right-moving ones. At equilibrium, the net sum is equal to zero. If the number of left-movers is for example higher than the one of right-movers, a net current can flow through the wire. If the Fermi level of the left-movers is increased by $e\Delta\mu/2$ (under an applied bias), the Fermi level of the right-movers will be decreased by the same amount.

The net increase in energy of the system is the excess number of electrons N in the left versus right moving states, times the energy added per electron ε_n:

$$E_k = N\,\varepsilon_n = \frac{e\Delta\mu}{2\delta}\,\frac{e\Delta\mu}{2} = \left(\frac{e\Delta\mu}{2}\right)^2 \frac{1}{\delta}\,, \tag{4.9}$$

where δ is the single carrier energy [142], which can be expressed in terms of the Fermi velocity v_F through the following expression:

$$\delta = \frac{hv_F}{l}\,. \tag{4.10}$$

The kinetic inductance per unit length is determined by equating Equations (4.9) to the energy that is stored in an inductor:

$$L_k = \frac{h}{2e^2 v_F}\,. \tag{4.11}$$

With $v_F \approx 10^8$ cm s^{-1}, the kinetic inductance is approximately 3 nH/μm.

C. Total Inductance

It is worth noticing that the kinetic inductance is significantly higher than the magnetic inductance (three orders of magnitude). Since the total effect of the two inductances is given by the series of the two,it follows that the inductive behavior of the nanotube is almost entirely given by the kinetic inductance.

A quantitative estimation of L_k for semiconducting CNTs remains still an open question. In CNT transistor modeling and analysis, L_k is taken to be in the same order of magnitude as the one calculated from Equations (4.11). Although this might seems a big approximation of the problem, it allows to have a rough estimation on the inductive behavior at high-frequencies.

However, as already mentioned, such low values for the inductance are not relevant for frequencies lower than several GHz. The applications here studied are thought to be used for much lower frequencies (max frequency around 2 MHz), hence the inductance will be from now on neglected in the equivalent circuit of the carbon nanotubes.

4.4.3 The Capacitive Contribution

Similarly to the inductance, the capacitance showed in the equivalent circuit of Figure 4.10 is the result of the sum of different contributions, which are herein discussed. The electronic capacitance of a one-dimensional system such as a CNT is a thermodynamic quantity that contains fundamental information about the ground state1. It is composed of an electrostatic component describing the interactions between electrons, and a kinetic term given by the electronic density of states.

A. Electrostatic Capacitance

Also in this case, the findings of the transmission lines theory can be applied to the CNTs [143]. In this respect, the capacitance is calculated by equating the capacitive energy to the stored electrostatic energy:

$$\frac{Q}{2C} = \frac{1}{2}\int_V E \cdot D \, dV \,, \tag{4.12}$$

where D is the displacement of the electric field within a dielectric material. The integration is done over the entire volume of the dielectric. The reason why this capacitance is defined as an electrostatic capacitance can be found in the expression in Equation (4.12). Indeed, within this approximation, the capacitance is calculated by relating a static charge with a static electric field.

Considering the specific geometry of interest, the electrostatic capacitance between a nanotube and a ground plane is finally given by

$$C_E = \frac{2\pi\epsilon}{\cosh^{-1}(sh/d)} \approx \frac{2\pi\epsilon}{\ln(h/d)} \,, \tag{4.13}$$

where the approximation leads to good results as long as $h > 2d$. It is noteworthy that, Equation (4.13) has the same formulation of the capacitance of a coaxial cable, where d is the internal radius and h the external one.

With the same values of d and h defined before when introducing the inductance, the electrostatic capacitance can be approximated numerically as

$$C_E \approx 40aF/\mu m \,. \tag{4.14}$$

B. Quantum Capacitance

From a classical point of view, the capacitance of a conductor is determined only by its geometry. When charged, the electrons distribute themselves in a way that minimizes their electrostatic energy. In quantum mechanics however, extra energies are introduced, which add a new contribution to the capacitance, the so-called quantum capacitance. While in a classical electron gas (of whatever dimensionality) adding an extra electron to the system does not cost any energy, in a quantum electron gas, due to the Pauli exclusion principle it is not possible to add an electron with energy less than the Fermi energy E_F [144].

CNTs have a rather low density of states per unit energy around the Fermi level. This causes the average energy spacing between the states to be much larger than in common metals [145]. When an applied potential is charging a nanotube, the Fermi level shifts by this large energy spacing for each state that has been either filled or depleted.

The rigorous expression of the quantum capacitance is

$$C_Q = \frac{\partial Q}{\partial V_A}\,, \tag{4.15}$$

where Q is the charge density and V_A the applied potential. In case the density of states is symmetric with respect to the Fermi level, the charge density can be written as

$$C_Q = \frac{\partial Q}{\partial V_A}\,, \tag{4.16}$$

where $g(E)$ is the density of states of the nanotube [146]. For a linear energy-wavevector relation, such as that near the Fermi level in graphene and in metallic CNTs, the density of states is constant. As proposed by Burke [138], if the applied voltage is such that the Fermi function is approximately zero before the first van Hove singularity, the quantum capacitance can be expressed as follows:

$$C_Q = \frac{2q^2}{hv_F}\,. \tag{4.17}$$

which comes out to be numerically equal to 100 $aF/\mu m$ when considering the Fermi velocity of graphene as equal to $8 \cdot 10^5\, m/s$.

From more recent calculations, values from the quantum capacitance of different nanotubes have been reported in a range from 140 $aF/\mu m$ up to more than 380 $aF/\mu m$ [147].

C. Total Capacitance

As the energies are simply additive, and since the capacitance is inversely proportional to the energy, the aforesaid capacitances are added in series, to yield the total capacitance:

$$C_{\text{tot}}^{-1} = C_E^{-1} + C_Q^{-1}. \tag{4.18}$$

With the values founded for the nanotubes in these particular configurations, the total capacitance varies between values from $\sim 28\ aF/\mu m$ to $\sim 36\ aF/\mu m$.

4.5 Parameter Extraction and Scaling

The equivalent circuit of each nanotube is compiled into individual sub-circuits that are saved in a library file. Every nanotube has a different resistance value (calculated following the theory of Chapter 3) and a different capacitance, due to the fact that the every nanotube in the network has a specific length.

Basically the program applies the same method already presented for the DC conductivity, and it only replaces the resistances with the complete equivalent circuit. However, this kind of simulation requires a further step. While in the former case of DC analysis, the small simulation domain could be extended to the real device dimension through a simple linear scaling, here few precautions must be taken. The more complicate topology of the circuit requires a different approach, in which the simulation is divided into two consecutive steps. During the first step, the area of the simulation domain is simulated and a macro-equivalent circuit is extracted. Afterwards, the extracted circuit is extended to the dimension of the entire device through series and parallel connections, as it is schematically illustrated in Figure 4.11. Finally the behavior of the entire network can be analyzed.

This approach is based on the assumption that every section of the entire device

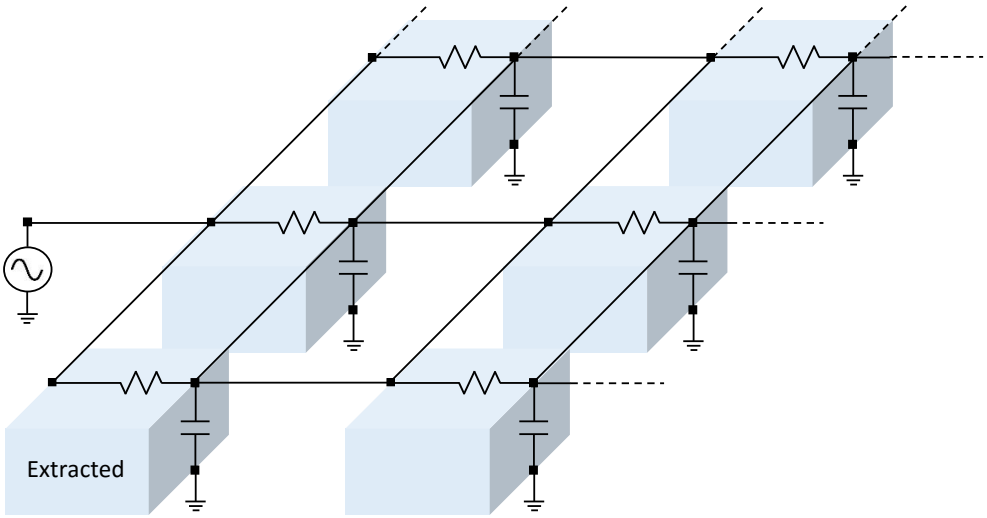

Figure 4.11: Schematic representation of the multi-level approach for the simulation of big devices. From the bottom-left block, the effective parameters are first extracted and then extended to the entire area of the real device.

can be reasonably described by the same equivalent circuit, an approximation that can be considered valid when the dimensions of the simulated area are much bigger than the dimensions of the single nanotubes. This hypothesis is supported by the same considerations given in the previous sections on the border effects and the simulation domains effects.

4.5.1 Parasitic Capacitance

Before continuing, it is useful to briefly summarize what has been done until this point. Conceptually, the simulation of the AC behavior of a network is divided into two consecutive steps. During the first one, the equivalent circuit of a single nanotube is calculated and inserted in a small portion of the network, which is then simulated with the same approach presented in the previous chapter. However, the higher complexity of the network does not allow a linear and uniform scaling up to the real device dimensions. Therefore, a second step has been introduced, in which the results from the small simulation domain are properly scaled as explained in the previous section.

Nonetheless, another consideration is needed. The entire device that is measured is a system composed by the CNT network and by an IDES structure like the one showed in Figure 4.1. As already mentioned, the metal electrodes are deposited

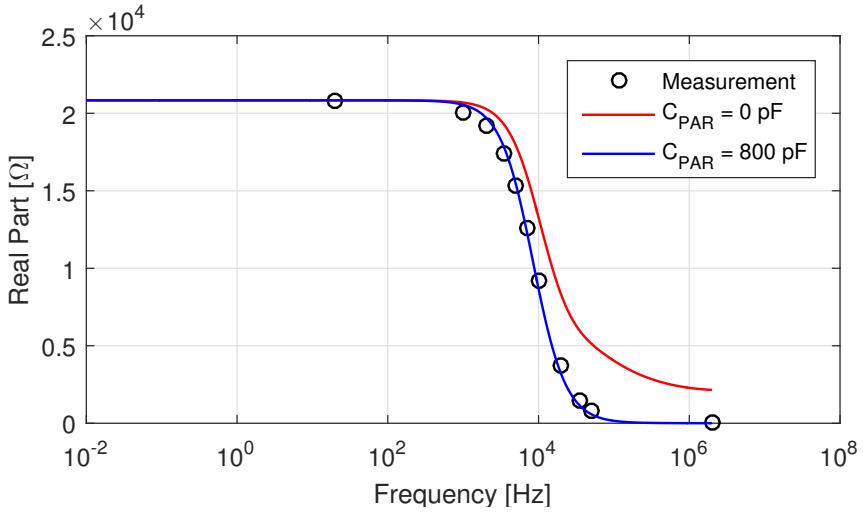

Figure 4.12: Plot of the real part of the complex impedance of a network versus the frequency of the applied electrical signal. The two continuous curves represent cases with different values for the parasitic capacitance; the black circles are the experimental measurements.

over a SiO_2 layer, which is grown over a heavily doped Si substrate. This particular configuration introduces a not negligible parasitic capacitance, which is estimated to be around 800 pF.

To understand the effect of the parasitic capacitance, it is useful to analyze Figure 4.12. As it comes out, the network simulated without considering the parasitic capacitance has a different behavior respect to what it is experimentally observed. The most important aspect, is that the slopes of the two curves are different. Both the curves resemble the behavior of a low-pass filter; however, the curve resulting from the measurements seems to be from a filter of one order higher. Indeed, changing the capacitance of the single nanotubes will simply shift the cut-off frequency of the curve, but not modify the slope of the curve. To keep the analogy with the filters, changing the capacitance will not increase the order of the circuit. On the other hand, by considering a global parasitic capacitance between the contacts and the substrate, one can see that the simulation fit perfectly the measured curve.

4.5.2 Frequency Behavior of CNT Films

In order to have the complete picture on the frequency response of CNT films, a last contribution must be considered. So far, it has been assumed that the CNTs are unaffected by the surrounding CNTs. It is well established that in

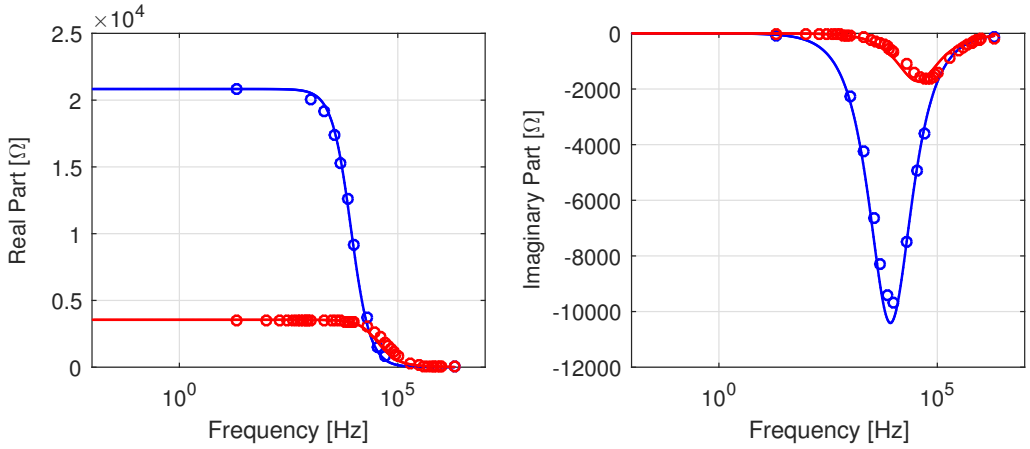

Figure 4.13: Real (left) and imaginary (right) part of the complex impedance versus the frequency of the applied signal. The continuous lines represent the simulations, while the circles are the measurements. The model has been validated for two networks with different densities of CNTs per unit of area.

densely packed circuits, with a lot of long interconnects, coupling effects between the wires are a serious issue. Although in this case the frequency range and the charge distribution is very different from the case of dense metallic interconnects, it is reasonable to expect a small contribution from some coupling effects between the nanotubes.

These assumptions are corroborated from the experimental measurements of networks with different densities of nanotubes. In this regard, Figure 4.13 shows the plot of the real and imaginary part of the complex impedence of two networks with different densities of nanotubes per unit of area. The simulations of the same networks show a remarkable good agreement with the measurements.

However, by taking a closer look to the behavior of the two networks, it emerges that the low density network has a lower cut-off frequency respect to the high density network. If the only contribution to the capacitance of the network would come solely from the single nanotubes' capacitances, this behavior would be contradictory with the expectations. In fact, one would expect an higher cumulative capacitance from the high density network and, as a consequence, a lower cut-off frequency.

As a matter of fact, by considering the capacitive contribution of the nanotubes in the two networks to be equal, it is impossible to fit the experimental data. One could then infer that somehow the nanotubes in the low density network have a higher intrinsic capacitance. As already described in Section 4.4.3, the

Table 4.2: Parameters for the simulation of the AC behavior of two networks with different densities.

	Low Density Film	**High Density Film**
Single CNT Capacitance	33 $aF/\mu m$	30 $aF/\mu m$
Parasitic Capacitance	800 pF	800 pF
Extracted Resistance	$10^7\,\Omega$	$1.7 \cdot 10^6\,\Omega$
Extracted Capacitance	$3.4 \cdot 10^{-14}\,F$	$2.6 \cdot 10^{-14}\,F$
Cut-off Frequency	$\sim 5.5\ kHz$	$\sim 24\ kHz$

predicted capacitance of a single nanotube for this device configuration would be something in between $\sim$ 28 $aF/\mu m$ to $\sim$ 36 $aF/\mu m$. The fitting of the experimental curves has been here obtained with a value of 33 $aF/\mu m$ for the low density network, and of 30 $aF/\mu m$ for the high density network. Both the values are perfectly in the range expected from the theoretical calculations.

However, it is important to give an explanation on why the nanotubes on the low density network have a higher capacitance respect to the ones in the high density network. On this regard, two considerations are crucial. Assuming that all the nanotubes are perfectly the same, with the same electrical properties and hence the same quantum capacitance. The same assumption does not hold for the electrostatic capacitance. In fact, while one could reasonably estimate the electrostatic capacitance of a low density network, this is less trivial when the network is rather dense. A low density network is very close to form a very thin monolayer, in which all the nanotubes can be considered to share the same distance from the ground plane. In a high density network, a not negligible percentage of nanotubes are on top of a layer of nanotubes. Due to this fact, the calculation of the electrostatic capacitance it is not straightforward. The nanotubes on top are screened by the nanotubes forming the first monolayer, hence they posses a much lower capacitance. In order to keep the model simple, this phenomenon can be included by considering that the average value of the nanotubes' capacitance is a bit lower than expected.

Moreover, one should consider the coupling capacitance between the nanotubes in the network. In a high density network, the nanotubes are much more connected between each other. This reduces the coupling capacitance between them, which is expected to be a bit higher in low density networks. The effect of these two phenomena combined makes the capacitance of the nanotubes in the low density network (in reality the average value) a bit higher than the one of the

high density network. The difference, which seems to be very small on the single nanotube (3 $aF/\mu m$), has however a big impact when extended to the entire network. The summary of all the parameters extracted and simulated is given in Table 4.2.

Chapter 5

Sensing the Environment

The subject of this chapter is the study of how a CNT film changes its electrical properties when exposed to different environmental changes. In the opening chapter, it has been highlighted that one of the main properties of CNTs is the ability to change their transport properties after interactions with certain molecules, which has made possible the realization of CNT-based gas sensors. The other interesting feature is that the nanotubes change their conductivity after a temperature variation, making them appealing for temperature-sensors applications as well.

Although these devices have been studied experimentally, not so much has been done from a numerical point of view. In this regard, simulations could help in the design of sensors with good performance. As it will be shown, many parameters, such as the density of nanotubes and the ratio metallic-semiconducting CNTs, have a substantial influence on the overall performance of the device.

Before getting to the heart of the matter, it is important to clarify some of the aspects concerning the doping of the nanotubes. As already mentioned in the first chapter, it has been demonstrated that oxygen molecules have a strong effect on the electronic structure of a nanotube, in a way that resemble a p-type doping effect. This core finding, will be explored through some simplified models in the first part of the chapter, in order to better understand the sensing mechanisms in the network, which will be presented in the last sections. Although temperature and molecules effects are treated in separate sections, it is worth mentioning that the two are intimately connected. In fact, all the parameters of interest in the adsorption (and de-adsorption) of the molecules are temperature-dependent.

5.1 Doping of the Nanotube

The observations reported on the p-type behavior of CNT-based devices have attributed the doping effect to the absorption of oxygen from the ambient air [86, 148, 149]. It has been shown, both theoretically [52] and experimentally [150], that CNTs are particularly sensitive to the absorption of some molecules, which induces a charge transfer mechanism, altering the conductive property of the nanotube. However, in single-CNT based FETs, the phenomenon is still part of a controversial debate, in which some groups claim that the main effect of the oxygen absorption is the adjustment of the Schottky barrier between the contacts and the nanotube [151, 152]. In spite of this argument, for CNT films, thermoelectric power measurements have proved that the main effect is a sort of bulk-doping of all the CNTs in the network, rather than a negligible effect of the contact metal [86, 148].

From the theoretical point of view, a rigorous treatment of the problem would require an *ab initio* calculation of the Hamiltonian and the overlap matrices (in atomic orbital basis) for the conducting channel and for each layer of the semi-infinite contacts, as well as the corresponding coupling matrices between them [153, 154]. Interesting studies on the modulation of the electronic transport of single-CNT devices with absorbed molecules have been carried on in details elsewhere [155, 156].

However, for the same motivations explained in Section 3.4.3, the approach here presented tries to maintain a relatively simple framework, by introducing some phenomenological models for the interactions between the nanotubes and the molecules.

5.2 Single CNTs and Molecules Interactions

Several research groups have been presented interesting results concerning the interaction between gas molecules and individual CNTs [52, 157, 53]. The most successful models are based on Density Functional Theory (DFT) calculations of the relaxed position of the molecule on the nanotube. In this work however, only the main results of these works will be presented and used as input for the implemented phenomenological models.

These complex calculations usually give three main parameters as output: the equilibrium tube-molecule distance, the adsorption energy, and the charge transfer. In general, the mechanisms of interaction has been identified to be physisoprtion. In fact, all the studied molecules are weakly binded to the nanotube, and the long equilibrium distance with no significant overlap of the electron densities excludes the possibility of the formation of chemical bonds. It is worth to mention that in these cases the nanotubes are assumed to be ideal, with no defects or preferential adsorption sites.

Most of the molecules have shown charge donors behavior, with the exception of O_2 and NO_2 that are acceptors instead. With the same exceptions, all the molecules have a weak binding energy (less than 0.2 eV), whereas for O_2 and NO_2 the charge transfer and adsorption energies are not negligible. To cite an example, NO_2 molecules on (10,0) SWNT have an adsoprtion energy in the range of 0.3-0.8 eV and distance of 0.2-0.3 nm [158]. These results can further support the considerations previously exposed for the oxygen molecules and the doping of the nanotubes. Furthermore, it has been observed that the binding energies are not too sensitive to the orientation of the molecule or to the position at which it is attached to the nanotube (energy differences in the order of k_BT at room temperature).

Regardless the type of molecule and nanotube, it is clear that the molecules have some effect on the nanotube. In a way, the charge transfer from the molecule to the nanotube, resemble a sort of gate effect on the nanotube itself. To be more specific, the molecule changes locally the potential profile of the nanotube, like if it is acting as a gate electrode. The idea is to take advantage of this analogy and the almost straightforward implementation of a gate effect in the NEGF formalism, in order to model the change in the transport due to molecules physisoprtion.

Another seminal results is that the molecules have almost the same charge transfer, distance and binding energy respect to the nanotube, regardless the chirality of the nanotube itself [52]. However, the same charge transfer can have different impacts on the transport depending on the chirality. This statement is further clarified in Figure 5.1, where the effect on a semiconducting CNT is compared with the one on a metallic CNT. The curves are obtained applying a small gate voltage, which is dependent on the charge transfer from the molecule to the nanotube. While in semiconducting nanotubes the change in the IV characteristic is

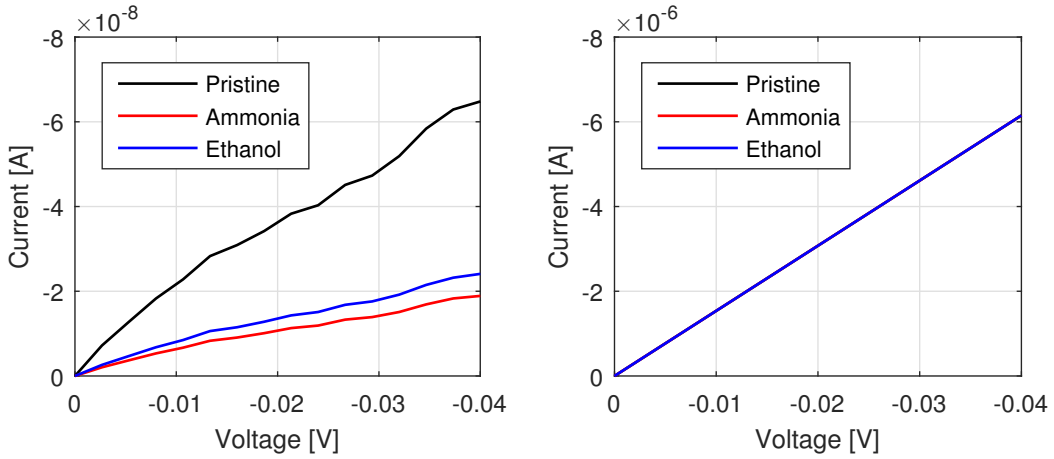

Figure 5.1: (Left) Effect of different gas species on the I-V curves of a semiconducting nanotube. (Right) Same plot for a metallic nanotube.

appreciable, the same does not hold for the metallic nanotubes. The explanation can be found in the band structure of the nanotube and on the magnitude of the applied gate. Due to the particular shape of the transmission rate of the semiconducting nanotubes (an example is shown in Figure 3.10) a small gate voltage can have a big impact in the transport, thanks to the activation or deactivation of the first sub-bands, which are relatively close to the Fermi level of a doped nanotube. On the other hand, in a metallic nanotube, the transmission rate shows a very flat trend in the energy region of interest, with the first sub-bands more far in energy respect to the case of a semiconducting nanotube. For this reason, the change in current is not evident, which is also the main reason why in the design of CNT film transistors it is desirable to have the lowest content of metallic CNTs in the network. Further details on these aspects will be treated more in details in the following Chapter where the theory of the transistors is described with a similar formalism.

5.2.1 Coverage Function and Sticking Probability

Until this point, the effect of the molecules on the nanotube has been introduced, pointing out that some molecules can either donate or extract charges from the nanotube, changing thus its way of conducting the current. The phenomenon has been introduced in the NEGF calculation as a sort of gating effect which alters the transport in the nanotube. In particular, it has been showed that the ammonia molecule donates electrons to the nanotube, acting as a donor. Due to the intrinsic p-type behavior of the nanotube, this resulted in a reduced

current, and as a consequence an higher resistance. This phenomenon is exactly the fundamental principle on which the CNT film-based sensors work, and it will be the subject of Section 5.3.

However, before moving to the entire film and its sensing ability, two other important concepts must be introduced, namely the *coverage function* and the *sticking probability*.

For the surface coverage, one of the most widely accepted model, is the Langmuir isotherm model [159], which describes the dependence of the surface coverage of an adsorbed gas on the pressure of the gas at a fixed temperature. There are many other types of isotherm models (among them Temkin and Freundlich) which differ in one or more of the assumptions made in deriving the expression for the surface coverage. Although the Langmuir isotherm is one of the simplest, it still provides a useful insight into the pressure dependence of the extent of surface adsorption. The expression is the following:

$$\theta = \frac{P}{v_0\sqrt{2\pi m k_B T}}\, e^{E_B/k_B T}\,, \tag{5.1}$$

where P is the pressure of the gas, v_0 the vibrational frequency of the molecule, m the mass of the molecule, T the temperature and E_B the binding energy. The most important aspect, which will be exploited in this work, is that the surface coverage is linearly dependent on the pressure of the gas.

The second fundamental concept is the sticking probability, which some times is included directly in the the surface coverage function. The sticking probability gives an indication of what percentage of the molecules which could potentially cover the surface will actually stick on the surface itself. This function depends on many parameters and so far no analytical model is accurate enough to describe its complexity. For this reason, most of the time the sticking probability and the surface coverage functions are merged together in semi-empirical models which describes with a reasonable level of accuracy the probability the a certain amount of molecules stick on a certain surface. In the proposed model, the sticking probability is a function of two main parameters: the thickness of the film and the surface coverage.

The first dependency is based on the fact that when the network is really dense, the molecules cannot reach the nanotubes that are lying on the substrate. To

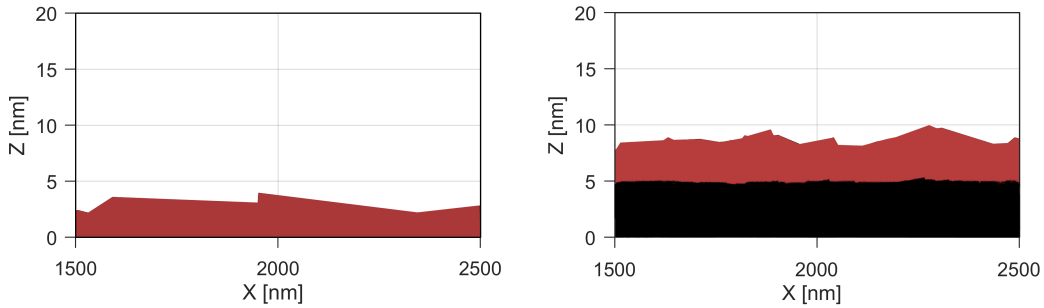

Figure 5.2: Schematic representation of the molecules coverage over the nanotubes of a thin network (left) and of a thick network (right). In red it is highlighted the region that is exposed to the molecules.

keep the model simple enough, this phenomenon is emulated by reducing the average sticking probability, to take into account that the molecules cannot be attached to these unreachable nanotubes. Mathematically, this has been expressed as function of the ratio between the average thickness of the film and the diameter of a single nanotube. As an example, if the thickness of the film is 10 times higher than the diameter of the nanotube, it means that the film is rather tick, and can be thought as the sum of ten mono-layers, stacked on top of each other. The sticking probability of such a film has to be lower than the one of a mono-layer film, in which all the nanotubes are exposed and reachable by the gas molecules. This hypothesis is schematically represented in Figure 5.2.

This theory is confirmed also by experiments in which has been shown that low density films are more sensitive to gas molecules adsorption [136]. In fact, one mono-layer has theoretically an higher ratio of adsorbed molecules per number of nanotubes, which turns out to have a greater impact on the overall resistance of the film.

The second dependency is related to the surface coverage. Although theoretically the molecules could cover a certain area defined by the surface coverage, there is no guarantee that they will stick and remain in equilibrium with the surface itself. The probability of sticking depends also on the electrostatic of the system, namely on how many molecules are already on the surface. From Equation 5.1, it seems that there is no limit to the surface coverage respect to the pressure of the gas; the coverage can in fact increase with increasing pressure, without any limit. While this equation guarantee accurate results for systems with a small amount of molecules, it must be re-adapted for this particular problem. Indeed, the coverage cannot just linearly increase, but rather saturate to

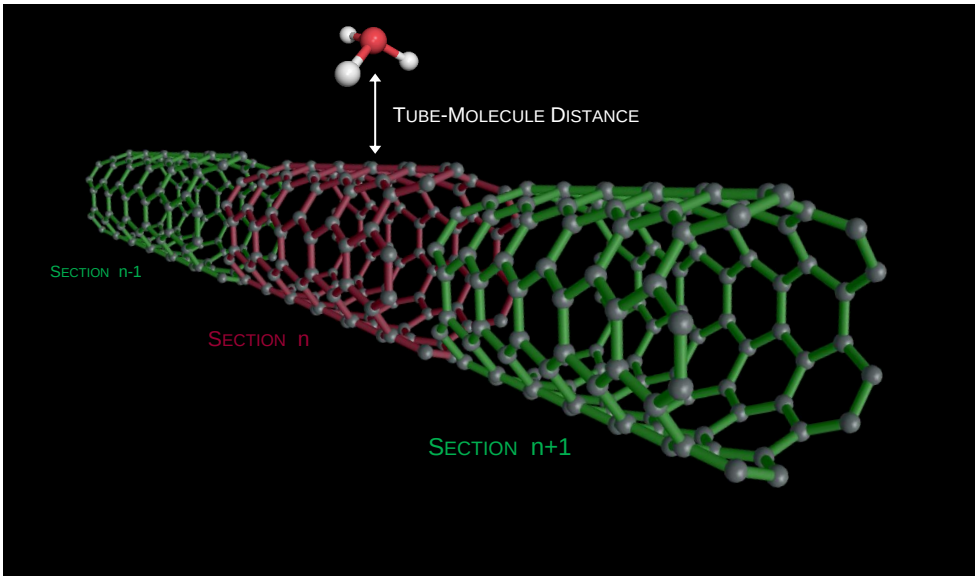

Figure 5.3: Schematic representation of the interaction between a section of a carbon nanotube and a gas molecule. In red the only region affected by the absorption of the molecule is highlighted. The other section are unaltered. The overall behavior is calculated through a weighted average between the "red regions" and the "green regions".

a certain value through a certain function.

Once the program has calculated the appropriate functions, it will assign to the nanotubes a certain number of molecules through a stochastic procedure. Every nanotube is divided into sections of the same length, and for each section a number is randomly extracted in a specific interval. If this number is less than the limit establish by the probability distribution, the number is accepted and a molecule is assign to the section. Figure 5.3 shows schematically this principle in a nanotube divided into three sections. To the second section, highlighted in red, a molecule has been assigned and therefore the local resistance has been changed with an induced gating effect by the molecule.

The length of the sections is typically very small, in the *nm* range. The total resistance of the nanotube is finally calculated with a weighted average of the resistance of the sections.

5.3 CNT film-based Gas Sensors

The model has been validated through comparison with some experimental measurements conducted on various films [160]. In the mentioned work, the CNT

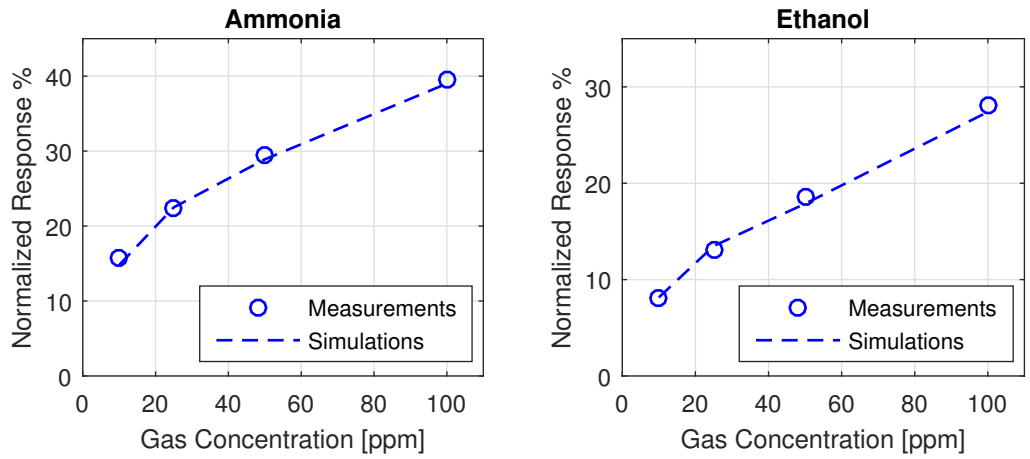

Figure 5.4: Plot that shows the comparison between simulations and experiments in terms of the normalized response of a CNT film to different gas concentrations. The left graph shows the case of an exposure to ammonia, while the right one the case of an exposure to ethanol.

films were deposited with a spray-coating technique over Si wafers with 200 nm of thermally grown SiO_2. An IDES structure, similar to the one introduced in Chapter 4, with a spacing between the fingers of 100 μm was evaporated on top of the substrate. The sensors were monitored in a gas chamber, in which a test gas was flown together with a carrier gas (N_2). The sensors were characterized in terms of the normalized response, defined as follow:

$$NR = \frac{R_f - R_i}{R_i} \tag{5.2}$$

where R_f is the resistance after exposure, while R_i the original resistance of the film. After the every exposure cycle the sensors were re-stabilized to their original resistance value through a passive recovery cycle, in which a high flux of the carrier gas at relatively high temperature was removing all the test gas molecules.

In this work, the model has been compared with these sensors for two different types of gases, namely ammonia (NH_3) and ethanol (C_2H_6O). The results are shown in Figure 5.4.

Both from the experiments and the simulations, it is clear that the resistance of the film increases after exposure to these two gases. In fact, as already mentioned in Section 5.2, most of the common gases are charge donor, while the CNTs are p-type. As a consequence, the effect of these molecules is to make the CNTs more intrinsic, increasing thus their resistance. The magnitude of

the change appears to be higher for the ammonia, indicating a higher charge transfer between the molecules and the nanotubes.

After a further look to the results, it is evident that the response is not linear with the concentration of the gas, as it would be expected if the surface coverage would be the only factor in the interactions between the nanotubes and the molecules. Indeed, the curves show a trend towards a saturation, which is more evident for the NH_3 molecules.

The function that fits properly the molecules coverage function, which is given as the product of the surface coverage and the sticking probability, has the following dependency to the pressure P:

$$MC = p_0 \, log(P)^t \,, \tag{5.3}$$

where p_0 is the normalized pressure and t a fitting exponent equal to 1.8.

5.3.1 Semiconducting Films

The comparison that has been showed in the previous section was based on a commercially available solution of unsorted SWNTs, which are 33% metallic and 67% semiconducting. While this kind of solution guarantee relatively good performance at a very reasonable cost, it represents not the optimum in terms of sensitivity of the devices. In fact, the high content of metallic nanotubes, reduces the performance of the sensors, due to the insensitivity of the metallic tubes to the adsorption of the molecules. As already shown in Section 5.2, due to the different band structure of the nanotubes, a small gating effect induced by the molecule does not produce an interesting change in the transport through the metallic nanotubes. On the other hand, semiconducting CNTs change considerably their resistance. This observation, naturally lead to the assumption that films with an high concentration of semiconducting CNTs can have a higher sensitivity respect to the unsorted solution. Although not experimentally verified in this work, some parametric simulation could help in estimate the magnitude of the increase in sensitivity when semiconducting solutions are utilized.

In this numerical experiment, four identical networks in which only the concentration of semiconducting nanotubes has been artificially changed, are compared between each other in terms of the normalized response. The results are

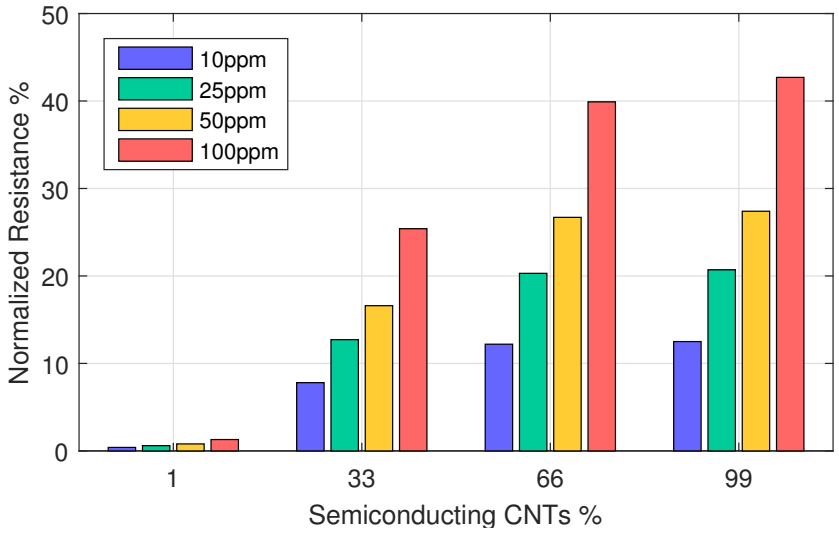

Figure 5.5: Sensitivity of different films in terms of normalized response of the film to different gas concentrations. Films with different concentrations of semiconducting nanotubes are compared between each other, showing that high concentrations of semiconducting nanotubes increase the sensitivity of the film.

presented in Figure 5.5. As expected, the film composed only by metallic nanotubes shows no appreciable variations when exposed to a certain amount of NH_3 molecules. The performance in terms of sensitivity increases considerably by increasing the amount of semiconducting nanotubes. However, by comparing the last two films, namely the film from the unsorted solution (66%) and the one from the semiconducting solution (99%), one can see only a small variation of few percent points between them. Such a small variation could not be enough to justify the higher costs related to the more expensive solution with sorted nanotubes.

5.4 Temperature Sensing

Historically, the first sensor ever developed was the thermometer. Although some of the principles of the thermometer were known to Greek philosophers of two thousand years ago, it is by the 18th century that with the introduction of standardized scales thermometers have been started to be widely used. In its broadest definition, a sensor is an object whose purpose is to detect events or changes in the surrounding environment, and to provide a corresponding output in response. According to this definition, a sensor is a type of transducer, a

device that converts one form of energy to another. A sensor can provide various types of output, which is typically either an electrical or optical signal. The nature of this signal is intimately related to the system in which the sensor is integrated. To cite an example, with the advent of the silicon integrated circuit, temperature sensors based on the band-gap of semiconductors (especially silicon) have widely spread in the market. These sensors can integrated easily on the substrate at a very low cost, and can provide signals easily readable by the circuitry.

Similarly, in the emerging field of flexible electronics, a temperature sensors must respect two main constraints: it has to be integrated on a flexible substrate and it has to produce output signals comparable to the one of the devices of interest. For these reasons, carbon nanotubes thin films are good candidate for such applications. Indeed, as already mentioned in the prefatory chapter, CNT films can be easily deposited over flexible substrate; moreover, the resistance of the film shows a dependency on the temperature of the substrate, which can be exploited for sensing purposes.

In the next few sections, all the temperature-dependent mechanisms in CNT films will be thoroughly analyzed, highlighting the importance of each of them in different working conditions and for different film typologies. Precisely, four main mechanisms have been individuated and studied:

- Temperature Dependency of Individual CNTs;
- Thermally-assisted Crossing of the Junctions;
- Mean Free Path and Scattering Events;
- De-adsorption of Oxygen Molecules.

5.4.1 Temperature Dependency of Individual CNTs

The first important aspect to be analyzed is how the transport along a single nanotube is affected by temperature changes. It is well known that semiconductors under certain conditions increase their conductivity when the temperature increases. The main reason is that the number of carriers that contributes to the current is increased by thermal excitation. The Fermi function, which defines the electronic states that are occupied by carriers, is well known to be temperature-dependent. Increasing the temperature, broadens the Fermi function and as a

consequence the number of carriers that contributes to the current.

Similar principles can be applied to carbon nanotubes. Not all the states (filled or empty) are contributing to the transport. It has been mathematically demonstrated that only the states close to the Fermi level are actually important for the transport [119]. The quantification of how much the states have to be close to the Fermi level is not trivial, but in general it is assumed to be in the energy range of a few k_BT. With the Landauer formalism introduced in Chapter 3, this is evident by taking a look at the integral in the current equation, here reported for simplicity:

$$I_i = (-\frac{q}{h}) \int_{-\infty}^{\infty} T(E)(f_1(E) - f_2(E))\, dE\,. \tag{5.4}$$

Apart from the transmission rate, what it is fundamental is the difference between the Fermi functions at the two contacts. Far from the Fermi level, the two Fermi functions $f_1(E)$ and $f_2(E)$ have practically the same value, hence the integral is zero. It is in the range close to E_F that the integral has a non-zero value, which multiplied by the transmission rate gives a certain current. By increasing the temperature, the window of energy in which the integral has a non-zero value increases, thus increasing the current.

While the effect of the temperature on the two Fermi function is always the same, regardless the species of the nanotube, that same is not true for the transmission rate $T(E)$. This fact has a major impact on the current-temperature behavior of the nanotubes, and it is what distinguishes the behavior of metallic and semiconducting nanotubes. From NEGF simulations, one can clearly see this difference, as reported in Figure 5.6.

Due to the different shape of the transmission rate (as shown in Figure 3.10), the effect of the temperature on the IV characteristic can be very different. In fact, in a metallic nanotube, the transmission rate has a non-zero value for a wide range of energies, with the first sub-bands far away from the Fermi level. The variation of the current is thus minimal, and not appreciable for the temperatures of interest in this study, as shown in Figure 5.6(b). On the other hand, semiconducting nanotubes have a narrower band-gap, with a Fermi level that, due to the doping, is close to the edge of one of the sub-bands. In this case, broadening the Fermi function can have a substantial effect on the current, due to a greater overlap of the function inside the integral. This particular case is

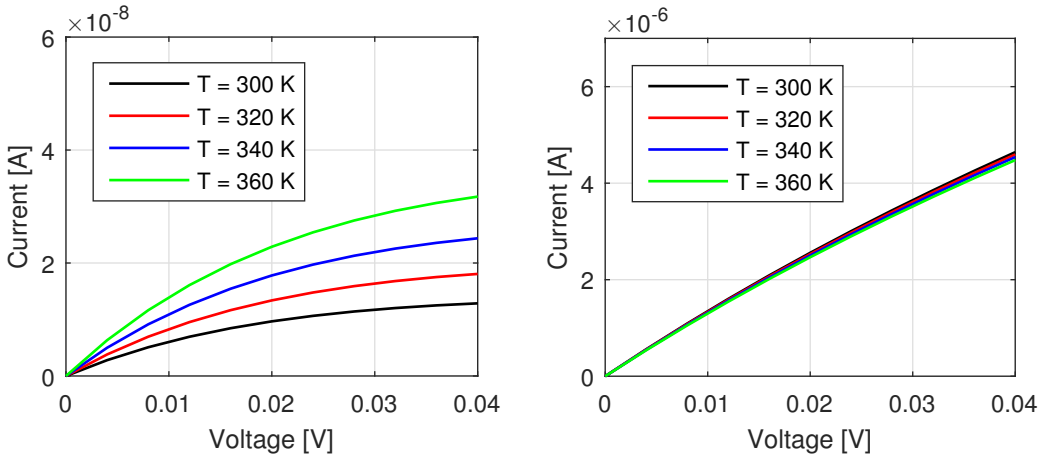

Figure 5.6: (Left) IV characteristics of a semiconducting nanotubes at different temperatures. (Right) same graph for a metallic nanotubes.

shown in Figure 5.6(a). It is worth to mention that in this simplified picture, the transmission rate is assumed to be constant with the temperature, neglecting every sort of thermal broadening of the density of states.

5.4.2 Mean Free Path and Scattering Events

In Chapter 3, it has been shown how to extend the theory of the coherent transport based on the NEGF formalism with phenomenological models for taking into account the mean free path and the scattering events. It has been highlighted that the the mean free path depends on the number of phonons, both acoustic and optical, and has the effect of reducing the current that flows in the nanotube. While in Section 3.5 the attention was focused more on the effect of the applied electric field on the mean free path, here the focus will be more on the temperature. Indeed, increasing the temperature has the effect of increasing the number of phonons, thus the number of scattering events. This effect is here modeled with a shorter mean free path, with the same formulations introduced in Section 3.5.

Figure 5.7 shows the mean free path versus the electric field for different temperatures. By considering low-electric fields, which are typical in these particular applications, one can see how the mean free path is reduced from approximately 1300 nm at room temperature to approximately 900 nm at 360 K. From this, a first consideration can be drawn: if the nanotubes are short (less than 900 nm), the effect of the temperature on the scattering is not influential on the resistance

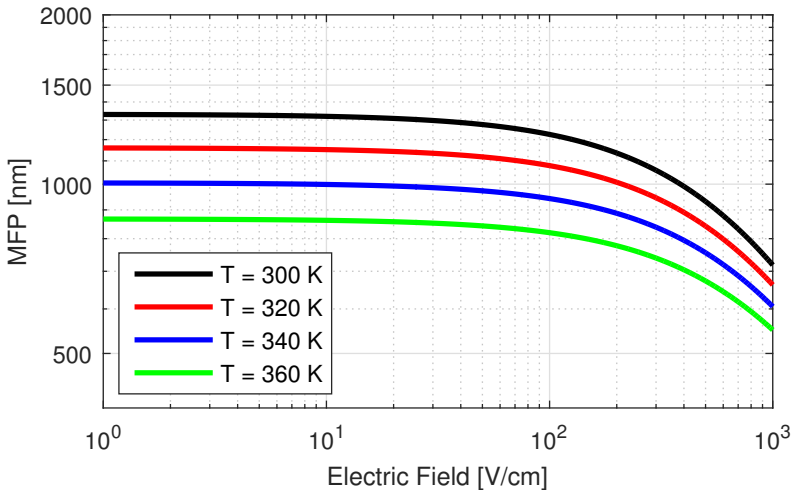

Figure 5.7: Variation of the mean-free-path for different temperatures. Increasing the temperature increases the number of phonons and reduces the MFP.

of the nanotube itself.

5.4.3 Thermally-assisted Crossing of the Junctions

The previous two phenomena analyzed were based on the transport along the nanotubes, and how the transport was affected by temperature variations. However, temperature changes can have an interesting effect also on the way the carriers cross the inter-tube junctions.

As already introduced in Chapter 3, the behavior of an inter-tube junction depends on the chirality of the two nanotubes forming the junction itself. It has been shown, that nanotube of the same class (metallic-metallic and semiconducting-semiconducting) form junctions with an I-V characteristic that is close to be linear, resembling the behavior of a simple resistor [55, 35]. However, it has been further observed, that a low temperatures the large-bias transport has a non-linearity in the IV characteristic, showing consistency with the theory of the Luttinger model. The experimental data have been fitted with the following phenomenological functional form:

$$I = C_1 T^{\alpha} V(1 + C_2(eV/k_B T)^{\alpha}) , \tag{5.5}$$

where C_1 and C_2 are two constants and the exponent α is equal to 2.1. It is worth noticing that Equation (5.5), produces a linear IV characteristic at room

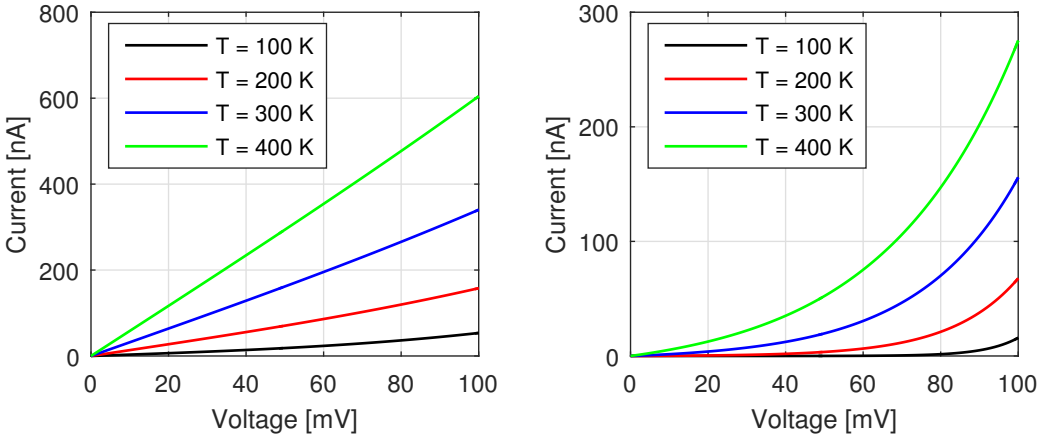

Figure 5.8: IV characteristics for different temperatures of the junctions described respectively by Equation (5.5) and Equation (5.6).

temperature. Furthermore, for the applications of interest here, it very unlikely to reach such high biases at the ends of a junction. Due to the lack of studies in the literature on semiconducting-semiconducting junctions, the same model of Equation (5.5) has been applied.

A different story emerges for metallic-semiconducting junctions. These junctions have shown energy barriers with a height approximately equal to half of the band-gap of the semiconducting nanotube, with a behavior that electrically brings to mind a Schottky diode. It is well known that when a carrier is supplied with some form of energy, it can overcome a barrier if the energy is greater than the height of the barrier. For conventional metal-semiconductor junctions this has been studied with different models that go by the name of thermionic emission effects. For the nanotubes, a proper model for this junctions has not yet been made, and the current state of the art is mostly based on semi-empirical models describing the experimental results. For this reason the model here implemented has a semi-empirical formulation:

$$I = I_0 \, T^{\alpha} \, e^{-\frac{\phi_B}{k_B T}} \left(e^{\frac{qV}{k_B T}} - 1 \right) \tag{5.6}$$

where I_0 is a fitting parameter equal to 10^{-12} and ϕ_B is the height of the Schottky barrier. Figure 5.8 shows the IV characteristics for different temperatures of the junctions described respectively by Equation (5.5) and Equation (5.6).

5.4.4 De-adsorption of Oxygen Molecules

Until this point three out of the four individuated phenomena have been treated and some conclusions can be already made. The current in the single nanotubes and at the junctions increases appreciably when the temperature increases. The increased scattering rate, which is evident for long nanotubes, is not strong enough to compensate the other two effects. As a consequence, one is reasonably led to think that the resistance of a CNT film should always monotonically decrease with the temperature. However, this is not what has been observed experimentally.

Barnes et al. have conducted several experiments on CNT films similar to the one studied in this thesis, and they observed a change in the trend of the resistance-temperature curve [161]. After a certain temperature, here and after referred to as critical temperature T_C, the resistance of the film, which was initially decreasing with the temperature, starts to increase. The curves assume a characteristic U-shape, with the resistance minimum in correspondence of the critical temperature.

Established that the increased scattering rate is not sufficient to counteract the other effects, there must be an additional mechanism which is activated by the temperature and that has an opposite effect, namely increasing the resistance of the film. Barnes et al. claimed that this effect was induced by thermal desorption of the attached oxygen molecules. Continuing what has been said at the beginning of the chapter, this assertion should not give rise to surprises. In fact, it has been shown that the oxygen molecules are attached to the nanotubes by weak electrostatic bonds, which can be easily broken if the necessary energy is given to the molecule. In case this energy exceeds the binding energy, the molecule can be detached, and the nanotube loses its doping, increasing thus the resistance.

By including this effect in the simulation it is possible to fit with good approximation the experimental results. In Figure 5.9, the comparison between the experimental measurements and the simulations with and without the desorption model are presented. Without considering the desorption model, the simulated curve shows a steeper slope than the experimental one. Furthermore, as it will be more clear in the next section, without the desorption model it is not possible to model the U-shape that appears under certain conditions.

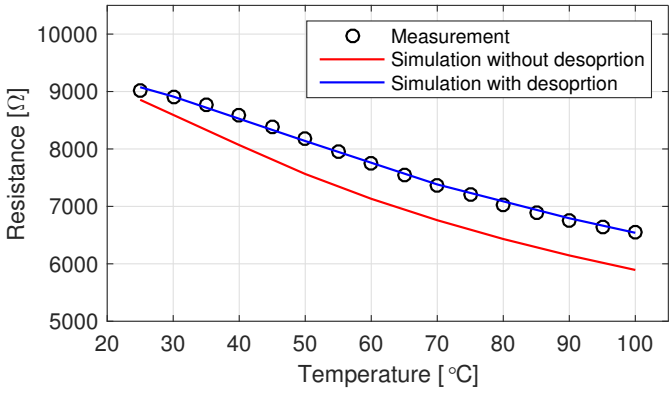

Figure 5.9: Comparison between the experimental measurements and the simulations with and without the desorption model.

The desorption model here used is based on the same formalism presented at the beginning of the chapter for the gas molecules. By increasing the temperature, the Fermi level of the semiconducting nanotubes is shifted towards the mid of the band-gap, making the nanotubes more intrinsic and less conductive. It is worth to mention that this mechanism reaches at some point a saturation; in the limit in which all the molecules are detached, the Fermi level would lie approximately in the mid of the band-gap. Consistently with what has been found experimentally by Barnes et al., metallic nanotubes are less affected by this phenomenon, due to their particular band structure.

It is important to notice that the desorption does not start abruptly at a certain temperature. Due to statistical fluctuations, it is reasonable to assume that the process of desorption starts already at room temperature, in a sort of dynamic equilibrium, in which molecules are constantly adsorbed and de-adsorbed; increasing the temperature makes these two rates unbalanced. The effect is really evident when the decrease of the film resistance starts to saturate. This is the case when, for example, there are no more carriers to be thermally excited.

5.5 CNT film-based Temperature Sensors

For the sake of clarity, it is important to summarize all the phenomena involved in the temperature sensing mechanisms presented in the previous sections.

1. The temperature tends to reduce the resistance of the semiconducting nanotubes and leaves almost unaltered the resistance of metallic nanotubes.

2. The mean free path of the nanotubes becomes shorter when the temperature increases; however the effect is sensible only for long nanotubes (longer than 1 μm).

3. The carriers are facilitate to overcome the barriers at the inter-tube junctions; as a result the resistance of the junctions becomes smaller when the temperature increases.

4. Increasing the temperature increases the vibrations of the molecules and the probability of detaching oxygen molecules from the nanotubes. The resistance increases due to a less pronounced oxygen-induced doping effect.

By combining this knowledge together with the models until here presented, it is possible to reasonably simulate the temperature behavior of CNT films. Figure 5.10 shows the comparison between experimentally measured films and the relative simulations in terms of the normalized resistance. The reason behind this choice for the plots is the same for the gas sensors; the variation of the resistance due to the sensing mechanisms (gas or temperature) is comparable to the variation of resistance due to the statistical fluctuations introduced in Chapter 4. The analysis has been made for films with different densities (from the top to the bottom of the figure the density of the film has been increased).

The first aspect that emerges from the figure is that the curves have a different shape. The last plot, which is related to a highly dense film, the normalized resistance decreases monotonically within the entire range of temperature, which goes from 30 °C to 90 °C. The almost perfect linearity of the characteristic makes this kind of film really interesting for temperature sensors on flexible substrates.

The second curve corresponds to a film with a density approximately around 18 CNTs/μm^2, and is referred to as a medium density film. In this case, the characteristic shows first a linear trend until 80 °C and afterwards a plateau in which the normalized resistance seems to saturate.

In the third and last case, with a film close to the percolation threshold, the point in which the curve changes its trend is moved towards lower temperatures. Indeed, after an initial linear decreasing section, the curve has a minimum at around 70 °C and starts afterwards to increase in the opposite direction. This curve shows exactly what was previously observed by Barnes et al., a U-shape in the resistance-temperature characteristic due to the desorption of the oxygen molecules.

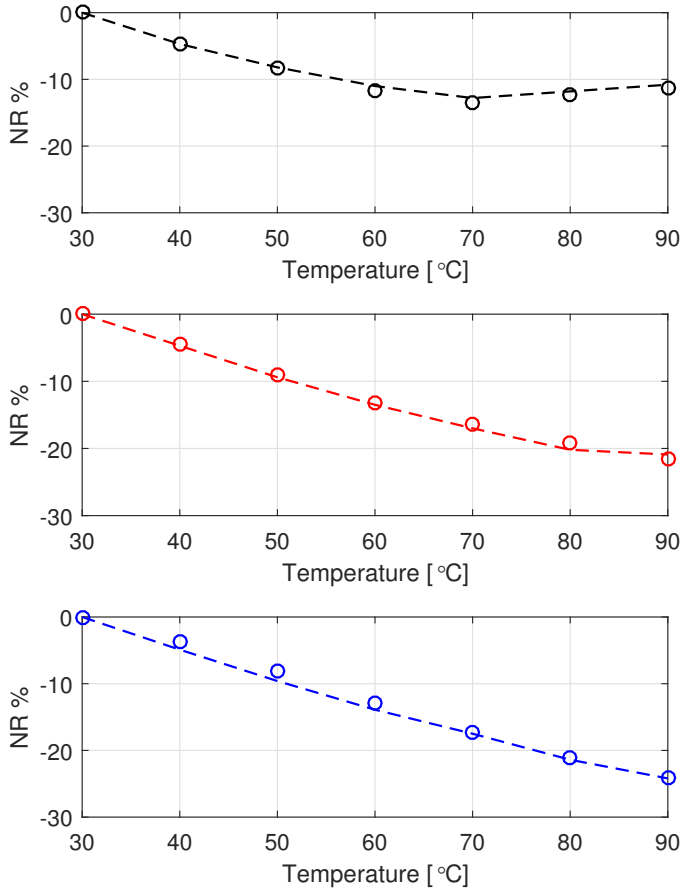

Figure 5.10: Comparison between experimentally measured films and the relative simulations in terms of the normalized resistance respect to temperature variations. From top to bottom the density of nanotubes per unit of area has been increased from almost the percolation threshold to a very dense network with more than 25 CNTs/μm^2.

The first important aspect is that the critical temperature in which the resistance has its minimum changes with the density of the film. From Figure 5.10 it seems that only the low-density film has the U-shape predicted by the desorption theory. However, to be more precise, the U-point does not disappear for denser film, but rather moves towards higher temperatures. This can be seen by the variation in the trend of the second curve, and can be expected for even higher temperatures for the third curve. The reason behind this behavior with different thicknesses can be found in what has been said at the beginning of the chapter and schematically represented in Figure 5.2. Thick films can be considered as two films in parallel: the one that is exposed on the top and the one that lies on the substrate. Due to the penetration length of the molecules, which is expected

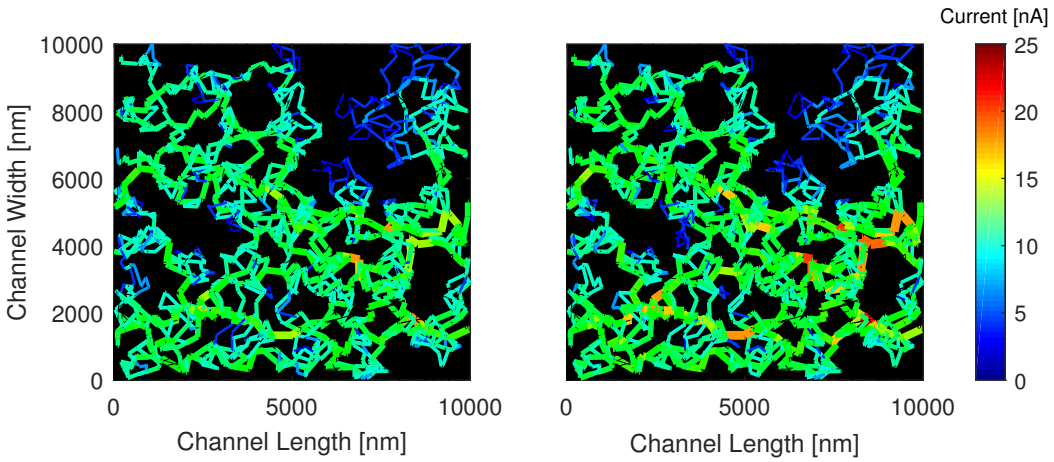

Figure 5.11: Current flow for a network simulated at 300 K (left) and 360 K (right). The film at higher temperature shows an increase of current especially for semiconducting nanotubes.

to be pressure-dependent, only the top film is affected by the molecules. The entire film can be conceptually modeled with a variable resistance (the one of the top film) and a fix one (the one of the film on the substrate). On the other hand, in thin films, the resistance of the entire film varies because all the nanotubes are exposed. Overall, a thin film is much more sensitive to fluctuations in the number of molecules respect to a thick film.

This effect, similarly with what has been done for the gas sensing, has been simulated by varying the average Fermi level of the film. In thin films, this variation is a bit more pronounced, because in principle all the nanotubes are shifting their Fermi level. In thick films, the variation is less marked, due to the fact that only a portion of nanotubes (the one on the top) are shifting their Fermi level. This choice of treating an average Fermi level, rather than different local Fermi levels is once again related to the necessity of limiting the number of IV characteristics to be pre-computed.

The Fermi level shifting can be well described with the following semi-empirical formulation:

$$E_F(T) = E_{F0} - \frac{\alpha T^2}{\beta + T}\,, \tag{5.7}$$

where E_{F0} represents the position of the Fermi level at 0 K, while α and β are two fitting parameters, respectively equal to 1e-4 eV K^{-}1 and 350 K.

To further address the resistance change in the network due to temperature

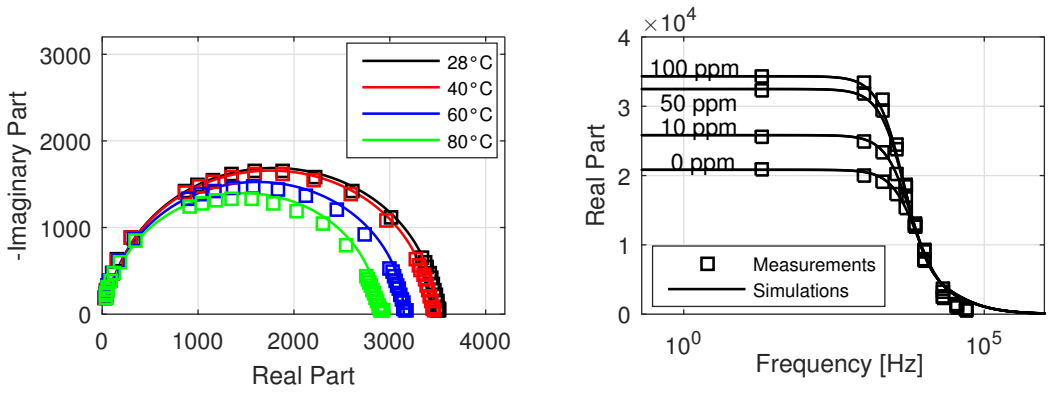

Figure 5.12: (Left) Nyquist plot of the complex impedence at different temperature. (Right) Real part of the complex impedance at different concentration of ammonia.

variations, it is helpful to graphically visualize how the current flow changes in response. Figure 5.11 shows the current flow for a network simulated at 300 K and at 360 K. The network at higher temperature shows an increase of the current in most of the nanotubes. However, this change is evident especially for semiconducting nanotubes, which is the consequence of the assumptions made when introducing the effects of the temperature on the single nanotubes.

5.5.1 Complex Impedance Characterization of Sensors

The program developed during this project has been structured in a modular way, in order to have the capability of combining different models together and have more flexibility during the design of the devices. An example of this is the possibility of combining the models for the frequency analysis (presented in the previous chapter) with the models for gas and temperature sensing.

In Figure 5.12 an example of two combined models for the analysis of temperature and gas sensor is showed. The first figure represents the Nyquist plot of a CNT film where the temperature of the substrate has been swept from room temperature to 80 °C. The good fit with the experiments is an indicator that the temperature acts primarily on the resistance of the nanotubes, leaving the capacitance almost unaltered. Similar conclusions can be drawn on the frequency behavior of the network, which is showed in the right figure. By exposing the film to different concentration of gas molecules (in this case ammonia), the main effect is on the resistance of the film, while the capacitive contributions do not experience any appreciable variation.

Chapter 6

Thin Film Transistor

This chapter is focused on the numerical study of CNT networks in transistor configuration. The intrinsically high charge carrier mobility and solution processability of CNTs renders them a good candidate for use as a channel material in TFTs. While transistors based on a single carbon nanotubes have previously shown extraordinary performance [10], the required fabrication processes typically lack reproducibility. The reasons for the poor reproducibilty are mainly two: first of all, the placement of individual CNTs between two electrodes is very difficult and requires very expensive process steps; secondly, due to the fact that the performance are strictly related to the chirality, orientation and contacting of the nanotube, it is very hard to fabricate several devices with similar characteristics. With the goal of overcoming such difficulties, preferably in a cost-efficient and scalable way, CNT networks have been also studied as material for TFT applications.

From the theoretical point of view, while many groups have studied transistors based on single nanotubes [162, 163, 164], not so much has been done concerning CNT networks. In this regard, following the same approach that has been presented until here, some of the aspects of single CNT transistors modelling have been extended to a network level. The "black boxes" introduced in Chapter 3, will now contain the equivalent circuit of a transistor; the value of the components of the equivalent circuit are obtained by extrapolation from the results of the NEGF calculations. This approach has the great advantage that guarantees simulations accurate enough for the devices under investigation, and, at the same time, the computational effort is not much greater than the one needed for the simulations presented so far.

6.1 Simplified Transistor Model for Single CNTs

Without revolutionizing the theory presented in Chapter 3, a third contact, namely the gate contact, can be added to the nanotube in the NEGF formalism. While until this point the attention has been focused on the low-bias conductance, often referred to as the linear response, for the transistor model the interest is on the full current-voltage characteristic. In this case, it is important to pay attention to the potential inside the nanotube, which arises in response to the voltages applied to the external contacts. The first aspect, which until this point has been neglected, is then to properly calculate the potential inside the channel. In Section 3.4, the NEGF formalism has been introduced together with the self-consistent calculation of the potential through the Poisson equation. However, the expression of the potential inside the channel has not been introduced so far. With the addition of the gate electrode, the problem of finding the potential becomes crucial.

The potential in the active region of the device is given by the sum of two contributions: the Laplace potential, and an additional term which is proportional to the change in the number of electrons. The first term, the Laplace potential, can be directly derived by solving the Laplace equation, in which the channel is assumed to be complete insulating:

$$\vec{\nabla} \cdot (\epsilon_r \vec{\nabla} V) = 0 \,, \tag{6.1}$$

where ϵ_r is the relative permittivity. The solution of this equation can be obtained in terms of a capacitive model, as schematically represented in Figure 6.1. This simplified model, already presented by Datta [119], offers a relative simple way to model the effects of the electrodes on the channel without complicating too much the self-consistent calculation of the potential.

In Figure 6.1, the three capacitances C_S, C_D and C_G are respectively the source, drain and gate capacitance. The potential energy in the channel is thus obtained by multiplying the electrostatic potentials by the electronic charges and the corresponding equivalent capacitance. The solution of equation (6.1) is then:

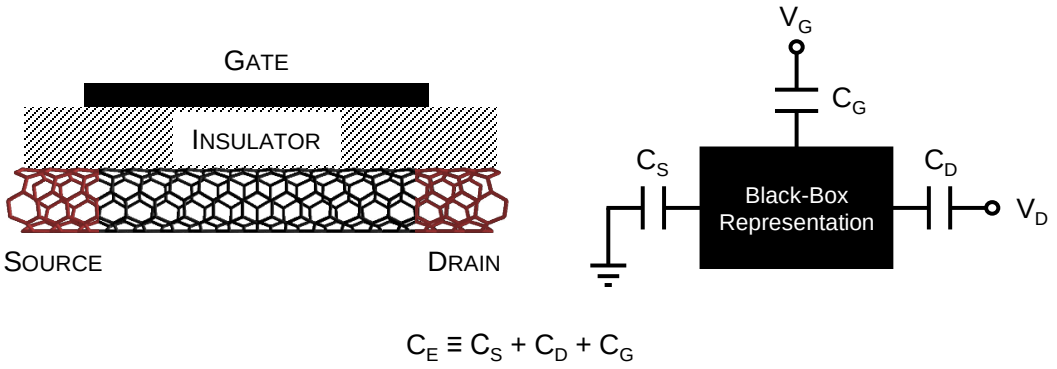

Figure 6.1: (Left) A device driven out of equilibrium by two contacts with different Fermi levels μ_1 and μ_2. (Right) Self-consistent procedure for determining the density matrix ρ from which all quantities of interest can be calculated.

$$U_L = \frac{C_G}{C_E}(-qV_G) + \frac{C_D}{C_E}(-qV_D)\,, \tag{6.2}$$

where the equivalent capacitance C_E is simply the sum of the three individual capacitance. In this case it has been assumed that the source is connected to ground, while the polarization is applied to the gate and drain contacts. The subscript L for the potential indicates that this is the Laplace contribution to the total potential. In fact, equation (6.2) must be completed with a further terms that takes into account the variations of electronic charges in the channel. The approximation in which the total potential is simply equal to the Laplace potential can be considered valid only when there are very few electronic states in the energy range between the electrochemical potentials at the source and drain contacts. However, this approximation it is not valid for metallic nanotubes, highly doped semiconducting nanotubes and with small energy-gap nanotubes, especially when large biases are applied.

Out of this reason, it is important to analyze the general case, in which also the variation in the electron density $\Delta\rho$ is considered. This requires the solution of the Poisson equation:

$$\vec{\nabla}\cdot(\epsilon_r\vec{\nabla}V) = -\Delta\rho/\epsilon_0\,. \tag{6.3}$$

The solution to the Poisson equation can be found once again through the capacitive model earlier introduced. The change in the charge can be rewritten as the sum of the charges on the three capacitors:

$$-q\Delta N = C_S V + C_G(V - V_G) + C_D(V - V_D)\,. \tag{6.4}$$

The total potential energy, is then the sum of the Laplace potential and the additional term proportional to the change of the number of electrons:

$$U = U_L + U_0 \Delta N\,, \tag{6.5}$$

with U_0 known as the *single-electron charging energy*:

$$U_0 \equiv \frac{q^2}{C_E}\,. \tag{6.6}$$

For the sake of completeness, it should be mentioned that the approximation made so far on the self-consistent calculation is considered valid as long as the single-electron charging energy is smaller or comparable to the thermal energy $k_B T$. When the U_0 exceeds greatly the thermal energy, the self-consistent method is not adequate anymore [119]. Since in this work only small conductors at room-temperature (or higher) are considered, the self-consistent method can be assumed valid.

6.1.1 Single CNT Transistor

By combining the concepts explained in the previous section together with the theory presented in Chapter 3, it is possible to compute the total IV characteristic of the desired nanotube-based transistor. In Figure 6.2 an example of two different nanotubes surrounded by the same gate dielectric is presented. The difference between the two output curves is due to the different chirality of the CNTs. Figure 6.2(a) shows the output characteristic of a semiconducting nanotubes, while Figure 6.2(b) the one of a metallic CNT. Both nanotubes are considered to be really short ($\sim$10 nm) in order to see the effect of the band structure on the curves. However, the same concepts can be easily extended to the case of longer nanotubes by considering the mean-free-path for the carriers.

As shown in the two curves, two main differences arise from the band structure of the nanotubes. First of all, the semiconducting nanotube shows a sort of saturation of the current, which is not present in the metallic one. Second of all,

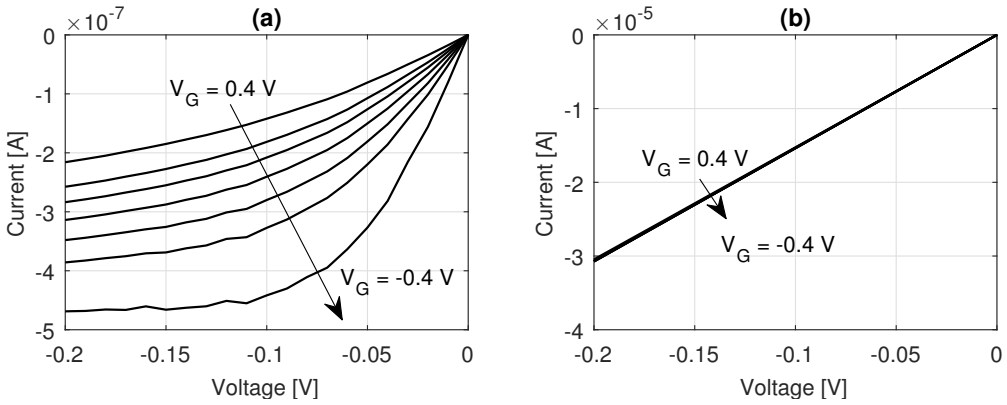

Figure 6.2: (a) Simulations of the output characteristic of a FET based on a single semiconducting nanotube. (b) Simulations of the output characteristic of a FET based on a single metallic nanotube. The gate voltage sweep in both cases ranges from -0.4 V to 0.4 V.

and perhaps the most interesting aspect for the TFTs, the metallic nanotubes do not show a modulation of the current due to the gate voltage.

Once again the reasons behind can be found in the different band structures, as shown previously in Figure 3.9 and Figure 3.10. In fact, while metallic nanotubes have available states in the entire energy range, in semiconducting nanotubes there is a gap of forbidden energies. When the applied voltage pushes one of the two electrochemical potential in this energy range, the current cannot increase linearly anymore due to the absence of available states and thus saturates. This is not valid for metallic nanotubes, where states are always available. It is worth to mention that other phenomena can cause saturation also in metallic nanotubes (e.g. scattering mechanisms) but this is usually the case only for very high voltages.

Out of the same reasons the gate modulation has two different behaviors depending on the chirality of the nanotube. The electrostatic influence on the channel is in principle the same, but the effect on the charges and the states is different. Especially concerning the states, the potential offset introduced by the gate has a big effect on the semiconducting nanotubes (due to the limited number of available states). On the other hand, in metallic nanotubes the change is not appreciable. For very high gate voltages also metallic nanotubes could change their transport properties due to the activation of other sub-bands. However, in such a case, second order effects start to play an important role and it is thus necessary to properly treat them with the non-coherent transport approximation. These cases are not relevant for the applications studied during this

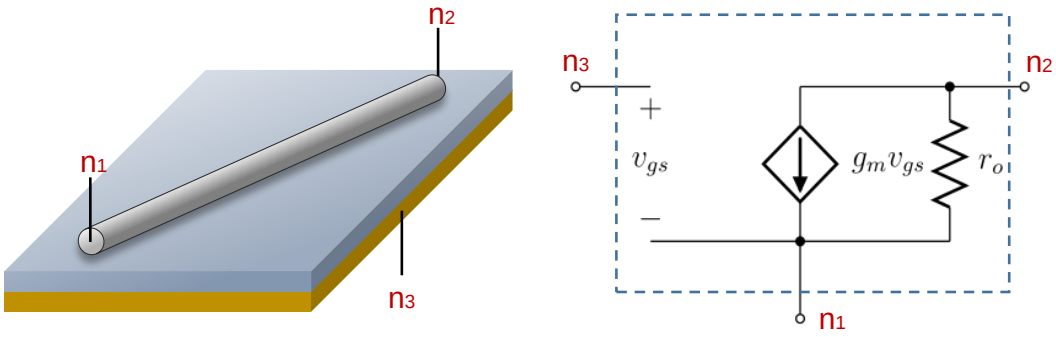

Figure 6.3: (Left) Schematic representation of a nanotube in FET configuration. (Right) Simplified small-signal equivalent circuit of a carbon nanotube.

project and therefore they will not be treated herein.

6.2 Extension of the Model to the Network

The extension of the model for the single nanotube to the entire network is done in the same way already presented in Chapter 4. The netlist for SPICE is written including specific sub-circuits that are connected between each other, with the so-called black-box approach. The transistor behavior of the nanotubes is represented through equivalent circuits, which constitute the sub-circuits forming the netlist of the entire network. A schematic of the single sub-circuit is reported in Figure 6.3.

The crucial point is the definition of the components in the sub-circuit, namely the voltage-controlled current generator and the output resistance of the channel. It is worth to mention that in the literature other groups have already worked in this direction, trying to define these components through semi-empirical models that could fit properly the measured devices [165, 166]. In this work however, the used approach is once again based on the NEGF calculation of the single species of nanotubes. The reason behind this choice is in part dictated by a matter of coherency with the models previously presented in the other chapters, and in part by the fact that the NEGF approach offers a level of details that is hard to match with other techniques.

6.2.1 Sub-circuit Definition

Without explaining the complete derivation of the equivalent circuit in Figure 6.3, which can be found elsewhere [167], here an overview of the components of the aforementioned circuits will be given. In its simplest form, the transistor can be represented by the only voltage-controlled current generator. However, due to the non-linearity of the channel, it is important to include also the output resistance of the channel, which gives a non-flat behavior of the characteristic curve in the saturation regime. In the small-signal approximation, the response of non-linear components becomes linear. In many applications, where signals much smaller than the bias are applied to the device, this approximation is considered valid. However, in case the signals are comparable to the bias, the equivalent circuit becomes much more complicate, and new components must be introduced. Due to the particular applications of interest to this work, the small-signal approximation can be considered valid with a good approximation. Nevertheless, in case of particular needs, the black-box approach allow a straightforward extension of the small-signal model.

The first and most important component is the voltage-controlled current generator. The value of the current in this element is given by the product of the trans-conductance g_m and the voltage that drops across the terminals of gate and source. For this reason, the first step is to calculate the value of g_m. The trans-conductance is simply the electrical characteristic that relates the current through the output of a device to the voltage across the input of the device itself. As every other characteristic of a transistor, the trans-conductance is defined for a specific bias point, which is fixed by the voltages across the device.

$$g_m \equiv \left.\frac{\partial I_D}{\partial V_{GS}}\right|_{V_{DS}} \tag{6.7}$$

The other electrical component that must be defined is the output resistance of the channel, which is the voltage derivative of the current. Similarly to the trans-conductance, also the output resistance is calculated for a specific bias point.

$$r_o \equiv \left.\frac{\partial V_{DS}}{\partial I_D}\right|_{V_{GS}} \tag{6.8}$$

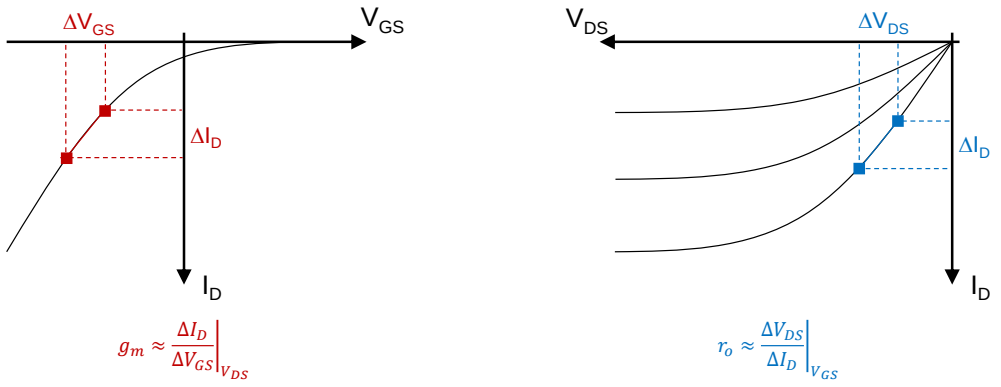

Figure 6.4: (Left) Graphical representation of the trans-conductance. (Right) Graphical representation of the output resistance.

Numerically, the derivative of equations (6.7) and (6.8) are calculated with the finite difference method (FDM). Figure 6.4 shows graphically the concept behind the calculation of the two quantities.

From the graph, it is clear that the trans-conductance is calculated as the slope of the transfer curve for a specific source-drain voltage, whereas the output resistance is calculated as the slope of the output curve for a specific gate-source voltage. The discretization of the functions has to be fine enough to guarantee a good accuracy for the calculations. This statement will be better clarified in the next section.

6.2.2 Assigning the Values to the Elements

For the reasons already explained in the previous chapters, the only way to utilize a multi-scale approach for the solution of this problem is to pre-compute all the possible curves before the actual simulation starts. In the previous cases, this step was rather straightforward, with the results of the pre-computation simply stored in some look-up tables that were subsequently loaded by the program each time during the creation of the netlist. While in the other cases the look-up table was simply a n-by-2 matrix, with n being the number of points along the IV-characteristic, here the problem is more complicate.

First of all, the pre-computer has to calculate all the possible cases, including all the gate-source potentials that can occur in the network. This increases greatly the number of curves that must be pre-computed, which means the number of calls to the NEGF solver. The range of possible gate-source potentials can be in

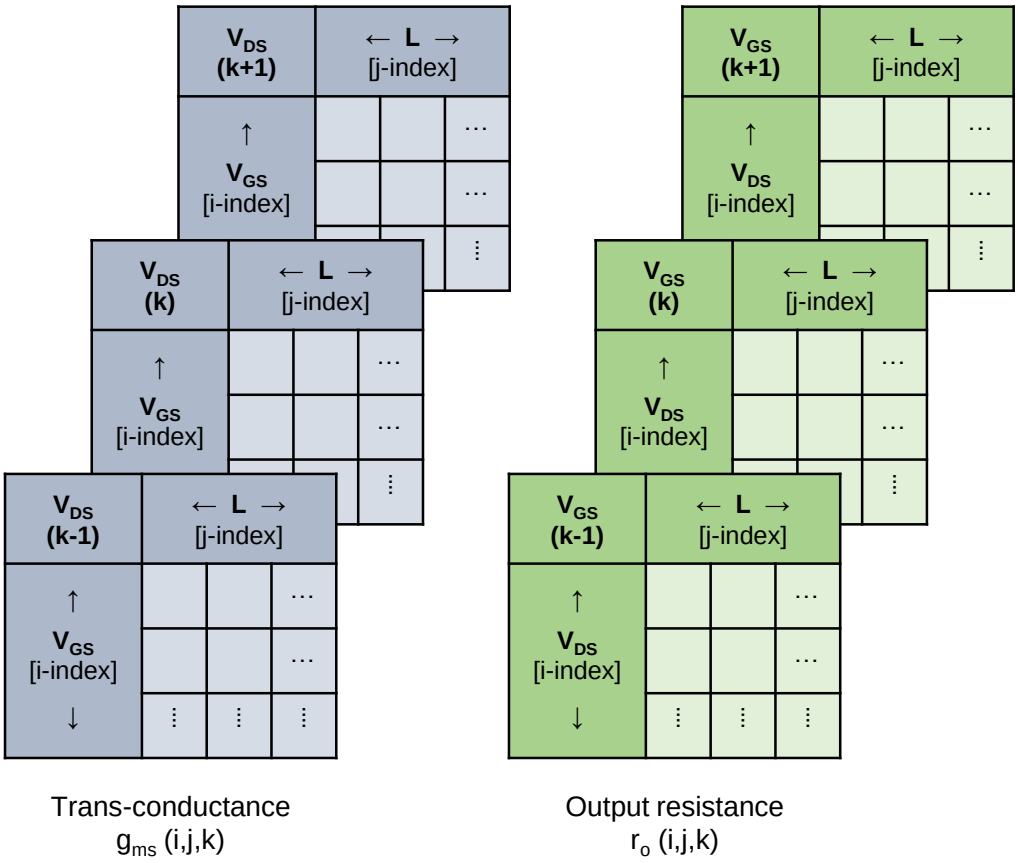

Figure 6.5: (Left) Set of look-up tables for the trans-conductance. (Right) Set of look-up tables for the output resistance.

some cases quite wide, and the discretization must be fine enough to guarantee accurate results. The number of points to be pre-computed varies according to the bias condition on the device. Typically, however, the simulation of a network used as transistor is up to 10 times slower than the simulation of a network used as sensor, due to greater number of curves that must be pre-computed.

Second of all, the simulation is not just slower, but requires also more attention in the assignment of the values to the elements. In fact, the pre-computer has to calculate not only the IV-characteristic (output characteristic of the single nanotube), but also the transfer characteristic, and from that extract the values of trans-conductance and output resistance. Furthermore, this has to be done for a number of possible scenarios that the user must predict a priori. To cite an example, in order to include the already mentioned scattering effects, the pre-computer has to calculate from the beginning the curves for different lengths of the nanotubes. Also in this case there is a certain number of pre-computed

lengths, and the program will afterward establish which is the length that is the closest to the length of the nanotube under investigation.

The result of this is a much more complicate look-up table, that can be visualized in a 3-dimensional space. The schematic idea is represented in Figure 6.5. After the pre-computation, the program assigns for each nanotube the corresponding value of trans-conductance and output resistance to the equivalent circuit of the nanotube itself. This is done by indexing the look-up table on the basis of the electrical condition at the external nodes of the equivalent circuits. The simulation is then performed as in all the other cases, through consecutive iterations of the self-consistent algorithm.

6.3 Effect of the Channel Length

The model has been validated by comparing the results from the simulation with the experimental measurements of devices with different channel lengths. The reason behind of this analysis is mainly due to an interesting behavior of the TFTs based on this technology. Figure 6.6 shows the comparisons for a transistor with a channel length of 4 μm and one with a channel length of 10 μm. As it is clear from the figure, the channel length has a huge impact on the output characteristics, both in terms of the current values and of the shape of the curve. In particular, the shorter channel has a current of one order of magnitude higher respect to the longer channel. Furthermore, while the longer channel shows saturation of the current, in the short channel the current seems to increase almost linearly. In a way, these differences resemble the short-channel effects typical also in inorganic transistors.

Before going further in considerations, it is worth to explain why a 4 μm channel behaves as a "short channel", whereas the 10 μm can be considered as a long channel. The reason is once again related to ratio between the length of the nanotubes and the one of the entire channel. Considering an average length for the nanotubes of 1 μm, it is easy to imagine that the probability of having percolation paths of few nanotubes is much higher in the 4 μm channel transistor. Indeed, shrinking the dimensions of the device could ultimately lead to the case of a single CNT transistor.

Such considerations could generate some concern. In fact, a single semicon-

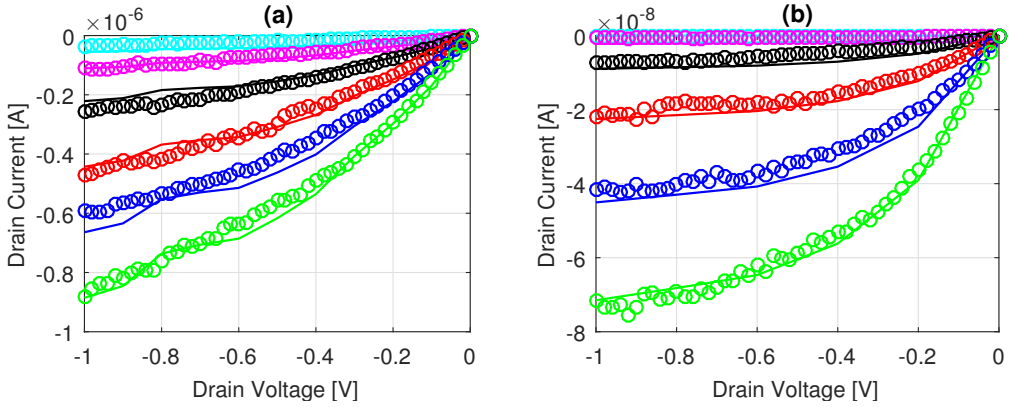

Figure 6.6: (a) Measurements versus simulations of the output characteristic of a TFT with 4 μm channel length. (b) Measurements versus simulations of the output characteristic of a TFT with 10 μm channel length. The gate voltage sweep in both cases ranges from 0 V to -2 V with steps of -0.4 V.

ducting CNT transistor shows typically a saturation of the current, as shown already in Figure 6.2. However, in the case of short channel TFTs more than one nanotube is contributing to the current, and perhaps more importantly, some of these nanotubes are not semiconducting. This can explain in principle the more linear behavior of the transistor and also the smaller impact of the gate electrode on the output characteristics.

However, there is an additional phenomenon that must be considered. If all the nanotubes are artificially set to be metallic, the curves in the case of the 4 μm channel show a better saturation, but still not as good as the ones of the 10 μm channel. The other reason is that the effect of the drain on the channel in a 4 μm channel is not negligible respect to the one of the gate contact. As shown in equation (6.4), the drain potential can play a significant role in the electrostatic of the nanotubes, altering the gating effect. This effect is conceptually very similar to the Drain-Induce Barrier Lowering (DIBL) effects of nano-transistors in inorganic electronic. In that case the strength of the drain potential is enough to tilt and lower the bands, causing higher injection of carriers and less saturation.

One further consideration is that the observed saturation is not due to the scattering mechanisms, since the potential drop on each nanotube is higher in the short channel transistor (due to the fact that the percolation paths have less nanotubes). In fact, if that would be the case, one should see much more pronounced saturation in the short channel transistor.

6.4 Effect of the Semiconducting Percentage

In the previous section, while addressing the problem on the saturation of the output curves, it has been mentioned the effect of the metallic nanotubes on the performance of the transistor. One of the most important figure of merit of transistors is the ratio between the current in the ON state and the one in the OFF state. Ideally, a good transistor would have an OFF-current equal to zero and an ON-current as high as possible. Furthermore, the transition between the two states should be abrupt: the transistor should be completely OFF under its voltage threshold (no current leakages that increase the power consumption) and completely ON immediately after the threshold. Therefore, the so-called I_{ON} to I_{OFF} ratio should be as high as possible. However, while the definition of the ON-current is straightforward, for the OFF-current there are often some disambiguates, especially regarding emerging technologies. One of the biggest problem is to individuate the voltage in which measure the OFF-current. Often, with new technologies, limiting the leakage current from the gate electrode can be very tricky. The direct consequence is that the leakage current is in the same order of the current measured between the source and drain electrodes. This increases the difficulty in defining the value of the OFF-current. Regardless the definition of the two currents, from what has been said until this point it is clear that the higher the concentration of semiconducting nanotubes, the higher is the ON-OFF ratio. In fact, while it is possible to switch a semiconducting nanotube between the ON and the OFF state by applying an appropriate gate potential, the same is not true for metallic nanotubes that are, by all means, always in the ON state. This obviously degrades the performance of the transistor, due to the leakage current that flows in the metallic nanotubes. This phenomenon is greatly reduced when the concentration of metallic nanotubes is very low. In such a case, even if the metallic nanotubes would be theoretically on, the majority of the percolation paths are made by high-impedance nanotubes; the overall current would be at the end very low, and the transistor could be considered in its OFF-state. It is thus fundamental to estimate numerically for which concentrations of metallic nanotubes the ON-OFF ratio can be considered acceptable. For this reason, a useful numerical experimental is to take a fixed morphology and artificially change the concentration of metallic and semiconducting nanotubes. In Figure 6.7 an example of such analysis is presented for three different concentration of semiconducting nanotubes.

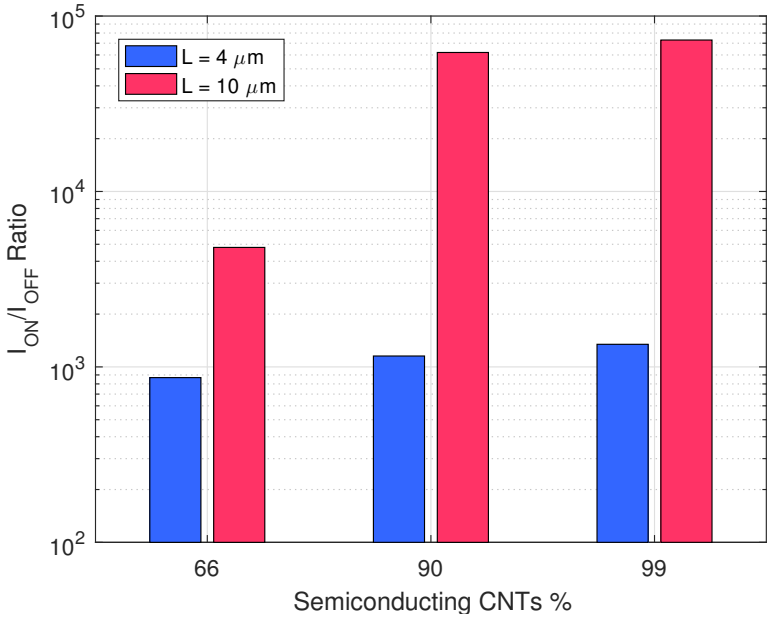

Figure 6.7: I_{ON}-I_{OFF} ratio versus the percentage of semiconducting nanotubes for two different channel lengths.

As expected the higher the concentration of semiconducting nanotubes, the higher the ON-OFF ratio. By looking at Figure 6.7, one can see that also the channel length plays a crucial role in the ON-OFF ratio. Indeed, by comparing the same concentrations of semiconducting nanotubes for two different channel lengths, it is clear that the ON-OFF ratio increases with the channel length. Once again, this phenomenon can be addressed to the percolative nature of the transport in the film. In a short channel, a metallic nanotube can have a huge impact on the overall transistor performance. Indeed, in a hypothetical case in which the nanotubes are long enough to connect directly the source and the drain, a single metallic nanotube could make the entire transistor always ON, even if all the other nanotubes are OFF. For this reason, longer channel lengths reduce the impact of the metallic nanotubes on the whole network, leading to higher ON-OFF ratios. However, after a certain channel length, the ON-OFF ratio tends to saturate. This effect can be studied in terms of the ratio between the average length of the nanotubes and the channel length. From the simulations and the experiments, it has been observed that when the length of the channel is approximately 9 times the length of the nanotubes, the improvements on the ON-OFF ratio start to be negligible.

Chapter 7

Conclusion and Outlook

The work conducted during this project has been introduced with an overview on the CNT film technology. Particular attention has been given to the motivations that pushed the researchers to experiment new technology based on CNTs. In order to completely grasp such motivations, it is important to understand the properties and limitations of the individual nanotubes. For this reason, after a short introduction on CNTs, a comparison among the different CNT-based technologies has been presented highlighting their strengths and weaknesses. In particular, the most interesting aspect of CNT films, namely the low-cost and scalable fabrication process, has made these devices extremely interesting for many emerging applications. Among them, transparent electrodes, sensors and TFTs are definitely the most studied and the closest to enter the market. To complete the foreword, an overview on the state-of-the-art of the modeling techniques used for the simulation of CNT films has been given, putting emphasis on the major flaws of the already available models. In this regard, this work attempts to overcome these limitations through a multi-scale approach that is able to capture the complex physics of the single nanotubes and extend it to the entire network with a circuit-level simulation methodology.

After the introduction, the software developed during this project has been extensively presented. The first important contribution to the numerical simulations of these devices is the introduction of a new algorithm which generates realistic three dimensional morphologies for the CNT films. By comparing experimental measurements and simulations, it has been demonstrated how the obsolete 2D models fail in representing the electrical behavior of the networks. With 2D models, the values of the resistance of the films are highly underestimated. This error, which can be up to 30% for very thin layers, has a

strong dependence on the thickness of the film and increases when the number of nanotubes increases. The reason behind it is merely geometrical, due to an overestimation of the number of junctions between the nanotubes. The low resistances calculated through 2D models are the result of an artifact: by considering all the nanotubes lying on the same plane, the number of junctions is actually much higher than the real number of junctions, since the information on the third dimension is completely lost.

The new algorithm for the generation of 3D networks is a step forward in the simulation of complex structures such as CNT films. However, it is fundamental also to correctly interpret the physics behind the transport in the nanotubes and across the junctions that connect more nanotubes. Simplistic approaches based on semi-empirical models could lead to inaccurate results, especially when it is important to evaluate the full IV characteristic of a nanotube or of a junction. For this reason, the developed program offers the capability of solving the transport equations of features in the nm scale with atomistic models based on the Non-Equilibrium Green's Function (NEGF) formalism. Important information such as the dispersion curves or the transmission rates along the nanotubes are computed in a time efficient but accurate way. These fundamental quantities are pre-computed at the beginning of every simulation steps, and then fed to a higher level simulation step, which includes the information of events that happen in a larger scale (μm range). Scattering phenomena have been introduced with a phenomenological model based on the computation of an effective mean-free-path. This allows to replicate realistic curves for nanotubes exceeding the lengths in which the coherent transport approximations are reasonably considered valid. Following the same approach, the information of the single entities in the film are connected all together in a schematic netlist that connects all the nodes in the network. Finally, a SPICE simulator performs the circuit-level simulation.

The validity of the software has been tested through the comparison with several different device architectures, ranging from simple resistive films to more complicate sensors and thin-film transistor configurations. The resistivity of different films has been thoroughly investigated in terms of thickness of the films and dimension of the devices. The simulations have shown good agreement with the experiments both in terms of absolute values of the resistance and in terms of the variability of the results due to the statistical fluctuations, which appears

to be more pronounced for low density films and for small area devices. Furthermore, the software has proven to be able to estimate correctly the percolation threshold of the networks. Purely resistive films have been also studied under AC stimuli, showing a behavior that resembles low-pass filters with cut-off frequencies in the order of few kHz. This has been possible by introducing the reactive behavior of the nanotubes with properly calculated capacitances and inductances. The modularity of the program allows the user to select every time the desired complexity of the sub-circuit that represents the entities in the network. More complicate models result in higher computational times. However, for all the simulations here presented, the computational effort is never prohibitive and it is possible to run all the instances even on mid-range laptops.

In parallel with the analysis of experimental measurements, a model for the physical interactions between the nanotubes and the surrounding atmosphere has been developed. Indeed, one of the most interesting peculiarity of the nanotubes is their ability to react and change their electrical properties upon exposure to different molecules, especially with oxygen. This particular feature of the nanotubes is often exploited in the realization of gas sensors, one of the most promising application for CNT thin films. Out of this reason, the modeling and simulation of CNT films-based gas sensors represents a significant part in this work. The rates of interaction between the CNTs and the molecules, as well as the impact of such interactions, have been taken from ab-initio simulations present in the literature and stored in a look-up table. With a procedure similar to the Montecarlo method, the program randomly extracts the rates and the quantities of interests by following certain probability distributions. These distributions are based mainly on two functions, the so-called coverage function and the sticking probability. Basically, these two functions describe the number of molecules that are interacting with the nanotubes, for a given pressure of the gas and temperature of the ambient.

Furthermore, staying on the subject of temperature effects, it has been proved that the CNTs have an interesting temperature-dependent resistive behavior that can be used to realize temperature sensors. Since the temperature affects also the number of sticking molecules, in the analysis of the temperature sensors it is always fundamental to define the surrounding ambient conditions (e.g. air, inert atmosphere, etc.). Indeed, the temperature has mainly four effects on the transport along the network: there is a temperature dependency of the indi-

vidual CNTs transport properties, a thermally-assisted crossing of the junctions between the nanotubes, a shorter mean-free-path due to scattering events and, perhaps the most important, the de-adsorption of the oxygen molecules. Both from the experiments and the simulations a dependency of the RTC (resistance temperature coefficient) on the morphology of the network is clearly evident. Furthermore, the concentration of semiconducting nanotubes plays a critical role in the resistance-temperature behavior of the films.

Finally, the CNT films have been studied in a three-terminal configuration, in which a gate electrode acts with the purpose of changing the conductance of the channel that lies between a source and a drain electrode. By adapting the powerful NEGF formalism and introducing the details on the potential inside the nanotubes, it is possible to reasonably model the electrostatic in transistor structures. The interaction between the contacts and the channel has been simplified through a capacitive model that weights the effect of the different electrodes on the electrostatic profile of the device. Although the idea behind the multiscale approach is the same used for the resistive networks and for the sensors, for the transistor model the pre-computation of the quantities of interest is not trivial. From the pre-computation the program extracts a set of values for the trans-conductance and the output resistance, which are the two quantities that constitutes the simplified equivalent circuit for a transistor. However, in this case the pre-computer has to calculate all the possible cases, including all the gate-source potentials that might occur in the network. The assignment of the elements is done through the indexing of a much more complicate look-up table that contains also all the possible lengths of the nanotubes. The simulations could reproduce with good accuracy the experimental results of transistor with different channel lengths. In particular, it has been observed that for short channels the current of the transistor is not saturating, but rather presents effects that resemble the short-channel effects in inorganic transistors with channels shorter than 100 nm. From the simulation this effect has been addressed mainly to two phenomena: the effect of metallic nanotubes (which is more pronounced in short channels) and the not-negligible effect of the drain on the electrostatic of the channel.

Concerning the metallic nanotubes, it has been observed that the lowest the concentration of metallic nanotubes, the highest is the I_{ON}-I_{OFF} ratio. This figure of merit has an interesting dependency also from the length of the chan-

nel. The ratio appears to increase with increasing the channel length, until it reaches a saturation for channel longer than 10 μm. However, these numbers are strictly dependent on the length of the nanotubes constituting the network. The definition of short and long channel is based on the ratio between the channel and the average length of the nanotubes. In the cases here studied, the ratio is approximately equal to 9.

The work accomplished in this project has still room for improvement and can be extended in different aspects. The developed program offers a powerful framework for different kind of simulations of complex structures such as CNT networks. By opportunely changing some of the modules of the program, it is possible to simulate other complicate structures like Si-nanowires, Ag-nanowires and even polymer chains. The simulations can be further extended to include the thermal transport in disorder media, a topic that has recently gain a lot of attention. The accuracy of the models can be increased by including some of the phenomena that are not treated in this work, by keeping in mind that everything has a certain impact on the computational costs.

Bibliography

[1] R. P. Feynman, "There's plenty of room at the bottom," *Engineering and science*, vol. 23, no. 5, pp. 22–36, 1960.

[2] 2011 Cientifica Report. [Online]. Available: http://www.cientifica.com

[3] European Commission, *Nanotechnology: the invisible giant tackling Europe's future challenges*. European Union, 2013.

[4] National Nanotechnology Initiative (NNI). [Online]. Available: http://www.nano.gov/

[5] The Nobel Prize in Chemistry 1996. [Online]. Available: http://www.nobelprize.org/nobel_prizes/chemistry/laureates/1996/

[6] S. Reich, C. Thomsen, and J. Maultzsch, *Carbon nanotubes: basic concepts and physical properties*. John Wiley & Sons, 2008.

[7] S. Iijima *et al.*, "Helical microtubules of graphitic carbon," *Nature*, vol. 354, no. 6348, pp. 56–58, 1991.

[8] P. Avouris, Z. Chen, and V. Perebeinos, "Carbon-based electronics," *Nature nanotechnology*, vol. 2, no. 10, pp. 605–615, 2007.

[9] M. Shim, A. Javey, N. W. Shi Kam, and H. Dai, "Polymer functionalization for air-stable n-type carbon nanotube field-effect transistors," *Journal of the American Chemical Society*, vol. 123, no. 46, pp. 11 512–11 513, 2001.

[10] T. Dürkop, S. Getty, E. Cobas, and M. Fuhrer, "Extraordinary mobility in semiconducting carbon nanotubes," *Nano letters*, vol. 4, no. 1, pp. 35–39, 2004.

[11] L. Hu, D. S. Hecht, and G. Gruner, "Carbon nanotube thin films: fabrication, properties, and applications," *Chemical Reviews*, vol. 110, no. 10, pp. 5790–5844, 2010.

[12] J.-C. Charlier, X. Blase, and S. Roche, "Electronic and transport properties of nanotubes," *Reviews of modern physics*, vol. 79, no. 2, p. 677, 2007.

[13] J. Mintmire and C. White, "Universal density of states for carbon nanotubes," *Physical Review Letters*, vol. 81, no. 12, p. 2506, 1998.

[14] X. Blase, L. X. Benedict, E. L. Shirley, and S. G. Louie, "Hybridization effects and metallicity in small radius carbon nanotubes," *Physical review letters*, vol. 72, no. 12, p. 1878, 1994.

[15] I. Cabria, J. Mintmire, and C. White, "Metallic and semiconducting narrow carbon nanotubes," *Physical Review B*, vol. 67, no. 12, p. 121406, 2003.

[16] V. Zólyomi and J. Kürti, "First-principles calculations for the electronic band structures of small diameter single-wall carbon nanotubes," *Physical Review B*, vol. 70, no. 8, p. 085403, 2004.

[17] D. Connétable, G.-M. Rignanese, J.-C. Charlier, and X. Blase, "Room temperature peierls distortion in small diameter nanotubes," *Physical review letters*, vol. 94, no. 1, p. 015503, 2005.

[18] A. Thess, R. Lee, P. Nikolaev, and H. Dai, "Crystalline ropes of metallic carbon nanotubes," *Science*, vol. 273, no. 5274, p. 483, 1996.

[19] D. Bethune, C. Klang, M. De Vries, G. Gorman, R. Savoy, J. Vazquez, and R. Beyers, "Cobalt-catalysed growth of carbon nanotubes with single-atomic-layer walls," *Nature*, vol. 363, pp. 605–607, 1993.

[20] C. Journet, W. Maser, P. Bernier, A. Loiseau, M. L. De La Chapelle, d. l. S. Lefrant, P. Deniard, R. Lee, and J. Fischer, "Large-scale production of single-walled carbon nanotubes by the electric-arc technique," *nature*, vol. 388, no. 6644, pp. 756–758, 1997.

[21] A. M. Cassell, J. A. Raymakers, J. Kong, and H. Dai, "Large scale cvd synthesis of single-walled carbon nanotubes," *The Journal of Physical Chemistry B*, vol. 103, no. 31, pp. 6484–6492, 1999.

[22] J. Liu, S. Fan, and H. Dai, "Recent advances in methods of forming carbon nanotubes," *MRS bulletin*, vol. 29, no. 04, pp. 244–250, 2004.

[23] J. Prasek, J. Drbohlavova, J. Chomoucka, J. Hubalek, O. Jasek, V. Adam,

and R. Kizek, "Methods for carbon nanotubes synthesis—review," *Journal of Materials Chemistry*, vol. 21, no. 40, pp. 15 872–15 884, 2011.

[24] S. Iijima and T. Ichihashi, "Single-shell carbon nanotubes of 1-nm diameter," *Nature*, vol. 363, pp. 603–605, 1993.

[25] B. Chen, S. Inoue, and Y. Ando, "Raman spectroscopic and thermogravimetric studies of high-crystallinity swnts synthesized by fh-arc discharge method," *Diamond and Related Materials*, vol. 18, no. 5, pp. 975–978, 2009.

[26] B. Chen, X. Zhao, S. Inoue, and Y. Ando, "Fabrication and dispersion evaluation of single-wall carbon nanotubes produced by fh-arc discharge method," *Journal of nanoscience and nanotechnology*, vol. 10, no. 6, pp. 3973–3977, 2010.

[27] T. Guo, P. Nikolaev, A. Thess, D. Colbert, and R. Smalley, "Catalytic growth of single-walled manotubes by laser vaporization," *Chemical physics letters*, vol. 243, no. 1, pp. 49–54, 1995.

[28] T. Ikegami, F. Nakanishi, M. Uchiyama, and K. Ebihara, "Optical measurement in carbon nanotubes formation by pulsed laser ablation," *Thin Solid Films*, vol. 457, no. 1, pp. 7–11, 2004.

[29] I. Kruusenberg, N. Alexeyeva, K. Tammeveski, J. Kozlova, L. Matisen, V. Sammelselg, J. Solla-Gullon, and J. M. Feliu, "Effect of purification of carbon nanotubes on their electrocatalytic properties for oxygen reduction in acid solution," *Carbon*, vol. 49, no. 12, pp. 4031–4039, 2011.

[30] N. Mubarak, F. Yusof, and M. Alkhatib, "The production of carbon nanotubes using two-stage chemical vapor deposition and their potential use in protein purification," *Chemical engineering journal*, vol. 168, no. 1, pp. 461–469, 2011.

[31] D. Bozovic, M. Bockrath, J. H. Hafner, C. M. Lieber, H. Park, and M. Tinkham, "Plastic deformations in mechanically strained single-walled carbon nanotubes," *Physical Review B*, vol. 67, no. 3, p. 033407, 2003.

[32] Q. Cao and J. A. Rogers, "Random networks and aligned arrays of single-walled carbon nanotubes for electronic device applications," *Nano Research*, vol. 1, no. 4, pp. 259–272, 2008.

[33] A. Javey, J. Guo, Q. Wang, M. Lundstrom, and H. Dai, "Ballistic carbon nanotube field-effect transistors," *nature*, vol. 424, no. 6949, pp. 654–657, 2003.

[34] N. Rouhi, D. Jain, and P. J. Burke, "High-performance semiconducting nanotube inks: Progress and prospects," *ACS nano*, vol. 5, no. 11, pp. 8471–8487, 2011.

[35] M. Fuhrer, J. Nygård, L. Shih, M. Forero, Y.-G. Yoon, H. J. Choi, J. Ihm, S. G. Louie, A. Zettl, P. L. McEuen *et al.*, "Crossed nanotube junctions," *Science*, vol. 288, no. 5465, pp. 494–497, 2000.

[36] E. Snow, J. Novak, P. Campbell, and D. Park, "Random networks of carbon nanotubes as an electronic material," *Applied Physics Letters*, vol. 82, no. 13, pp. 2145–2147, 2003.

[37] E. Snow, J. Novak, M. Lay, E. Houser, F. Perkins, and P. Campbell, "Carbon nanotube networks: Nanomaterial for macroelectronic applications," *Journal of Vacuum Science & Technology B*, vol. 22, no. 4, pp. 1990–1994, 2004.

[38] E. Joselevich and C. M. Lieber, "Vectorial growth of metallic and semiconducting single-wall carbon nanotubes," *Nano Letters*, vol. 2, no. 10, pp. 1137–1141, 2002.

[39] Y. Zhang, A. Chang, J. Cao, Q. Wang, W. Kim, Y. Li, N. Morris, E. Yenilmez, J. Kong, and H. Dai, "Electric-field-directed growth of aligned single-walled carbon nanotubes," *Applied physics letters*, vol. 79, no. 19, pp. 3155–3157, 2001.

[40] T. Sreekumar, T. Liu, S. Kumar, L. M. Ericson, R. H. Hauge, and R. E. Smalley, "Single-wall carbon nanotube films," *Chemistry of Materials*, vol. 15, no. 1, pp. 175–178, 2003.

[41] L. Hu, D. Hecht, and G. Grüner, "Percolation in transparent and conducting carbon nanotube networks," *Nano Letters*, vol. 4, no. 12, pp. 2513–2517, 2004.

[42] S. Kim, J. Yim, X. Wang, D. D. Bradley, S. Lee, and J. C. deMello, "Spin- and spray-deposited single-walled carbon-nanotube electrodes for organic solar cells," *Advanced Functional Materials*, vol. 20, no. 14, pp. 2310–2316, 2010.

[43] A. Abdellah, A. Yaqub, C. Ferrari, B. Fabel, P. Lugli, and G. Scarpa, "Spray deposition of highly uniform cnt films and their application in gas sensing," in *Nanotechnology (IEEE-NANO), 2011 11th IEEE Conference on.* IEEE, 2011, pp. 1118–1123.

[44] A. Abdellah, A. Abdelhalim, M. Horn, G. Scarpa, and P. Lugli, "Scalable spray deposition process for high performance carbon nanotube gas sensors," *Nanotechnology, IEEE Transactions on*, vol. 12, no. 2, pp. 174–181, 2013.

[45] A. Abdelhalim, A. Abdellah, G. Scarpa, and P. Lugli, "Fabrication of carbon nanotube thin films on flexible substrates by spray deposition and transfer printing," *Carbon*, vol. 61, pp. 72–79, 2013.

[46] R. C. Tenent, T. M. Barnes, J. D. Bergeson, A. J. Ferguson, B. To, L. M. Gedvilas, M. J. Heben, and J. L. Blackburn, "Ultrasmooth, large-area, high-uniformity, conductive transparent single-walled-carbon-nanotube films for photovoltaics produced by ultrasonic spraying," *Advanced materials*, vol. 21, no. 31, pp. 3210–3216, 2009.

[47] T. Takahashi, K. Tsunoda, H. Yajima, and T. Ishii, "Dispersion and purification of single-wall carbon nanotubes using carboxymethylcellulose," *Japanese journal of applied physics*, vol. 43, no. 6R, p. 3636, 2004.

[48] A. Abdellah, A. Abdelhalim, F. Loghin, P. Köhler, Z. Ahmad, G. Scarpa, and P. Lugli, "Flexible carbon nanotube based gas sensors fabricated by large-scale spray deposition," *Sensors Journal, IEEE*, vol. 13, no. 10, pp. 4014–4021, 2013.

[49] D. Hecht, L. Hu, and G. Gruner, "Conductivity scaling with bundle length and diameter in single walled carbon nanotube networks," *Applied Physics Letters*, vol. 89, no. 13, pp. 133 112–133 112, 2006.

[50] W. Zhou, J. Vavro, N. M. Nemes, J. E. Fischer, F. Borondics, K. Kamaras, and D. Tanner, "Charge transfer and fermi level shift in p-doped single-walled carbon nanotubes," *Physical Review B*, vol. 71, no. 20, p. 205423, 2005.

[51] D.-W. Shin, J. H. Lee, Y.-H. Kim, S. M. Yu, S.-Y. Park, and J.-B. Yoo, "A role of hno3 on transparent conducting film with single-walled carbon nanotubes," *Nanotechnology*, vol. 20, no. 47, p. 475703, 2009.

[52] J. Zhao, A. Buldum, J. Han, and J. P. Lu, "Gas molecule adsorption in carbon nanotubes and nanotube bundles," *Nanotechnology*, vol. 13, no. 2, p. 195, 2002.

[53] D. Kang, N. Park, J.-h. Ko, E. Bae, and W. Park, "Oxygen-induced p-type doping of a long individual single-walled carbon nanotube," *Nanotechnology*, vol. 16, no. 8, p. 1048, 2005.

[54] M. Itkis, D. Perea, S. Niyogi, S. Rickard, M. Hamon, H. Hu, B. Zhao, and R. Haddon, "Purity evaluation of as-prepared single-walled carbon nanotube soot by use of solution-phase near-ir spectroscopy," *Nano Letters*, vol. 3, no. 3, pp. 309–314, 2003.

[55] Z. Yao, H. W. C. Postma, L. Balents, and C. Dekker, "Carbon nanotube intramolecular junctions," *Nature*, vol. 402, no. 6759, pp. 273–276, 1999.

[56] A. A. Odintsov, "Schottky barriers in carbon nanotube heterojunctions," *Physical Review Letters*, vol. 85, no. 1, p. 150, 2000.

[57] Y. Zhang, Y. Zhang, X. Xian, J. Zhang, and Z. Liu, "Sorting out semiconducting single-walled carbon nanotube arrays by preferential destruction of metallic tubes using xenon-lamp irradiation," *The Journal of Physical Chemistry C*, vol. 112, no. 10, pp. 3849–3856, 2008.

[58] D. Zhang, K. Ryu, X. Liu, E. Polikarpov, J. Ly, M. E. Tompson, and C. Zhou, "Transparent, conductive, and flexible carbon nanotube films and their application in organic light-emitting diodes," *Nano Letters*, vol. 6, no. 9, pp. 1880–1886, 2006.

[59] Y.-M. Chien, F. Lefevre, I. Shih, and R. Izquierdo, "A solution processed top emission oled with transparent carbon nanotube electrodes," *Nanotechnology*, vol. 21, no. 13, p. 134020, 2010.

[60] M. Ha, Y. Xia, A. A. Green, W. Zhang, M. J. Renn, C. H. Kim, M. C. Hersam, and C. D. Frisbie, "Printed, sub-3v digital circuits on plastic from aqueous carbon nanotube inks," *ACS nano*, vol. 4, no. 8, pp. 4388–4395, 2010.

[61] C. Wang, J. Zhang, and C. Zhou, "Macroelectronic integrated circuits using high-performance separated carbon nanotube thin-film transistors," *Acs Nano*, vol. 4, no. 12, pp. 7123–7132, 2010.

[62] J. Li, Y. Lu, Q. Ye, M. Cinke, J. Han, and M. Meyyappan, "Carbon nanotube sensors for gas and organic vapor detection," *Nano letters*, vol. 3, no. 7, pp. 929–933, 2003.

[63] E. Bekyarova, M. Davis, T. Burch, M. Itkis, B. Zhao, S. Sunshine, and R. Haddon, "Chemically functionalized single-walled carbon nanotubes as ammonia sensors," *The Journal of Physical Chemistry B*, vol. 108, no. 51, pp. 19 717–19 720, 2004.

[64] M. Penza, R. Rossi, M. Alvisi, G. Cassano, and E. Serra, "Functional characterization of carbon nanotube networked films functionalized with tuned loading of au nanoclusters for gas sensing applications," *Sensors and Actuators B: Chemical*, vol. 140, no. 1, pp. 176–184, 2009.

[65] U. G. Survey, "Mineral commodity summaries 2015: U.s. geological survey," 2015, 196 p.

[66] L.-j. Meng and M. Dos Santos, "Properties of indium tin oxide films prepared by rf reactive magnetron sputtering at different substrate temperature," *Thin Solid Films*, vol. 322, no. 1, pp. 56–62, 1998.

[67] K. Sok Won, K. Manil, K. Inkoo, C. Minwoo, and R. Ji-Wook, "Optical properties of sputtered indium tin oxide thin films," *Journal of Korean Physical Society*, vol. 59, p. 3280, 2011.

[68] Y. Leterrier, L. Medico, F. Demarco, J.-A. Månson, U. Betz, M. Escola, M. K. Olsson, and F. Atamny, "Mechanical integrity of transparent conductive oxide films for flexible polymer-based displays," *Thin Solid Films*, vol. 460, no. 1, pp. 156–166, 2004.

[69] S. Ye, A. R. Rathmell, Z. Chen, I. E. Stewart, and B. J. Wiley, "Metal nanowire networks: the next generation of transparent conductors," *Advanced Materials*, vol. 26, no. 39, pp. 6670–6687, 2014.

[70] D. Langley, G. Giusti, C. Mayousse, C. Celle, D. Bellet, and J.-P. Simonato, "Flexible transparent conductive materials based on silver nanowire networks: a review," *Nanotechnology*, vol. 24, no. 45, p. 452001, 2013.

[71] G. Gruner, "Carbon nanotube films for transparent and plastic electronics," *J. Mater. Chem.*, vol. 16, no. 35, pp. 3533–3539, 2006.

[72] G. Gruner, "Carbon nanonets spark new electronics," *Scientific American*, vol. 296, no. 5, pp. 76–83, 2007.

[73] Z. Wu, Z. Chen, X. Du, J. M. Logan, J. Sippel, M. Nikolou, K. Kamaras, J. R. Reynolds, D. B. Tanner, A. F. Hebard *et al.*, "Transparent, conductive carbon nanotube films," *Science*, vol. 305, no. 5688, pp. 1273–1276, 2004.

[74] Z. Li, H. R. Kandel, E. Dervishi, V. Saini, Y. Xu, A. R. Biris, D. Lupu, G. J. Salamo, and A. S. Biris, "Comparative study on different carbon nanotube materials in terms of transparent conductive coatings," *Langmuir*, vol. 24, no. 6, pp. 2655–2662, 2008.

[75] B.-S. Kong, D.-H. Jung, S.-K. Oh, C.-S. Han, and H.-T. Jung, "Single-walled carbon nanotube gold nanohybrids: application in highly effective transparent and conductive films," *The Journal of Physical Chemistry C*, vol. 111, no. 23, pp. 8377–8382, 2007.

[76] M. Kaempgen, M. Lebert, M. Haluska, N. Nicoloso, and S. Roth, "Sonochemical optimization of the conductivity of single wall carbon nanotube networks," *Advanced Materials*, vol. 20, no. 3, pp. 616–620, 2008.

[77] A. A. Green and M. C. Hersam, "Colored semitransparent conductive coatings consisting of monodisperse metallic single-walled carbon nanotubes," *Nano letters*, vol. 8, no. 5, pp. 1417–1422, 2008.

[78] I. Heller, A. M. Janssens, J. Männik, E. D. Minot, S. G. Lemay, and C. Dekker, "Identifying the mechanism of biosensing with carbon nanotube transistors," *Nano Letters*, vol. 8, no. 2, pp. 591–595, 2008.

[79] E. D. Minot, A. M. Janssens, I. Heller, H. A. Heering, C. Dekker, and S. G. Lemay, "Carbon nanotube biosensors: the critical role of the reference electrode," *Applied Physics Letters*, vol. 91, no. 9, p. 093507, 2007.

[80] K. Maehashi, T. Katsura, K. Kerman, Y. Takamura, K. Matsumoto, and E. Tamiya, "Label-free protein biosensor based on aptamer-modified carbon nanotube field-effect transistors," *Analytical Chemistry*, vol. 79, no. 2, pp. 782–787, 2007.

[81] D. Lee and T. Cui, "Low-cost, transparent, and flexible single-walled carbon nanotube nanocomposite based ion-sensitive field-effect transistors

for ph/glucose sensing," *Biosensors and Bioelectronics*, vol. 25, no. 10, pp. 2259–2264, 2010.

[82] A. Münzer, K. Melzer, M. Heimgreiter, and G. Scarpa, "Random cnt network and regioregular poly (3-hexylthiophen) fets for ph sensing applications: A comparison," *Biochimica et Biophysica Acta (BBA)-General Subjects*, vol. 1830, no. 9, pp. 4353–4358, 2013.

[83] K. Melzer, A. Münzer, E. Jaworska, K. Maksymiuk, A. Michalska, and G. Scarpa, "Selective ion-sensing with membrane-functionalized electrolyte-gated carbon nanotube field-effect transistors," *Analyst*, vol. 139, no. 19, pp. 4947–4954, 2014.

[84] K. Melzer, V. D. Bhatt, T. Schuster, E. Jaworska, K. Maksymiuk, A. Michalska, P. Lugli, and G. Scarpa, "Flexible electrolyte-gated ion-selective sensors based on carbon nanotube networks," *Sensors Journal, IEEE*, vol. 15, no. 6, pp. 3127–3134, 2015.

[85] J. Kong, N. R. Franklin, C. Zhou, M. G. Chapline, S. Peng, K. Cho, and H. Dai, "Nanotube molecular wires as chemical sensors," *Science*, vol. 287, no. 5453, pp. 622–625, 2000.

[86] P. G. Collins, K. Bradley, M. Ishigami, and A. Zettl, "Extreme oxygen sensitivity of electronic properties of carbon nanotubes," *science*, vol. 287, no. 5459, pp. 1801–1804, 2000.

[87] S. Colasanti, V. D. Bhatt, and P. Lugli, "3d modeling of cnt networks for sensing applications," in *Ph. D. Research in Microelectronics and Electronics (PRIME), 2014 10th Conference on.* IEEE, 2014, pp. 1–4.

[88] S. Colasanti, V. Robbiano, F. C. Loghin, A. Abdelhalim, V. D. Bhatt, A. Abdellah, F. Cacialli, and P. Lugli, "Experimental and computational study on the temperature behavior of cnt networks," *IEEE Transactions on Nanotechnology*, vol. 15, no. 2, pp. 171–178, 2016.

[89] C. D. Dimitrakopoulos and P. R. Malenfant, "Organic thin film transistors for large area electronics," *Advanced Materials*, vol. 14, no. 2, pp. 99–117, 2002.

[90] Y. D. Park, J. A. Lim, Y. Jang, M. Hwang, H. S. Lee, D. H. Lee, H.-J. Lee, J.-B. Baek, and K. Cho, "Enhancement of the field-effect mobility

of poly (3-hexylthiophene)/functionalized carbon nanotube hybrid transistors," *Organic Electronics*, vol. 9, no. 3, pp. 317–322, 2008.

[91] G. P. Siddons, D. Merchin, J. H. Back, J. K. Jeong, and M. Shim, "Highly efficient gating and doping of carbon nanotubes with polymer electrolytes," *Nano Letters*, vol. 4, no. 5, pp. 927–931, 2004.

[92] A. Javey, H. Kim, M. Brink, Q. Wang, A. Ural, J. Guo, P. McIntyre, P. McEuen, M. Lundstrom, and H. Dai, "High-κ dielectrics for advanced carbon-nanotube transistors and logic gates," *Nature materials*, vol. 1, no. 4, pp. 241–246, 2002.

[93] EDA Consortium Market Statistics Service (MSS). [Online]. Available: http://www.edac.org/initiatives/committees/mss

[94] D. Stauffer and A. Aharony, *Introduction to percolation theory*. CRC press, 1994.

[95] G. Pike and C. Seager, "Percolation and conductivity: A computer study. I," *Physical review B*, vol. 10, no. 4, pp. 1421–1434, 1974.

[96] C. Seager and G. Pike, "Percolation and conductivity: A computer study. II," *Physical Review B*, vol. 10, no. 4, pp. 1435–1446, 1974.

[97] S. Kirkpatrick, "Percolation and conduction," *Rev. Mod. Phys.*, vol. 45, pp. 574–588, Oct 1973.

[98] I. Balberg and N. Binenbaum, "Computer study of the percolation threshold in a two-dimensional anisotropic system of conducting sticks," *Phys. Rev. B*, vol. 28, pp. 3799–3812, Oct 1983.

[99] S. Kumar, J. Murthy, and M. Alam, "Percolating conduction in finite nanotube networks," *Physical review letters*, vol. 95, no. 6, p. 066802, 2005.

[100] J. Guo and M. A. Alam, "Carrier transport and light-spot movement in carbon-nanotube infrared emitters," *Applied Physics Letters*, vol. 86, no. 2, p. 023105, 2005.

[101] S. Kumar, N. Pimparkar, J. Murthy, and M. Alam, "Theory of transfer characteristics of nanotube network transistors," *Applied physics letters*, vol. 88, no. 12, p. 123505, 2006.

[102] A. Behnam and A. Ural, "Computational study of geometry-dependent

resistivity scaling in single-walled carbon nanotube films," *Physical Review B*, vol. 75, no. 12, p. 125432, 2007.

[103] C. Kocabas, N. Pimparkar, O. Yesilyurt, S. Kang, M. Alam, and J. Rogers, "Experimental and theoretical studies of transport through large scale, partially aligned arrays of single-walled carbon nanotubes in thin film type transistors," *Nano letters*, vol. 7, no. 5, pp. 1195–1202, 2007.

[104] M. A. Topinka, M. W. Rowell, D. Goldhaber-Gordon, M. D. McGehee, D. S. Hecht, and G. Gruner, "Charge transport in interpenetrating networks of semiconducting and metallic carbon nanotubes," *Nano letters*, vol. 9, no. 5, pp. 1866–1871, 2009.

[105] D. Jack, C. Yeh, Z. Liang, S. Li, J. Park, and J. Fielding, "Electrical conductivity modeling and experimental study of densely packed swcnt networks," *Nanotechnology*, vol. 21, no. 19, p. 195703, 2010.

[106] L.-P. Simoneau, J. Villeneuve, C. M. Aguirre, R. Martel, P. Desjardins, and A. Rochefort, "Influence of statistical distributions on the electrical properties of disordered and aligned carbon nanotube networks," *Journal of Applied Physics*, vol. 114, no. 11, p. 114312, 2013.

[107] Linear Technology, LTspice IV. [Online]. Available: http://www.linear.com/designtools/software/

[108] S. Datta, *Electronic transport in mesoscopic systems*. Cambridge university press, 1997.

[109] Z. Ren, R. Venugopal, S. Goasguen, S. Datta, and M. S. Lundstrom, "nanoMOS 2.5: A two-dimensional simulator for quantum transport in double-gate MOSFETs," *IEEE Trans. Electron Devices*, vol. 50, no. 9, pp. 1914–1925, 2003.

[110] A. Rahman, A. Ghosh, and M. Lundstrom, "Assessment of Ge n-MOSFETs by quantum simulation," in *IEDM Tech. Dig.*, 2003, pp. 19–4.

[111] P. Damle, T. Rakshit, M. Paulsson, and S. Datta, "Current-voltage characteristics of molecular conductors: two versus three terminal," *IEEE Trans. Nanotechnol.*, vol. 1, no. 3, pp. 145–153, 2002.

[112] J. Guo, S. Datta, and M. Lundstrom, "A numerical study of scaling issues

for Schottky-barrier carbon nanotube transistors," *IEEE Trans. Electron Devices*, vol. 51, no. 2, pp. 172–177, 2004.

[113] S. Datta, "Nanoscale device modeling: the Green's function method," *Superlattices and microstructures*, vol. 28, no. 4, pp. 253–278, 2000.

[114] S. Datta, "The non-equilibrium Green's function (NEGF) formalism: An elementary introduction," in *IEDM Tech. Dig.*, 2002, pp. 703–706.

[115] A. Trellakis, T. Andlauer, and P. Vogl, "Efficient solution of the Schrödinger-Poisson equations in semiconductor device simulations," in *Large-Scale Scientific Computing*. Springer, 2006, pp. 602–609.

[116] R. Venugopal, Z. Ren, S. Datta, M. Lundstrom, and D. Jovanovic, "Simulating quantum transport in nanoscale transistors: Real versus mode-space approaches," *Journal of Applied Physics*, vol. 92, no. 7, pp. 3730–3739, 2002.

[117] M. Anantram, M. S. Lundstrom, and D. E. Nikonov, "Modeling of nanoscale devices," *Proceedings of the IEEE*, vol. 96, no. 9, pp. 1511–1550, 2008.

[118] J. C. Slater and G. F. Koster, "Simplified lcao method for the periodic potential problem," *Phys. Rev.*, vol. 94, pp. 1498–1524, Jun 1954.

[119] S. Datta, *Quantum transport: atom to transistor*. Cambridge University Press, 2005.

[120] C. T. White and T. N. Todorov, "Carbon nanotubes as long ballistic conductors," *Nature*, vol. 393, no. 6682, pp. 240–242, 1998.

[121] M. Lundstrom, *Fundamentals of carrier transport*. Cambridge University Press, 2009.

[122] J.-Y. Park, S. Rosenblatt, Y. Yaish, V. Sazonova, H. Üstünel, S. Braig, T. Arias, P. W. Brouwer, and P. L. McEuen, "Electron-phonon scattering in metallic single-walled carbon nanotubes," *Nano Letters*, vol. 4, no. 3, pp. 517–520, 2004.

[123] E. Pop, D. A. Mann, K. E. Goodson, and H. Dai, "Electrical and thermal transport in metallic single-wall carbon nanotubes on insulating substrates," *Journal of Applied Physics*, vol. 101, no. 9, p. 093710, 2007.

[124] A. Javey, J. Guo, M. Paulsson, Q. Wang, D. Mann, M. Lundstrom, and

H. Dai, "High-field quasiballistic transport in short carbon nanotubes," *Physical Review Letters*, vol. 92, no. 10, p. 106804, 2004.

[125] Z. Yao, C. L. Kane, and C. Dekker, "High-field electrical transport in single-wall carbon nanotubes," *Physical Review Letters*, vol. 84, no. 13, p. 2941, 2000.

[126] D. Ferry, *Semiconductor transport*. CRC Press, 2000.

[127] E. Pop, D. Mann, J. Cao, Q. Wang, K. Goodson, and H. Dai, "Negative differential conductance and hot phonons in suspended nanotube molecular wires," *Physical Review Letters*, vol. 95, no. 15, p. 155505, 2005.

[128] H. C. d'Honincthun, S. Galdin-Retailleau, J. Sée, and P. Dollfus, "Electron-phonon scattering and ballistic behavior in semiconducting carbon nanotubes," *Applied Physics Letters*, vol. 87, no. 17, p. 172112, 2005.

[129] J. Liu, M. J. Casavant, M. Cox, D. Walters, P. Boul, W. Lu, A. Rimberg, K. Smith, D. T. Colbert, and R. E. Smalley, "Controlled deposition of individual single-walled carbon nanotubes on chemically functionalized templates," *Chemical Physics Letters*, vol. 303, no. 1, pp. 125–129, 1999.

[130] A. Buldum and J. P. Lu, "Contact resistance between carbon nanotubes," *Physical Review B*, vol. 63, no. 16, p. 161403, 2001.

[131] B. I. Dunlap, "Relating carbon tubules," *Physical Review B*, vol. 49, no. 8, p. 5643, 1994.

[132] P. Lambin, A. Fonseca, J. Vigneron, J. Nagy, and A. Lucas, "Structural and electronic properties of bent carbon nanotubes," *Chemical Physics Letters*, vol. 245, no. 1, pp. 85–89, 1995.

[133] L. Chico, V. H. Crespi, L. X. Benedict, S. G. Louie, and M. L. Cohen, "Pure carbon nanoscale devices: nanotube heterojunctions," *Physical Review Letters*, vol. 76, no. 6, p. 971, 1996.

[134] D. W. Brenner, "Empirical potential for hydrocarbons for use in simulating the chemical vapor deposition of diamond films," *Physical Review B*, vol. 42, no. 15, p. 9458, 1990.

[135] R. Serway and J. Gordon, *Principles of Physics*, ser. Principles of Physics. Saunders College Pub., 1998, no. v. 2.

[136] A. Abdelhalim, M. Winkler, F. Loghin, C. Zeiser, P. Lugli, and A. Abdellah, "Highly sensitive and selective carbon nanotube-based gas sensor arrays functionalized with different metallic nanoparticles," *Sensors and Actuators B: Chemical*, vol. 220, pp. 1288–1296, 2015.

[137] P. J. Burke, "An rf circuit model for carbon nanotubes," in *Nanotechnology, 2002. IEEE-NANO 2002. Proceedings of the 2002 2nd IEEE Conference on.* IEEE, 2002, pp. 393–396.

[138] P. J. Burke, "Luttinger liquid theory as a model of the gigahertz electrical properties of carbon nanotubes," *Nanotechnology, IEEE Transactions on*, vol. 1, no. 3, pp. 129–144, 2002.

[139] N. Ashcroft and N. Mermin, *Solid State Physics.* Philadelphia: Saunders College, 1976.

[140] R. Collier, *Transmission Lines: Equivalent Circuits, Electromagnetic Theory, and Photons.* Cambridge University Press, 2013.

[141] H.-S. P. Wong and D. Akinwande, *Carbon nanotube and graphene device physics.* Cambridge University Press, 2011.

[142] M. W. Bockrath, "Carbon nanotubes: electrons in one dimension," Ph.D. dissertation, University of California, Berkeley, 1999.

[143] S. Ramo, J. R. Whinnery, and T. Van Duzer, *Fields and waves in communication electronics.* John Wiley & Sons, 2008.

[144] S. Ilani, L. A. Donev, M. Kindermann, and P. L. McEuen, "Measurement of the quantum capacitance of interacting electrons in carbon nanotubes," *Nature Physics*, vol. 2, no. 10, pp. 687–691, 2006.

[145] I. Heller, J. Kong, K. A. Williams, C. Dekker, and S. G. Lemay, "Electrochemistry at single-walled carbon nanotubes: the role of band structure and quantum capacitance," *Journal of the American Chemical Society*, vol. 128, no. 22, pp. 7353–7359, 2006.

[146] D. John, L. Castro, and D. Pulfrey, "Quantum capacitance in nanoscale device modeling," *Journal of Applied Physics*, vol. 96, no. 9, pp. 5180–5184, 2004.

[147] V. Parkash and A. K. Goel, "Quantum capacitance extraction for car-

bon nanotube interconnects," *Nanoscale research letters*, vol. 5, no. 9, pp. 1424–1430, 2010.

[148] G. Sumanasekera, C. Adu, S. Fang, and P. Eklund, "Effects of gas adsorption and collisions on electrical transport in single-walled carbon nanotubes," *Physical Review Letters*, vol. 85, no. 5, p. 1096, 2000.

[149] S.-H. Jhi, S. G. Louie, and M. L. Cohen, "Electronic properties of oxidized carbon nanotubes," *Physical Review Letters*, vol. 85, no. 8, p. 1710, 2000.

[150] D. Kang, N. Park, J. Hyun, E. Bae, J. Ko, J. Kim, and W. Park, "Adsorption-induced conversion of the carbon nanotube field effect transistor from ambipolar to unipolar behavior," *Applied Physics Letters*, vol. 86, no. 9, p. 093105, 2005.

[151] V. Derycke, R. Martel, J. Appenzeller, and P. Avouris, "Controlling doping and carrier injection in carbon nanotube transistors," *Applied Physics Letters*, vol. 80, no. 15, pp. 2773–2775, 2002.

[152] S. Heinze, J. Tersoff, R. Martel, V. Derycke, J. Appenzeller, and P. Avouris, "Carbon nanotubes as schottky barrier transistors," *Physical Review Letters*, vol. 89, no. 10, p. 106801, 2002.

[153] A. A. Farajian, R. V. Belosludov, H. Mizuseki, and Y. Kawazoe, "A general-purpose approach for calculating transport in contact–molecule–contact systems: Tarabord implementation and application to a polythiophene-based nanodevice," *Thin Solid Films*, vol. 499, no. 1, pp. 269–274, 2006.

[154] M. L. Sancho, J. L. Sancho, and J. Rubio, "Quick iterative scheme for the calculation of transfer matrices: application to mo (100)," *Journal of Physics F: Metal Physics*, vol. 14, no. 5, p. 1205, 1984.

[155] A. Pecchia, M. Gheorghe, A. Di Carlo, and P. Lugli, "Modulation of the electronic transport properties of carbon nanotubes with adsorbed molecules," *Synthetic metals*, vol. 138, no. 1, pp. 89–93, 2003.

[156] A. Sadrzadeh, A. A. Farajian, and B. I. Yakobson, "Electron transport of nanotube-based gas sensors: An ab initio study," *Applied Physics Letters*, vol. 92, no. 2, p. 022103, 2008.

[157] S. Peng, K. Cho, P. Qi, and H. Dai, "Ab initio study of cnt no 2 gas sensor," *Chemical Physics Letters*, vol. 387, no. 4, pp. 271–276, 2004.

[158] K. Seo, K. A. Park, C. Kim, S. Han, B. Kim, and Y. H. Lee, "Chirality-and diameter-dependent reactivity of no2 on carbon nanotube walls," *Journal of the American Chemical Society*, vol. 127, no. 45, pp. 15 724–15 729, 2005.

[159] G. A. Somorjai and Y. Li, *Introduction to surface chemistry and catalysis*. John Wiley & Sons, 2010.

[160] A. Abdelhalim, "Fabrication and characterization of carbon nanotube thin-films for gas sensing applications," Ph.D. dissertation, München, Technische Universität München, Diss., 2015, 2015.

[161] T. Barnes, J. Blackburn, J. van de Lagemaat, T. Coutts, and M. Heben, "Reversibility, dopant desorption, and tunneling in the temperature-dependent conductivity of type-separated, conductive carbon nanotube networks." *ACS nano*, vol. 2, no. 9, pp. 1968–1976, 2008.

[162] L. Latessa, A. Pecchia, A. Di Carlo, G. Scarpa, and P. Lugli, "Simulation of carbon nanotube field-effect devices," in *Nanotechnology, 2004. 4th IEEE Conference on*. IEEE, 2004, pp. 10–12.

[163] L. Latessa, A. Pecchia, and A. Di Carlo, "Dft modeling of bulk-modulated carbon nanotube field-effect transistors," *IEEE transactions on nanotechnology*, vol. 6, no. 1, pp. 13–21, 2007.

[164] S. Frégonèse, H. C. d'Honincthun, J. Goguet, C. Maneux, T. Zimmer, J.-P. Bourgoin, P. Dollfus, and S. Galdin-Retailleau, "Computationally efficient physics-based compact cntfet model for circuit design," *IEEE Transactions on Electron Devices*, vol. 55, no. 6, pp. 1317–1327, 2008.

[165] J. Deng and H.-S. P. Wong, "A compact spice model for carbon-nanotube field-effect transistors including nonidealities and its application—part i: Model of the intrinsic channel region," *IEEE Transactions on Electron Devices*, vol. 54, no. 12, pp. 3186–3194, 2007.

[166] J. Deng and H.-S. P. Wong, "A compact spice model for carbon-nanotube field-effect transistors including nonidealities and its application—part ii: Full device model and circuit performance benchmarking," *IEEE Transactions on Electron Devices*, vol. 54, no. 12, pp. 3195–3205, 2007.

[167] S. M. Sze and K. K. Ng, *Physics of semiconductor devices*. John wiley & sons, 2006.

List of Publications

Peer Reviewed Journals

- **S. Colasanti**, V. Robbiano, F. C. Loghin, V. D. Bhatt, A. Abdellah, F. Cacialli, and P. Lugli, "Experimental and Computational Study on the Temperature Behavior of CNT Networks", IEEE Transactions on Nanotechnology, vol. 15, no. 2, 2015.
- **S. Colasanti**, V. D. Bhatt, A. Abdelhalim, and P. Lugli, "3D Percolative Model Based Multiscale Simulation of Randomly Aligned Networks of Carbon Nanotubes", IEEE Transactions on Electron Devices, vol. 63, no. 3, 2016.

Conference Proceedings

- **S. Colasanti**, V. D. Bhatt, and P. Lugli, "3D Modeling of CNT Networks for Sensing Applications", The 10th Conference on Ph. D. Research in Microelectronics and Electronics (PRIME), 2014.
- **S. Colasanti**, H. Nesswetter, C. G. Zimmermann, P. Lugli, "Modeling and parametric simulation of triple junction solar cell for space applications", The 41st IEEE Photovoltaic Specialist Conference (PVSC), 2014.
- **S. Colasanti**, V. D. Bhatt, A. Abdellah, and P. Lugli, "3D self-consistent percolative model for networks of randomly aligned carbon nanotubes", The 19th International Conference on Electron Dynamics in Semiconductors, Optoelectronics and Nanostructures (EDISON'19), 2015.
- **S. Colasanti**, V. D. Bhatt, A. Abdelhalim, A. Abdellah, and P. Lugli, "A 3D Self-Consistent Percolative Model for AC-DC Electrical Analysis of Carbon Nanotubes Networks", The 20th International Conference on Simulation of Semiconductor Processes and Devices (SISPAD), 2015.
- P. Lugli, A. Abdellah, A. Abdelhalim, A. Albrecht, M. Becherer, E. Ca-

gatay, **S. Colasanti**, A. Falco, F. Loghin, S. El-Molla, J. F. Salmeron, A. Rivadeneyra, "Fabrication, characterization and modeling of flexible electronic components based on CNT networks", 2016 IEEE International Symposium on Circuits and Systems (ISCAS), 2016.

- E. Bezzeccheri, **S. Colasanti**, A. Falco, R. Liguori, A. Rubino, P. Lugli, "Comparative modeling of vertical and planar organic phototransistors with 2D drift-diffusion simulations", VIII International Conference On "Times Of Polymers And Composites": From Aerospace to Nanotechnology, 2016.

Acknowledgment

The possibility and success of this work would not have been likely without the trust, patience and support of several individuals and organizations. I hereby thank all those who contributed to this work in any way.

First, I would like to thank my supervisor Prof. Paolo Lugli for giving me the chance to work on a very exciting topic in an amazing environment. His continuous support contributed greatly to the success of this work. Further I want to thank Mrs. Lucia Weik, for her kind help and cooperation.

I want to express my gratitude to all my colleagues and friends: Claudio Ciceroni, Bogdan Popescu, Dan Popescu, Alaa Abdellah, Ahmed Abdelhalim, Florin Loghin, Mohamed Montasser, Arseny Basta, Ahmed Mahmoud, Vijay Deep Bhatt, Aniello Falco, Emanuele Bezzeccheri, Tim Albes, Pietro Luppina, Alina Lyuleeva, Morten Schmidt, Engin Cagatay, Angela Bernunzo, Marius Loch and Marco Bobinger.

I want to thank the CONTEST Project for the financial support and for the possibility of travelling around Europe and meeting other fellow scientists. Among them I would like to mention a few people that eventually have become good friends of mine: Valentina Robbiano, Luca Santarelli, Matjaz Ogrinc, Nagarajan Palavesam and Tekfouy Lim.

A special comment goes to a person that has become much more than a friend, Katharina Melzer. Her help and continuous encouragement allowed me to keep going on even in very complicated moments.

Finally, there are no words that could express how grateful I am to my family. I owe everything to them and I would have never become who I am without their permanent support. My last thought goes to my father, who I am sure would have wanted to see me reaching this goal.